NTT Technical Review

10
2019

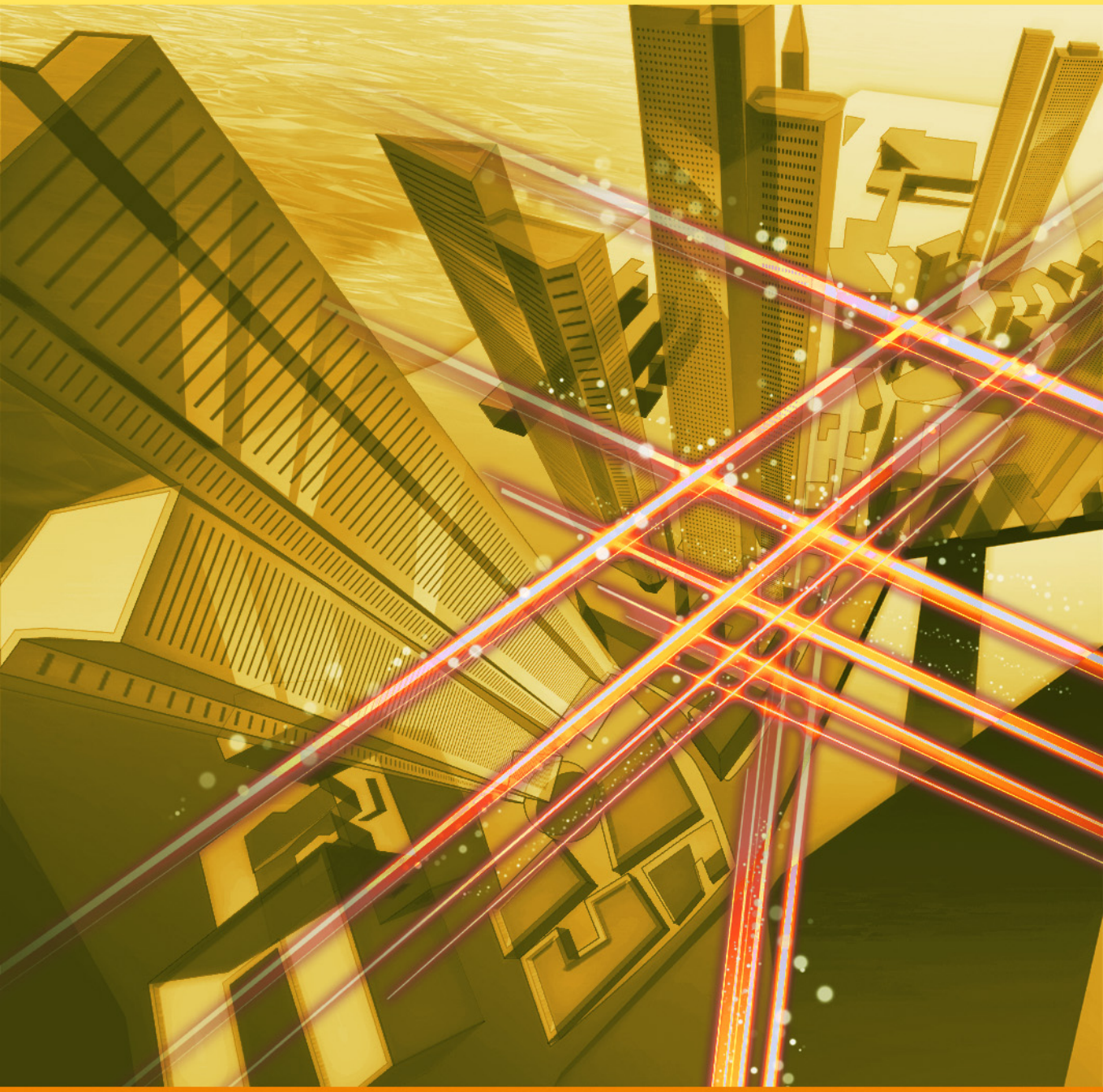

October 2019 Vol. 17 No. 10

NTT Technical Review

October 2019 Vol. 17 No. 10

Feature Articles: Creating Novel Functional Materials

- Overview of Novel Materials Creation Research at NTT
- Creation of Novel Material Sr_3OsO_6 with the Highest Ferromagnetic Transition Temperature among Insulators
- Magnetically Purified Erbium-doped Oxide Crystal—Towards Creating a Quantum-information-manipulation Platform
- MBE Growth and Element-distinctive Atomic-resolution Characterization of High Temperature Superconductors
- High-quality Atomic-layer Materials Fabricated by Chemical Vapor Deposition
- Development of Next-generation Wide-bandgap Semiconductors
- Crystal Growth of Wurtzite GaP Nanowires for Solar-water-splitting Devices

Regular Articles

- High Power and High Efficiency Operation of Semiconductor Optical Amplifier Assisted Extended Reach Electroabsorption Modulated DFB Laser (AXEL) for Extension of Transmission Distance

Global Standardization Activities

- Surviving in the Digital Transformation Era; Technical Trends and Issues from the Perspective of The Telecommunication Technology Committee

Practical Field Information about Telecommunication Technologies

- Introduction to Troubleshooting Cases Related to Telephone Systems in Customer Premises

External Awards/Papers Published in Technical Journals and Conference Proceedings

Overview of Novel Materials Creation Research at NTT

Hideki Yamamoto and Hideki Gotoh

Abstract

The activities of NTT Basic Research Laboratories include creating novel materials with fascinating functions through materials design and arrangement control of atoms, molecules, and crystals in materials. The purpose is to make progress in materials science and eventually contribute to the development of information and communication technology. While our research covers a vast range of materials, we introduce some of the latest research accomplishments in inorganic materials, for example, oxides and nitrides, in the Feature Articles in this issue. In particular, we highlight thin films (less than a micrometer thick), atomic layer materials (less than a nanometer thick), and nanowires.

Keywords: creation of novel materials, functionalization, device fabrication

1. Significance of research on novel functional materials

The development of novel functional materials has been contributing to advances in fundamental science as well as the development of new and/or high-performance devices; the latter has sometimes brought about breakthroughs even in the design concept of devices and has had a substantial impact on our societies. Examples of such novel materials include superconducting oxides (Nobel Physics Prize in 1987); fullerenes, a football-like structure comprising 60 carbon atoms (Nobel Chemistry Prize in 1996); graphene, an extremely thin graphite layer of single-atom thickness (Nobel Physics Prize in 2010); and nitride semiconductors, the essential constituents of blue light-emitting diodes (LEDs) (Nobel Physics Prize in 2014). In fact, some alternative materials have been proposed to overcome the limits of miniaturization in silicon (Si)-based integrated circuits (Moore's law limit) [1]. Another good example is InP (indium phosphide), rather new compared with Si and gallium arsenide (GaAs), which is essential for ultrahigh-speed-operable optical devices in optical communications [2].

The development of novel functional materials and fabrication of devices exploiting them are always challenges, and one has to start with basic research. To achieve designated but yet-unrealized functions, two approaches are possible. One is to create/synthesize brand-new materials/compounds, and the other is to improve the quality of some already existing materials and alternately stack them followed by processing in the nanometer range.

Tremendous efforts have been made here at NTT Basic Research Laboratories using both approaches. We have been exploiting our unique and state-of-the-art apparatuses and technologies for materials creation, which, at least partially, we developed through our own efforts. In the Feature Articles in this issue, we describe our latest accomplishments in such materials science research. Because of space limitations, we regrettably had to omit recent developments in bio-soft materials research previously featured in 2016 [3].

2. Materials creation using thin-film synthesis methods

In this section, we explain what thin-film specimens are and how they are prepared.

2.1 Thin-film specimens

The phrase *synthesis of novel materials* may bring

to mind reactions of reagents in beakers and flasks as well as calcination and sintering of various ingredient powders in furnaces. However, our approach involves synthesis by means of thin-film growth methods. Generally, thin films are specimens whose thicknesses are in the range between 0.1 nm (atomic monolayer) and 10 μm; here, 1 nm is 1/1000 μm, and 1 μm is 1/1000 mm. Researchers and experts use the term *growth* for the preparation of films, as our thin-film specimens are grown on single-crystalline substrates in an atomic- or molecular-layer-by-layer manner, leading to single-crystalline thin films. Note that solids in which atoms are periodically and orderly arranged and thus form lattices are called crystals, and crystals that have only a single atomic arrangement over an entire volume are called single crystals.

2.2 Thin-film growth methods

We have mainly adopted two kinds of thin-film growth methods: molecular beam epitaxy (MBE) and metal-organic vapor phase epitaxy (MOVPE); the term epitaxy comes from the Greek roots *epi*, meaning *above* and *taxis*, meaning *an ordered manner*. In MBE, thin films are formed on heated single-crystalline substrates in an ultrahigh vacuum (UHV) chamber (~10 trillion times lower than the atmospheric pressure) by reaction between the constituent elements that are supplied as atomic or molecular beams. In MOVPE, thin films are also formed on heated single-crystalline substrates but in a reactor furnace, in which metal-organic substances containing the constituent cations are flowed with a carrier gas, for example, H_2 (hydrogen gas) or N_2 (nitrogen gas), along with an anion source gas, for example, NH_3 (ammonia gas). The latter method belongs to a broader category called chemical vapor deposition (CVD), where the metal-organic sources are not necessarily used.

Both methods were originally developed for growing high-quality thin films of known materials and also for fabricating junctions and superlattices consisting of various known materials. To search for brand-new materials that are non-existent in nature, MBE is the more suitable method, as the film growth proceeds under conditions far from the thermodynamic equilibrium. Actually, as exemplified in the Feature Articles in this issue, MBE is used to fabricate the brand-new ferromagnetic material Sr_3OsO_6 (Sr: strontium, Os: osmium, O: oxygen) [4], as well as $CaCuO_2$ (Ca: calcium, Cu: copper, O: oxygen) having the infinite-layer structure (IL-$CaCuO_2$) [5], c-BN (cubic-structured boron nitride) [6], and lightly erbium-doped CeO_2 (cerium oxide) thin films [7]; IL-$CaCuO_2$ and c-BN are thermodynamically metastable, and high pressure is required to synthesize them in bulk forms.

In contrast, in MOVPE and CVD, thin-film growth proceeds under conditions close to the thermodynamic equilibrium, and, hence, dislocation density in the thin films can be reduced. This means that high-crystalline-quality films are rather readily achieved. Accordingly, MOVPE has been widely exploited in the fabrication of nitride-based light-emitting devices and transistors, for example, GaN (gallium nitride)-based devices. Two of the Feature Articles in this issue explain the fabrication of atomic-layer-thick graphene and h-BN (hexagonal boron nitride) by CVD [8] and GaP (gallium phosphide) nanowires by MOVPE [9].

3. MBE as a synthesis method *sui generis* for brand-new materials

NTT Basic Research Laboratories is one of the most advanced research organizations in the world, in that some brand-new materials have been synthesized using MBE. MBE is a thin-film growth technique developed in the late 1960s to crystallize and investigate GaAs epilayers and has been applied to grow thin epitaxial structures made of various known materials. Here, we start with an explanation of how the unique characteristics of our MBE apparatuses allow for the creation of novel materials. A schematic illustration of our MBE set-up *sui generis*, which is totally tuned up for the growth of multi-cation oxides (complex oxides) [10], is shown in **Fig. 1**.

One of the unique features of our MBE system is that the flux rates of multiple cations supplied at a certain moment are simultaneously monitored and the results are fed back in real time to the power supplies of the evaporators, which allows for precise control and stable supply of the atomic fluxes of each constituent cation; the flux rates are monitored by electron impact emission spectroscopy (EIES). In EIES, atomic fluxes are impacted with accelerated electrons, and each flux emits light of characteristic wavelengths. Although the intensity of the emitted light is too weak to detect with the human eye, the EIES equipment can measure the intensity of the emitted light in a wavelength-specific manner and transform the optical signals into electrical ones. In this manner, one can obtain information on what and how many atoms are supplied.

It is worth mentioning that the principle of EIES

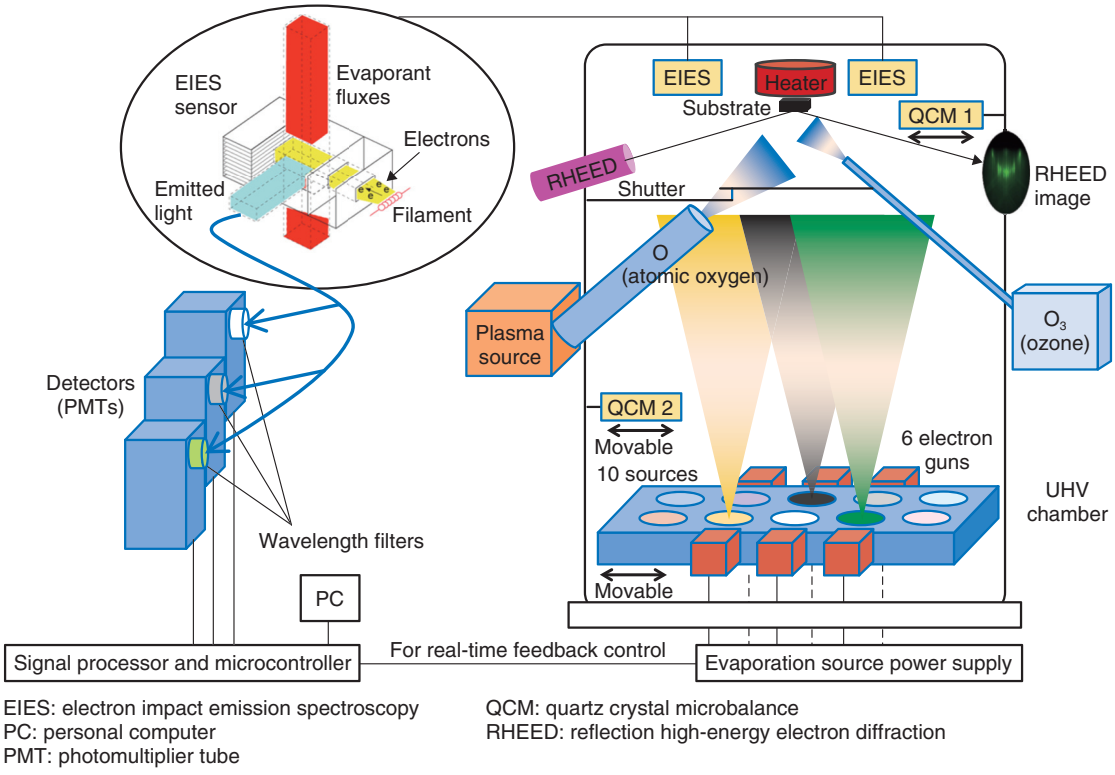

Fig. 1. Schematic illustration of our MBE system for growing complex oxide thin films.

takes after that of a flame reaction, which may have been learned in one's high school days. Instead of being impacted with electrons, a flame reaction takes place when materials are heated in a flame. In doing so, light with element-specific wavelengths is emitted, for example, greenish yellow light for Ba (barium) and bright red light for Sr (strontium). The flame reaction is utilized in fireworks, where one can enjoy multiple combinations of beautiful colors achieved by various combinations of pyrotechnic materials.

Another characteristic feature of our MBE system is the capability of introducing reactive atomic oxygen (O) or ozone (O_3) gas, which enables oxidation of the cation species under UHV; typically, oxygen exists as O_2 (oxygen molecules). We can also grow nitride thin films, for example, c-BN, if the oxygen gas source is replaced by an atomic nitrogen (N) gas source [11].

Furthermore, modern MBE systems are equipped with a reflection high-energy electron diffraction (RHEED) capability, which is also the case with ours and allows for real-time monitoring of crystal structure and crystallinity of thin films during the growth. In RHEED, a high-energy electron beam is incident to the sample surface under grazing incident angle, and hence, this method is surface sensitive. As the operation of RHEED requires a high vacuum, RHEED is a method highly compatible with MBE. Note that in our labs, we can also monitor thin-film growth in real time with MOVPE using a method other than RHEED. These advantages of our MBE system have enabled us to discover novel superconductors [12, 13] and a magnetic material [14], while some important growth parameters such as the flux ratio of cations, substrate materials, substrate temperature, and oxidation strength are systematically varied.

Outstanding developments in measurement techniques and equipment are another important factor that has enabled materials science research using thin-film specimens. Nowadays, cutting-edge characterization methods can be applied to thin-film specimens due to their sufficiently high sensitivity. Since the thicknesses of thin-film specimens are limited to, at most, a few hundred atomic/molecular layers, detailed investigation of their properties had been elusive until a couple of decades ago even when one succeeded in synthesizing new materials in thin-film forms. In stark contrast, atomic-resolution scanning

transmission electron microscopes as well as magnetometers with an ultrahigh sensitivity adequate for investigating the magnetic properties of 300-nm-thick specimens have been developed and exploited in our daily research, as represented by the accomplishments presented in these Feature Articles. The use of thin-film specimens in the search for novel materials has the following advantages as compared with bulk specimens: less consumption of reagents (less use of natural resources), higher-throughput screening, and higher compatibility with device fabrication processes.

4. Functionalization: from material synthesis to device fabrication

To achieve devices that exhibit designated functions by exploiting various properties inherent to individual materials, just the existence of certain materials or the availability of their thin films is not enough. We explain here the functionalization and device fabrication processes using an aluminium nitride (AlN)-based LED as an example of a typical semiconductor device (**Fig. 2**). The AlN-based diodes emit light with the shortest wavelength among any solid-state semiconductor-based light sources, as has been described in a previous NTT Technical Review article [15].

The AlN-based LEDs are prepared by MOVPE (**Fig. 3**). The existence of the chemical substance, AlN, had been well-known, and accordingly, AlN itself is not a new material. However, to make AlN usable as a functional semiconducting material requires the accumulation of a vast amount of research, which is comparable to that for the creation of new materials.

First, the crystalline quality of AlN itself needs to be substantially improved (Phase I). This is because the emergence of inherent functionality is hindered when (thin-film) crystals include polycrystalline portions and/or a high density of defects. Next, doping control is required (Phase II). To fabricate LEDs, or more generally, some semiconductor-based devices, it is necessary to deliberately introduce heterovalent impurities into pristine materials (here, AlN) and achieve a situation in which positive and negative carriers (holes and electrons, respectively) exist in different regions. Accordingly, in phase II, research efforts are focused on how to achieve effective doping without dramatically deteriorating the crystallinity of the thin films. Finally, the design and fabrication of stacking structures (schematically shown in Fig. 2) need to be investigated (Phase III). For example, one should optimize the thickness of each stacking layer and the number of repetition periods in the superlattice layers. In addition, the stacking layers are lithographed and etched until device structures exhibiting certain functions are eventually completed.

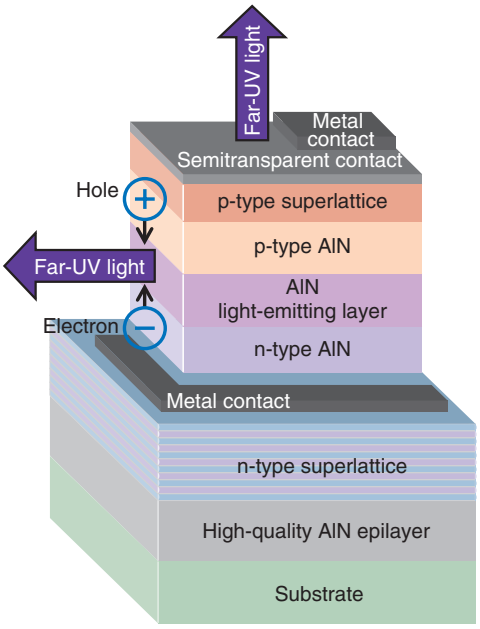

UV: ultraviolet

Fig. 2. Schematic illustration of the structure of AlN-based LED.

5. Towards further creation of novel functional materials

As described above, materials science research requires vast amounts of time and effort as well as long-term strategies [16]; it follows the saying, "Endurance makes you strong." This is especially true for research on the creation of hitherto-undiscovered materials but with fascinating properties. Such research may be likened to *Phase Zero*, and is sometimes compared to a journey for seeking the Holy Grail, borrowing the phrase of Prof. Emeritus M. R. Beasley of Stanford University.

Nevertheless, materials science research is a dreamful activity that inherently has the potential for yielding something exciting, as far as taking methodologically correct approaches. For example, on the assumption that a useful room-temperature superconductor is discovered, it will lead to disruptive innovation

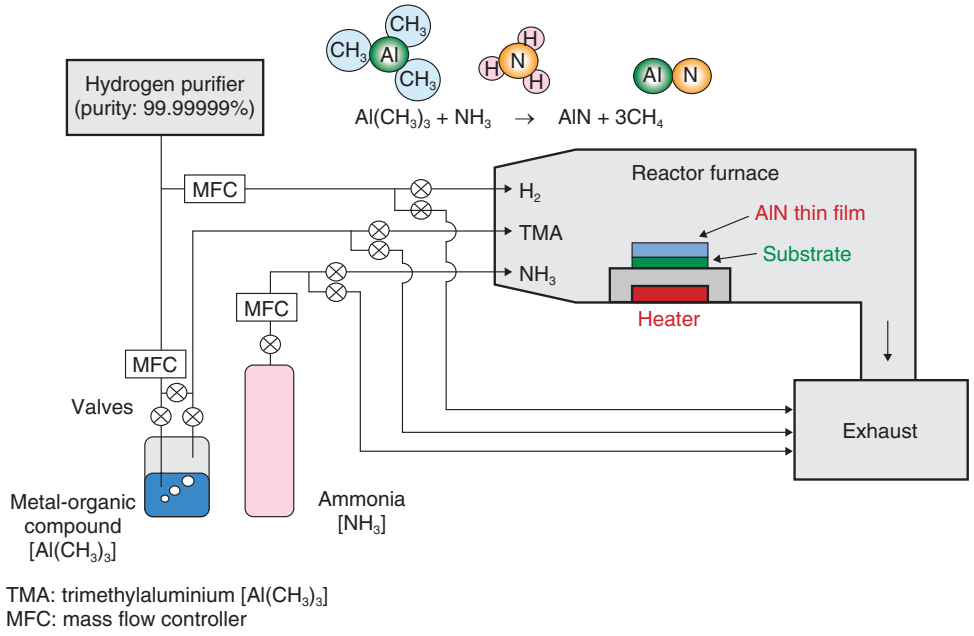

Fig. 3. Schematic illustration of our MOVPE system and chemical reaction during the growth of AlN.

[17] that allows for lossless direct current power feeding as well as lossless intra- and inter-chip connections.

Materials science research has relied on the three conventional paradigms of science: experiment, theory, and computation. Individual materials are first synthesized and characterized. Their molecular/crystal/electronic structures are subsequently determined with the aid of theoretical and computational studies. Finally, functional structures and/or devices are designed and fabricated. Recently, a fourth paradigm called materials informatics (MI) has emerged, where the compositions and structures of materials having desired functions are predicted by utilizing machine learning techniques along with materials databases and/or theoretical calculations [18]. While further progress in MI is desirable to see its bona fide capability and potential, we hope to promote our materials science research further by combining our advantages of thin-film synthesis technologies already in hand and the newly developed approach, MI.

References

[1] H. Hasegawa, M. Akazawa, A. Domanowska, and B. Adamowicz, "Surface Passivation of III-V Semiconductors for Future CMOS Devices—Past Research, Present Status and Key Issues for Future," Appl. Surf. Sci., Vol. 256, No. 19, pp. 5698–5707, 2010.

[2] M. Nagatani, H. Wakita, Y. Ogiso, H. Yamazaki, M. Ida, and H. Nosaka, "Ultrahigh-speed Optical Front-end Device Technology for Beyond-100-GBaud Optical Transmission Systems," NTT Technical Review, Vol. 17. No. 5, pp. 27–33, 2019. https://www.ntt-review.jp/archive/ntttechnical.php?contents=ntr201905fa4.html

[3] "Feature Articles: Forefront Research on Bio-soft Materials," NTT Technical Review, Vol. 14, No. 8, 2016. https://www.ntt-review.jp/archive/2016/201608.html

[4] Y. K. Wakabayashi, Y. Krockenberger, Y. Taniyasu, and H. Yamamoto, "Creation of Novel Material Sr_3OsO_6 with the Highest Ferromagnetic Transition Temperature among Insulators," NTT Technical Review, Vol. 17, No. 10, pp. 7–11, 2019. https://www.ntt-review.jp/archive/ntttechnical.php?contents=ntr201910fa2.html

[5] A. Ikeda, Y. Krockenberger, Y. Taniyasu, and H. Yamamoto, "MBE Growth and Element-distinctive Atomic-resolution Characterization of High Temperature Superconductors," NTT Technical Review, Vol. 17, No. 10, pp. 18–23, 2019. https://www.ntt-review.jp/archive/ntttechnical.php?contents=ntr201910fa4.html

[6] K. Hirama, Y. Taniyasu, H. Yamamoto, and K. Kumakura, "Development of Next-generation Wide-bandgap Semiconductors," NTT Technical Review, Vol. 17, No. 10, pp. 30–35, 2019. https://www.ntt-review.jp/archive/ntttechnical.php?contents=ntr201910fa6.html

[7] T. Tawara and T. Inaba, "Magnetically Purified Erbium-doped Oxide Crystal—Towards Creating a Quantum-information-manipulation Platform," NTT Technical Review, Vol. 17, No. 10, pp. 12–17, 2019. https://www.ntt-review.jp/archive/ntttechnical.php?contents=ntr201910fa3.html

[8] S. Wang and Y. Taniyasu, "High-quality Atomic-layer Materials Fabricated by Chemical Vapor Deposition," NTT Technical Review, Vol. 17, No. 10, pp. 24–29, 2019. https://www.ntt-review.jp/archive/ntttechnical.php?contents=ntr201910fa5.html

[9] K. Tateno and K. Kumakura, "Crystal Growth of Wurtzite GaP Nanowires for Solar-water-splitting Devices," NTT Technical

Review, Vol. 17, No. 10, pp. 36–41, 2019.
https://www.ntt-review.jp/archive/ntttechnical.php?contents=ntr201910fa7.html
[10] H. Yamamoto, Y. Krockenberger, and M. Naito, "Augmented Methods for Growth and Development of Novel Multi-cation Oxides," Proc. of SPIE OPTO, Vol.8987, 89870V, San Francisco, CA, USA, Feb. 2014.
[11] K. Hirama, Y. Taniyasu, S. Karimoto, H. Yamamoto, and K. Kumakura, "Heteroepitaxial Growth of Single-domain Cubic Boron Nitride Films by Ion-beam-assisted MBE," Appl. Phys. Express, Vol. 10, No. 3, 035501/1-4, 2017.
[12] H. Yamamoto, Y. Krockenberger, and M. Naito, "Epitaxial Growth of Superconducting Oxides," Epitaxial Growth of Complex Metal Oxides, pp. 95–127, Woodhead Publishing, Cambridge, 2015.
[13] M. Naito, Y. Krockenberger, A. Ikeda, and H. Yamamoto, "Reassessment of the Electronic State, Magnetism, and Superconductivity in high-T_c Cuprates with the Nd_2CuO_4 Structure," Physica C, Vol. 523, pp. 28–54, 2016.
[14] Y. K. Wakabayashi, Y. Krockenberger, N. Tsujimoto, T. Boykin, S. Tsuneyuki, Y. Taniyasu, and H. Yamamoto, "Ferromagnetism above 1000 K in a Highly Cation-ordered Double-perovskite Insulator Sr_3OsO_6," Nat. Commun, Vol. 10, 535, 2019.
[15] Y. Taniyasu and M. Kasu, "Improved Emission Efficiency of 210-nm Deep-ultraviolet Aluminum Nitride Light-emitting Diode," NTT Technical Review, Vol. 8, No. 8, 2010.
https://www.ntt-review.jp/archive/ntttechnical.php?contents=ntr201008sf2.html
[16] I. Yokohama, "Materials Research Activities," NTT Technical Review, Vol. 8, No. 8, 2010.
https://www.ntt-review.jp/archive/ntttechnical.php?contents=ntr201008sf1.html
[17] C. M. Christensen, "The Innovator's Dilemma: When New Technologies Cause Great Firms to Fail," Harvard Business Review Press, Boston, 1997.
[18] T. Lookman, F. J. Alexander, and K. Rajan, "Information Science for Materials Discovery and Design," Springer, Cham, 2016.

Hideki Yamamoto
Senior Research Scientist, Supervisor, Executive Manager of Materials Science Laboratory, NTT Basic Research Laboratories.
He received a B.S., M.S., and Ph.D. in chemistry from the University of Tokyo in 1990, 1992, and 1995. He joined NTT in 1995. His principal research fields are thin film growth, surface science, and superconductivity. He was a visiting scholar at the Geballe Laboratory for Advanced Materials, Stanford University, USA (2004–2005). He received the 2nd Young Scientist Presentation Award (1997) from the Japan Society of Applied Physics (JSAP) and the 20th Superconductivity Science and Technology Award (2017) from the Forum of Superconductivity Science and Technology, the Society of Non-traditional Technology. He is a member of JSAP, the Physical Society of Japan, the Japan Society of Vacuum and Surface Science, the American Physical Society, and the Materials Research Society.

Hideki Gotoh
Director, NTT Basic Research Laboratories; Executive Manager of Optical Science Laboratory, NTT Basic Research Laboratories.
He received a B.S., M.S., and Ph.D. in engineering from Hiroshima University in 1991, 1993, and 2000. Since joining NTT Basic Research Laboratories in 1993, he has been working on optical physics and device applications of semiconductor nanostructures. He was a visiting scientist at the University of Illinois at Urbana-Champaign in 2006. He is a member of JSAP and the Optical Society.

Creation of Novel Material Sr_3OsO_6 with the Highest Ferromagnetic Transition Temperature among Insulators

Yuki K. Wakabayashi, Yoshiharu Krockenberger, Yoshitaka Taniyasu, and Hideki Yamamoto

Abstract

We have synthesized a novel material, Sr_3OsO_6 (Sr: strontium, Os: osmium, O: oxygen) using a unique oxide thin-film growth technique that has been developed over many years at NTT Basic Research Laboratories. The Curie temperature (T_C) value of this material, estimated from the magnetic measurements, is above 780°C, surpassing the T_C record among insulators for the first time in 88 years by more than 100°C. As Sr_3OsO_6 has been synthesized in a single-crystalline thin film form, this brand-new material is expected to be readily implemented in high-performance magnetic device applications such as magnetoresistive random access memories and magnetic sensors that work above room temperature.

Keywords: molecular beam epitaxy, magnetic oxide, spin-orbit coupling

1. Introduction

Ferromagnetism is a magnetic state in a material that gives it the properties of a magnet. In the ferromagnetic state, the net magnetic moment is large since the magnetic moments of the constituent atoms are aligned (**Fig. 1**). A ferromagnetic insulator is a magnet in which electric current cannot flow due to its high resistivity. Ferromagnetic insulators include maghemite, the first magnet that humans discovered and used as a compass. Today, ferromagnetic insulators are widely used as permanent magnets and in the microwave devices incorporated into, for instance, smartphones, cars, and computers—and such technology could not have been developed without ferromagnetic insulators. Spintronic devices, in which both the electrical and magnetic properties of electrons are utilized simultaneously, are now being extensively investigated to achieve high-speed devices with low power consumption. Ferromagnetic insulators will also serve as essential constituents that make such spintronic devices viable.

In conjunction with trends in computerization, there has been a steadily growing demand for practical devices with higher performance. In terms of temperature, stable operation even above 200°C is required. However, the record Curie temperature (T_C), which is the crucial factor determining the temperature range in which any ferri/ferromagnetic system remains stable, has stood in insulators ever since ferrite magnets[*1] were first developed over eight decades ago in the 1930s. Therefore, researchers have sought to develop the next generation of ferromagnetic insulators with high T_C values as well as to establish guiding principles to search for such materials.

*1 Ferrite magnets: Ferrite magnets are ferromagnetic insulators developed in the 1930s in Japan. They have been the most widely used magnets in the world. The major components are iron oxides, and many ferrite magnets also contain Co (cobalt), Ni (nickel), Mn (manganese), and other elements.

Fig. 1. Schematic diagram of ferromagnetism and paramagnetism.

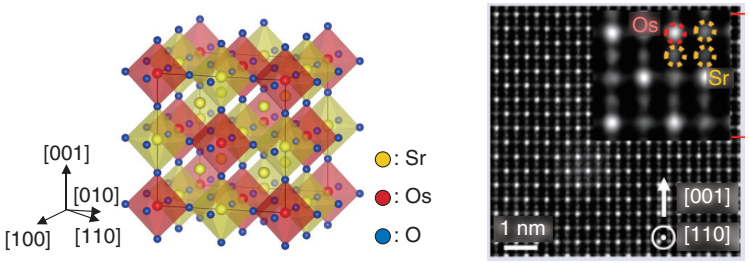

(a) Schematic diagram
O: oxygen, Os: osmium, Sr: strontium

(b) Microscopy image

Fig. 2. Crystal structure of Sr_3OsO_6 (double perovskite).

2. Preparation of high-quality Sr_3OsO_6 thin films

Solids in which atoms are periodically and orderly arranged and thus form lattices are called crystals. Crystals that have only a single atomic arrangement over an entire volume are known as single crystals. Samples whose thicknesses range from one atomic layer to about several tens of micrometers (1 μm = 1×10^{-6} m) are called thin films. Single-crystalline thin films are synthesized on single-crystalline substrates. For microfabrication of high-performance devices, it is necessary to prepare samples in the form of single-crystalline thin films with submicrometer thicknesses. In this study, single-crystalline Sr_3OsO_6 thin films with a thickness of 300 nm (1 nm = 1×10^{-9} m) were synthesized on single-crystalline $SrTiO_3$ (strontium titanate) substrates [1].

A schematic diagram of the double perovskite structure of Sr_3OsO_6 is shown in **Fig. 2(a)**. The yellow, red, and blue spheres respectively indicate Sr (strontium), Os (osmium), and O (oxygen) atoms. Sr_3OsO_6 is a novel material synthesized in this study for the first time. In crystals, atoms are regularly ordered and form lattices. There are many kinds of atomic arrangements (crystal structures), and representative ones have specific names. One such arrangement is known as double perovskite, in which the lattice is twice as large as the perovskite structure. Many complex oxides are known to have the perovskite structure. Iodides and chlorides that have the perovskite structure have also been extensively studied recently to develop the next generation of solar cells [2].

To grow high-quality Sr_3OsO_6 thin films, precise control of the flux rate of each constituent cation (Sr, Os) is mandatory. Generally, controlling the flux of Os is a challenge because of its high melting point (3033°C). Nevertheless, we have succeeded in precisely controlling both the Sr and Os flux rates. We accomplished this by monitoring the flux rates with an atomic emission spectrometer and feeding them back to the evaporation source power supplies in real time, which enabled the synthesis of Sr_3OsO_6 thin films with the Sr and Os atoms arranged in a highly ordered structure. An atomic resolution microscopy (scanning transmission electron microscopy) image of an Sr_3OsO_6 film viewed along the [110] direction

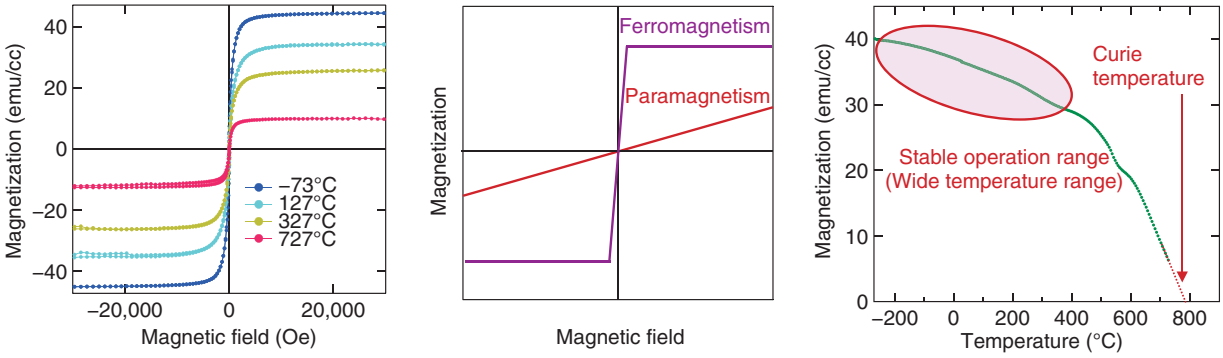

(a) Magnetization versus magnetic field

(b) Schematic diagram of ferromagnetism

(c) Magnetization versus temperature

Fig. 3. Magnetic properties of Sr_3OsO_6.

is shown in **Fig. 2(b)**. We can clearly see the atomic ordering depicted in Fig. 2(a).

3. Ferromagnetism above 780°C in Sr_3OsO_6

As described above, we have synthesized the novel material Sr_3OsO_6 having the highest T_C among insulators by using a unique oxide thin-film growth technique that we have developed over many years. First, we measured the electrical and optical properties of the Sr_3OsO_6 thin films. The resistivity at room temperature was 75 Ω·cm, which is about 10^9 times as large as typical metals such as Au (gold) and Cu (copper). Also, resistivity increased exponentially as the temperature decreased. Furthermore, the optical band gap of Sr_3OsO_6 was found to be about 2.65 eV. All these results indicate that Sr_3OsO_6 is an insulator.

Next, we examined magnetic properties. The magnetization versus applied magnetic field curves of an Sr_3OsO_6 film is shown in **Fig. 3(a)**. It shows ferromagnetic behavior (**Fig. 3(b)**) with a finite magnetization even at the high temperature of 727°C. The magnetization versus temperature curve of an Sr_3OsO_6 film is shown in **Fig. 3(c)**. The applied magnetic field was 2000 Oe. The gradual change in the magnetization up to about 400°C is suitable for high-performance magnetic devices that can be stably operated at high temperatures (above room temperature). The T_C value, at which ferromagnetism disappears, is above 780°C, surpassing the T_C record among insulators for the first time in 88 years by more than 100°C.

In addition to the experiments, density functional theory[*2] calculations were carried out by the Tsuneyuki Research Group at the University of Tokyo. These calculations revealed that the ferromagnetic insulating state of Sr_3OsO_6 originates from the large spin-orbit coupling of the 5*d* element Os. The spin-orbit coupling consists of interactions between the spin magnetic moment coming from the axial rotation of electrons and the orbital magnetic moment coming from the revolution of the charged particles (electrons) around the nucleus (**Fig. 4**). The elements in the lower rows of the periodic table are heavier than those in the higher rows, and they have a larger spin-orbit coupling. Thus, the spin-orbit coupling in Os is larger than in Fe (iron) and Co (cobalt), which are used in typical magnets. This insight into the mechanism of the emergent high-temperature ferromagnetism will open a new avenue for developing functional materials in which elements having large spin-orbit coupling play a role.

This novel material Sr_3OsO_6 has been synthesized in the form of single-crystalline thin films, which have high compatibility with device fabrication processes. This is in marked contrast to typical new oxides often synthesized in a powder or sintered polycrystalline form. Thus, Sr_3OsO_6 is expected to be readily implemented in high-performance magnetic device applications such as magnetoresistive random

*2 Density functional theory: This theory states that the energies of electrons in solids can be determined by using spatially dependent electron density $n(r)$. The word *functional*, which means the function of another function, is used since the energy is calculated as a function of $n(r)$, which is already a function of r. The electronic states of materials can be calculated and predicted from the fundamental equation that electrons follow based on this theory, without experimental data.

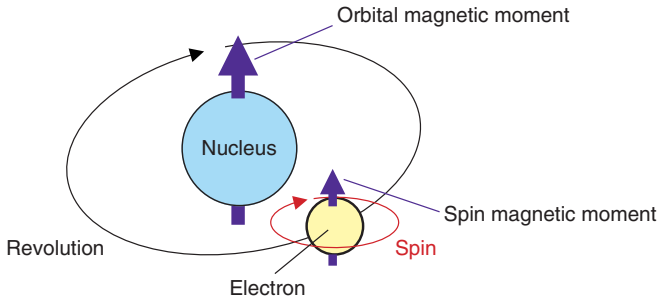

Fig. 4. Spin-orbit coupling.

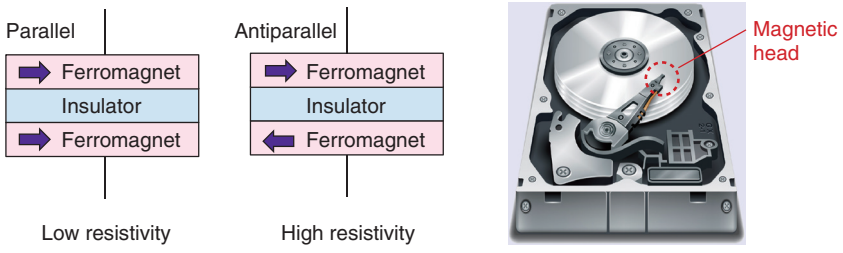

(a) Tunnel magnetoresistance effect

(b) Magnetic head of hard disc drives

Fig. 5. Tunnel magnetoresistance and its application.

access memories (MRAMs) and magnetic sensors that work above room temperature.

4. Future outlook

In our quest to better understand the fundamentals of ferromagnetism, we will further investigate the electronic structures of Sr_3OsO_6 using advanced spectroscopy techniques provided by synchrotron radiation facilities.*3 As part of efforts to develop high-performance magnetic devices that can be operated at high temperatures, we are working on fabricating some test devices using Sr_3OsO_6 to examine the tunnel magnetoresistance effect. This effect occurs when the tunnel resistance of an insulator sandwiched between two ferromagnets changes depending on the magnetic configuration of the ferromagnets (parallel or antiparallel) (**Fig. 5(a)**). The tunnel magnetoresistance effect has been widely utilized in commercial devices such as hard disc drives (**Fig. 5(b)**), MRAMs, and magnetic sensors. Therefore, demonstration of the tunnel magnetoresistance effect in Sr_3OsO_6 will lead to progress in developing high-performance magnetic devices that work at high temperatures.

References

[1] Y. K. Wakabayashi, Y. Krockenberger, N. Tsujimoto, T. Boykin, S. Tsuneyuki, Y. Taniyasu, and H. Yamamoto, "Ferromagnetism above 1000 K in a Highly Cation-ordered Double-perovskite Insulator Sr_3OsO_6," Nat. Commun., Vol. 10, 535, 2019.

[2] M. Liu, M. B. Johnston, and H. J. Snaith, "Efficient Planar Heterojunction Perovskite Solar Cells by Vapour Deposition," Nature, Vol. 501, pp. 395–398, 2013.

*3 Synchrotron radiation facilities: In synchrotron radiation facilities, we can use light with various wavelengths (synchrotron radiation) such as ultraviolet rays and X-rays. Synchrotron radiation is emitted from accelerated electrons that travel in a huge ring in an ultrahigh-vacuum environment. The versatile capabilities of such synchrotron facilities include emissions of intense and variable-wavelength light, and this enables us to perform many kinds of high-resolution spectroscopy to investigate the physical properties of specimens in detail. Therefore, synchrotron radiation facilities are also very useful for materials science research. In Japan, there are several synchrotron facilities in operation, including SPring-8 in Hyogo Prefecture and the Photon Factory in Ibaraki Prefecture.

Yuki K. Wakabayashi
Researcher, NTT Basic Research Laboratories.

He received a B.S. in solid-state physics from Osaka University in 2012, and an M.S. and Ph.D. in electrical engineering from the University of Tokyo in 2014 and 2017. Since joining NTT in 2017, he has been conducting research on thin film growth of ferromagnetic oxides. He received the English Presentation Award by the Spintronics Committee of the Japan Society of Applied Physics (JSAP) at the 62nd Spring Meeting of JSAP in 2015, the Young Researcher Best Poster Award at the 9th International Conference on Physics and Applications of Spin-Related Phenomena in Solids in 2016, and the 45th JSAP Presentation Award at the 66th Spring Meeting of JSAP in 2019.

Yoshiharu Krockenberger
Senior Researcher, Low-Dimensional Nanomaterials Research Group, NTT Basic Research Laboratories.

He received a diploma in physics from the Technical University of Munich in 2002 and a Ph.D. in physics from the Darmstadt University of Technology, Germany, in 2006. His principal research areas are superconductivity, strongly correlated electron systems, and thin film growth. He has been working at NTT since 2010. He also worked as a research scientist at RIKEN, Advanced Science Institutes, in the cross-correlated materials research group of Prof. Y. Tokura (2006–2010).

Yoshitaka Taniyasu
Senior Researcher, Group Leader of Low-Dimensional Nanomaterials Research Group, NTT Basic Research Laboratories.

He received a B.E., M.S., and Dr. Eng. in electrical engineering from Chiba University in 1996, 1998, and 2001. He joined NTT Basic Research Laboratories in 2001. He has been engaged in wide-bandgap semiconductor research. He received the Young Scientist Award at the 2007 Semiconducting and Insulating Materials Conference, the Young Scientist Award of the International Symposium on Compound Semiconductors 2011, the Commendation for Science and Technology by the Minister of Education, Culture, Sports, Science and Technology of Japan (the Young Scientists' Prize) in 2011, and the Japan Society for the Promotion of Science Prize in 2019.

Hideki Yamamoto
Senior Research Scientist, Supervisor, Executive Manager of Materials Science Laboratory, NTT Basic Research Laboratories.

He received a B.S., M.S., and Ph.D. in chemistry from the University of Tokyo in 1990, 1992, and 1995. He joined NTT in 1995. His principal research fields are thin film growth, surface science, and superconductivity. He was a visiting scholar at the Geballe Laboratory for Advanced Materials, Stanford University, USA (2004–2005). He received the 2nd Young Scientist Presentation Award (1997) from JSAP and the 20th Superconductivity Science and Technology Award (2017) from the Forum of Superconductivity Science and Technology, the Society of Non-traditional Technology. He is a member of JSAP, the Physical Society of Japan, the Japan Society of Vacuum and Surface Science, the American Physical Society, and the Materials Research Society.

Magnetically Purified Erbium-doped Oxide Crystal—Towards Creating a Quantum-information-manipulation Platform

Takehiko Tawara and Tomohiro Inaba

Abstract

Erbium (Er) is a rare-earth element that is expected to be a platform for manipulation of quantum information by utilizing telecommunication-wavelength photons. However, high-quality epitaxial growth of Er-doped host crystals is difficult, and the memory time of quantum information, which determines the performance of quantum manipulation, is much shorter than theoretically predicted. We investigated a good-compatibility rare-earth oxide as a host crystal for Er. The host oxide crystal, cerium oxide (CeO_2), had its nuclear spin removed (i.e., magnetically purified). The nuclear spin is the main factor that shortens the lifetime of quantum-information retention time. In this article, we describe high-quality epitaxial growth of CeO_2 and its optical properties as a thin film grown on a silicon substrate.

Keywords: rare-earth oxide, erbium, molecular beam epitaxy

1. Erbium-doped oxide and its application as a quantum-state-manipulation platform

It has long been known that adding rare-earth atoms to uniform solid crystals forms a determinative, discrete, and less-fluctuating ideal energy quantum level that is robust against changes in the external environment such as differences in host materials and temperature. This is because rare-earth atoms have a unique electron configuration; that is, their 4*f* electron orbit is electrically shielded from the outside world. In recent years, researchers have been actively studying the application of such superior quantum levels of rare-earth atoms as the platforms of quantum-information-manipulation devices (especially photon memories) used in quantum-information communication.

Quantum-information manipulation is defined as follows: photons responsible for the transmission of quantum information are transferred to electrons in a material, some operations are added to the electron state, and the photons are re-emitted as photons carrying that information. At that time, the electronic state (quantum level) of the material to which the information is transferred must have a slight fluctuation in energy (so that a long time is taken to lose any quantum information). A rare-earth atom is outstanding as an element that meets this requirement. Of the rare-earth elements, only erbium (Er) can interact with the optical-telecommunication photons (i.e., those having a wavelength of 1.55 μm). Accordingly, Er-doped crystals are promising as a platform for quantum-information-manipulation devices in quantum optical communication using existing optical-fiber networks [1].

The question that arises is what kind of Er-doped crystals are specifically required. First, Er needs to be added in a *diluted* manner. That is because if the distance between the doped Er atoms is too close, energy (i.e., quantum information) will be exchanged between the Er atoms, and the information will be lost instantaneously [2]. The distance between Er

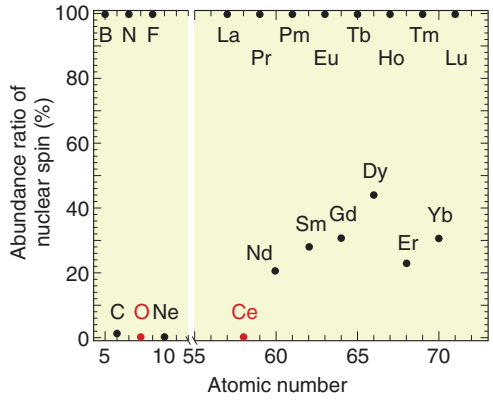

B: boron, C: carbon, Ce: cerium, Dy: dysprosium, Er: erbium, Eu: europium, F: fluorine, Gd: gadolinium, Ho: holmium, La: lanthanum, Lu: lutetium, N: nitrogen, Nd: neodymium, Ne: neon, O: oxygen, Pm: promethium, Pr: praseodymium, Sm: samarium, Tb: terbium, Tm: thulium, Yb: Ytterbium

Fig. 1. Natural abundance ratio of isotopes with nuclear spin of different atoms.

atoms must therefore be sufficient so that the atoms are separated (diluted). Moreover, the host crystal to which Er is added strongly influences the quantum level characteristics of Er, particularly the degree of fluctuation of quantum levels. For example, when each atom that composes the host crystal has nuclear spin, large magnetic fluctuation occurs, and the quantum level fluctuation becomes large. This fluctuation is also a factor contributing to losing quantum information in a short time.

For more efficient manipulation of quantum information, it is necessary to strongly confine the light in the host crystal and enhance its interaction with Er. Technology for fabricating optical circuits (e.g., optical resonators, waveguides, and multiplexing/demultiplexing devices) used in silicon (Si) photonics is useful to achieve this. It is therefore desirable to form the host crystal as a thin film on a Si substrate.

Some rare-earth oxides are candidate materials that can be grown as thin films on a Si substrate with less magnetic fluctuation. The crystal structure of a rare-earth oxide is similar to that of Si, and its lattice constant is exactly twice that of Si. This indicates that epitaxial growth of such an oxide on a Si substrate is possible. Among the many rare-earth atoms, only cerium (Ce) has no nuclear spin (**Fig. 1**). Thus, Ce has excellent characteristics; namely, it has no magnetic fluctuation and does not affect the quantum state of Er.

Incidentally, since the natural abundance ratio of isotopes with nuclear spin is very small for oxygen, cerium oxide (CeO_2) is the most promising candidate for an Er-doped host crystal on a Si substrate. However, although CeO_2 has been studied as a polishing agent, reduction catalyst, and other purposes [3], there are no published research examples of it being used as an Er-doped host crystal—as the basis of a quantum-information manipulation platform—or as an epitaxial-crystal thin film on a Si substrate.

2. Crystal growth of Er-doped CeO_2 thin films

An Er-doped CeO_2 film was grown to a thickness of 30 nm at 640°C on a surface-cleaned Si (111) substrate by using molecular beam epitaxy [4]. The rare-earth materials used, high-purity (> 99.99%) Er and Ce metals, were oxidized with O^* (oxygen-atom radicals) to form a rare-earth oxide film. To obtain high-quality crystals of CeO_2 as a host matrix, it is necessary to adjust the supply ratio of Ce and O^* so that the formed thin film has a stoichiometric composition (in this case, a stoichiometry of Ce:O = 1:2). Crystal quality was therefore investigated by changing the amount of Ce supply under a constant O^* supply.

Reflection high-energy electron diffraction (RHEED) images after crystal growth are shown in **Fig. 2**. When the amount of Ce supplied is small and the oxidizing power is excessive (Fig. 2(a), (b)), the halo-like pattern (showing an amorphous state) is obtained, and when the amount of Ce supplied is large and the oxidizing power is insufficient (Fig. 2(d), (e)), ring-like patterns (showing a polycrystalline state) appear.

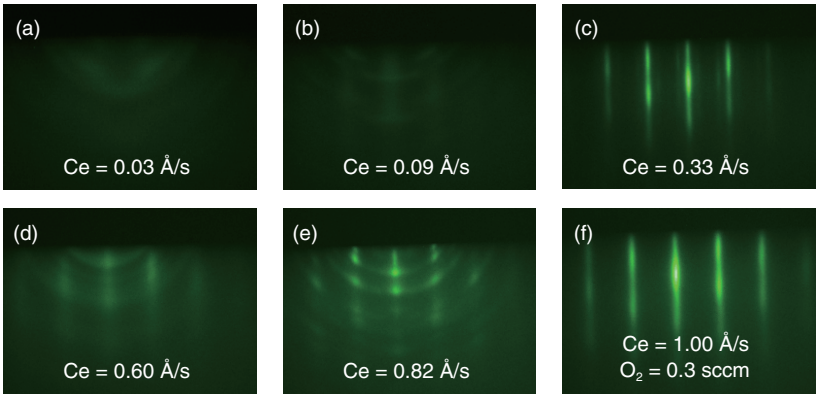

Sccm: standard cubic centimeters per minute

Fig. 2. RHEED images taken after crystal growth.

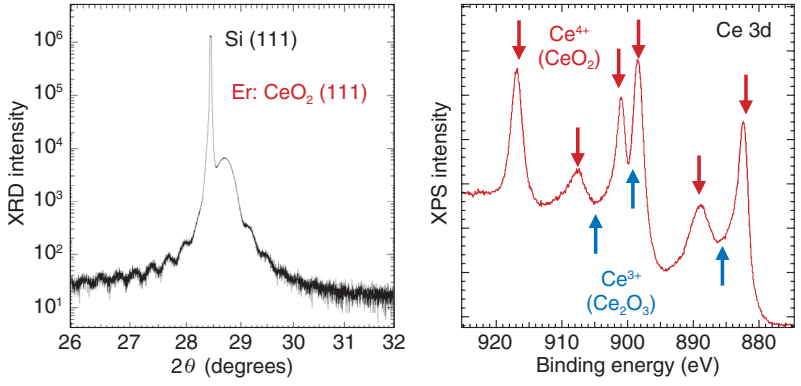

(a) XRD spectrum (b) XPS spectra of Ce 3d orbital

Fig. 3. Structural characteristics of CeO_2.

In contrast, in Fig. 2(c), a streak pattern (indicating a flat surface and single-crystal growth) is observed, and it can be seen that a thin film close to stoichiometry is formed by supplying that amount of Ce. It can also be seen that the streak pattern is maintained even when each supply amount is increased while the supply ratio of Ce to O^* is kept constant (Fig. 2(f)). Therefore, when Er is added as a dopant, it is possible to change the Er concentration while keeping the crystal quality constant by changing the crystal growth rate of the host CeO_2 crystal.

In addition to the cubic fluorite structure targeted in this study, CeO_2 has multiple crystal structures such as cubic bixbyite (Ce_2O_3) and hexagonal. Since the above-described RHEED images cannot distinguish these differences in crystal structure, the crystal structure was examined in more detail by using X-ray diffraction (XRD) spectroscopy and X-ray photoelectron spectroscopy (XPS).

The crystal lattice spacing estimated from the XRD spectrum shown in **Fig. 3(a)** is 3.11 Å, which corresponds to cubic CeO_2 and indicates that the hexagonal crystal structure does not exist. Moreover, from the spacing of the periodic satellite peaks observed when the crystal is grown uniformly at the atomic level, it is clear that the thickness of the grown CeO_2 film is 26.4 nm, which agrees fairly well with the assumed grown-film thickness. The charge states of the Ce atoms, estimated from the XPS spectra of the Ce 3d orbital shown in **Fig. 3(b)**, are all Ce^{4+} in the case of fluorite CeO_2, and Ce^{3+} does not exist in the case of bixbyite Ce_2O_3. The above results demonstrate

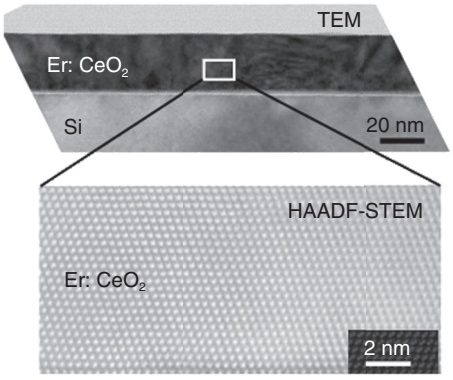

HAADF-STEM: high-angle annular dark-field scanning TEM

Fig. 4. Cross-sectional TEM image of grown Er-doped CeO_2.

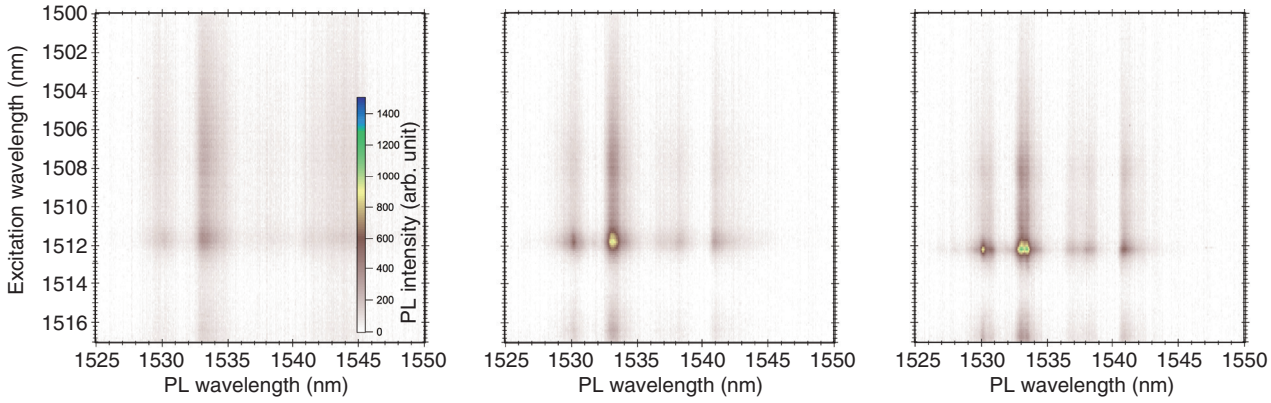

(a) Er concentration: 4% (b) Er concentration: 2% (c) Er concentration: 1%

Fig. 5. Color plot of dependence of PL on excitation wavelength.

that the grown CeO_2 thin film is the desired cubic fluorite CeO_2.

A cross-sectional TEM (transmission electron microscopy) image of the grown Er-doped CeO_2 is shown in **Fig. 4**. From this image, it can be seen that in addition to an extremely flat surface, a very high quality Er-doped CeO_2 thin-film crystal without crystal defects or different crystal-structure phases is obtained. It is thus concluded that a high-quality Er-doped CeO_2 thin film was epitaxially grown on a Si substrate for the first time.

3. Optical properties of Er-doped CeO_2 thin-film crystal

The optical properties of the high-quality Er-doped CeO_2 thin-film crystals were investigated. Color plots of the dependence of photoluminescence (PL) on excitation wavelength are shown in **Fig. 5**. In the PL measurement, energy is applied to a sample by irradiating the sample with a laser to excite electrons in the sample to a high-energy (excitation) state, and the light emitted when these excited electrons return to a low-energy state is observed. In this investigation, the Er concentration was changed from 4% (Fig. 5(a)) to 1% (Fig. 5(c)), and the PL measurement was performed at a temperature of 4K. It can be seen that for all Er-doping concentrations, sharp PL emission appears at a PL wavelength (horizontal axis) of 1533 nm against an excitation wavelength (vertical axis) of 1512 nm. This result indicates that the dopant Er atoms replace Ce sites in the parent CeO_2 crystal and

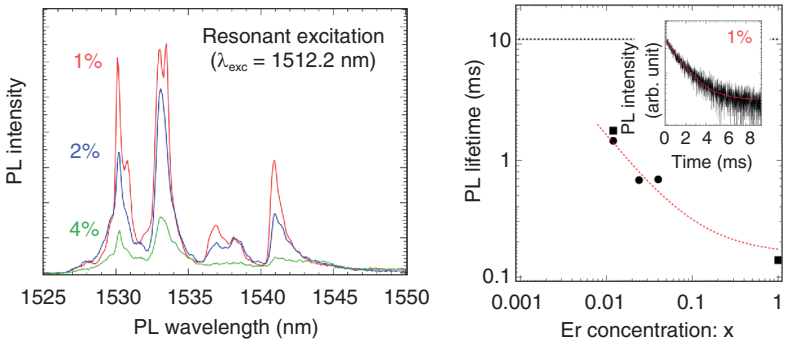

(a) PL spectrum (b) PL lifetime

Fig. 6. Dependence of PL spectrum and PL lifetime on Er-doping concentration.

are optically activated. In other words, in this Er-concentration range, Er atoms do not exist between crystal lattices, or they form Er clusters. Multiple PL emission peaks appear because the energy level of the doped Er is split due to the crystal field of the CeO_2 host.

This emission spectrum is compared in detail in **Fig. 6(a)**. For all Er concentrations, the emission peak appears at the same wavelength; at the same time, the emission intensity increases as Er concentration decreases. This result can be explained by the fact that as Er concentration decreases, the distance between the Er atoms increases, so the Er atoms become isolated in the host crystal. As a result, the non-emission process involving energy transfer by Er-Er atomic interaction is suppressed (and emission efficiency is enhanced).

This suppression of the non-radiative process by diluting the doped Er also changes the PL-emission lifetime. The dependence of PL-emission lifetime on Er concentration is shown in **Fig. 6(b)**. The PL-emission lifetime is measured by the intensity change of the emission from the sample appearing after the laser irradiation in the time domain (inset of Fig. 6(b)). It is clear from the figure that the PL-emission lifetime is extended as the Er concentration is reduced. The dotted line in the figure shows a PL-emission lifetime of about 11 ms when 0.001% of extremely dilute Er is added to a YSi_2O_5 host crystal (which has conventionally been used as a quantum optics crystal), and that value is considered to be the intrinsic PL-emission lifetime of Er in a solid; that is, the Er-Er atomic interaction can be ignored.

For the Er-doped CeO_2 used in this investigation, the minimum Er concentration was 1%. By lowering the Er concentration by another order of magnitude, it is expected that (i) the Er-Er interaction can be completely suppressed, and (ii) the Er atoms can be completely isolated in the solid. Also, in regard to the PL-emission characteristics, we observed the formation of a definite energy state, enhancement of PL-emission efficiency, and prolongation of PL-emission lifetime. In conclusion, Er-doped CeO_2 thin films with high quality in terms of both crystal structure and optical characteristics were successfully obtained.

4. Future development

It is expected that with the high-quality Er-doped CeO_2 thin film obtained in this investigation, the memory time of quantum information will be longer than that possible with a conventionally doped host crystal. We plan to fabricate an optical waveguide structure on a crystal surface in order to evaluate the quantum-information memory time and achieve on-chip manipulation of the quantum state by using telecom-band photons.

References

[1] T. Tawara, H. Omi, T. Hozumi, R. Kaji, S. Adachi, H. Gotoh, and T. Sogawa, "Population Dynamics in Epitaxial Er_2O_3 Thin Films Grown on Si(111)," Appl. Phys. Lett., Vol. 102, No. 24, 241918, 2013.
[2] T. Tawara, Y. Kawakami, H. Omi, R. Kaji, S. Adachi, and H. Gotoh, "Mechanism of Concentration Quenching in Epitaxial $(Er_xSc_{1-x})_2O_3$ Thin Layers," Opt. Mat. Express, Vol. 7, No. 3, pp. 1097–1104, 2017.
[3] E. J. Schelter, "Cerium under the Lens," Nat. Chem., Vol. 5, No. 4, p. 348, 2013.
[4] T. Inaba, T. Tawara, H. Omi, H. Yamamoto, and H. Gotoh, "Epitaxial Growth and Optical Properties of Er-doped CeO_2 on Si(111)," Opt. Mat. Express, Vol. 8, No. 9, pp. 2843–2849, 2018.

Takehiko Tawara
Senior Research Scientist, Supervisor, Quantum Optical Physics Research Group, Optical Science Laboratory, NTT Basic Research Laboratories and NTT Nanophotonics Center.

He received a B.S. in applied physics from Nihon University, Tokyo, in 1996 and an M.S. and Ph.D. in engineering from Hokkaido University in 1998 and 2001. He joined NTT Basic Research Laboratories in 2001. Since then, he has engaged in the study of semiconductor nanostructure fabrication and optical characterization of semiconductor quantum systems. He is a member of the Japan Society of Applied Physics (JSAP) and the Optical Society (OSA).

Tomohiro Inaba
Research Scientist, Quantum Optical Physics Research Group, Optical Science Laboratory, NTT Basic Research Laboratories.

He received a B.S., M.S., and Ph.D. in material science and engineering from Osaka University in 2013, 2015, and 2018. He joined NTT Basic Research Laboratories in 2018. His current research interests are thin film growth, fabrication technology, and optical properties. He is a member of JSAP.

MBE Growth and Element-distinctive Atomic-resolution Characterization of High Temperature Superconductors

Ai Ikeda, Yoshiharu Krockenberger, Yoshitaka Taniyasu, and Hideki Yamamoto

Abstract

Cuprate superconductors are in the material family that have the highest superconducting transition temperature (T_c) of ~130 K under ambient pressure. The infinite-layer structure is the essential building block of high-T_c cuprates with a T_c of over 100 K and is therefore vital to understand the mechanism of high-T_c superconductivity. While the infinite-layer phase is inaccessible using bulk single-crystal synthesis methods, we synthesized single-crystalline thin films of the infinite-layer cuprates using our unique oxide molecular beam epitaxy setup. To clarify the relationship between their microscopic crystal structures and electronic responses, we performed atomic-resolution electron microscopy measurements of the CuO_2 (copper peroxide) planes in the infinite-layer cuprates, the playground of high-T_c superconductivity.

Keywords: superconductivity, oxide molecular beam epitaxy, scanning transmission electron microscopy

1. Introduction

Superconductivity is a phenomenon in quantum materials that allows for lossless transportation of electrical current, and thus of energy and information. The quantum phenomenon, superconductivity, had been observed only below –140°C (~130 K) until very recent reports on hydrides, that is, sulfur hydride (H_3S) and lanthanum hydride (LaH_{10}). These materials show significantly higher superconducting transition temperatures (T_cs): –70°C (~200 K) for H_3S [1] and even close to room temperature for LaH_{10} [2]. Synthesizing these hydrides, however, requires extremely high pressure, specifically, ~2 million times higher (~200 GPa) than the atmospheric pressure. To make matters more complicated, their crystal structures are altered when the pressure is reduced after synthesis. In other words, the superconducting phases can exist only under an extremely high pressure comparable to that at the core of the Earth. Accordingly, practical applications using these hydrides remain elusive despite the significance of their discoveries from an academic point of view.

In contrast, cuprates are superconductors that exhibit the highest T_c under ambient pressure. Among them, $YBa_2Cu_3O_{7-\delta}$ (yttrium barium copper oxide) as well as $Bi_2Sr_2Ca_2Cu_3O_{10+\delta}$ (bismuth strontium calcium copper oxide), both of which show higher T_c (~90 K and ~110 K, respectively) than the boiling point of nitrogen (77 K), have already yielded practical applications as superconducting cables and microwave filters. However, the mechanism of high-T_c superconductivity in cuprates remains unclarified despite immense efforts for over three decades, which has been hampering the strategic search of novel superconducting materials with a higher T_c.

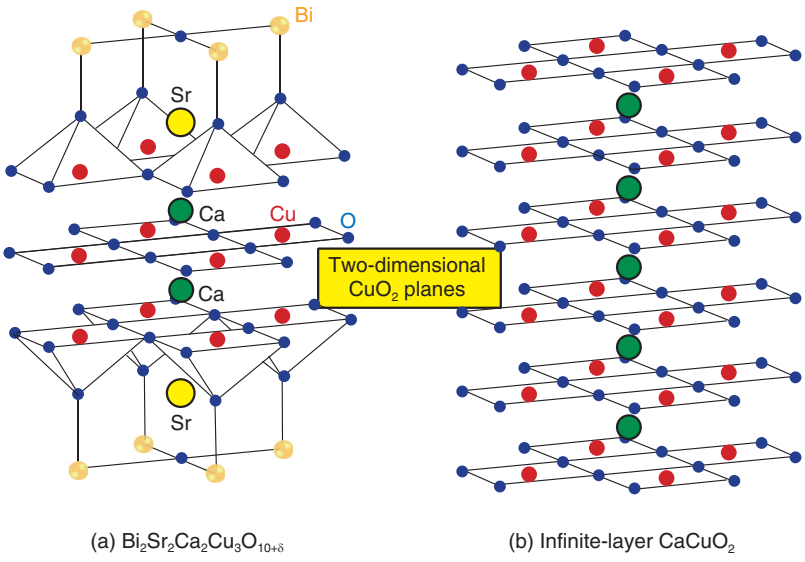

(a) $Bi_2Sr_2Ca_2Cu_3O_{10+\delta}$ (b) Infinite-layer $CaCuO_2$

Bi: bismuth, Ca: calcium, Cu: copper, O: oxygen, Sr: strontium

Fig. 1. Crystal structures of cuprate superconductors.

Nonetheless, the fundamental structural ingredient of high-T_c cuprates is fortunately well known: copper peroxide (CuO_2) planes, as exemplified by $Bi_2Sr_2Ca_2Cu_3O_{10+\delta}$ (**Fig. 1(a)**). Two-dimensional CuO_2 planes are made up of copper (Cu) and oxygen (O) and are separated by bismuth (Bi), strontium (Sr), calcium (Ca), and O. The formal valences of O and Cu are 2– and 2+, respectively, so the CuO_2 plane is not charge-neutral and cannot exist independently. Instead, the minimal structural unit that is compassable is charge-neutral calcium copper oxide ($CaCuO_2$) (**Fig. 1(b)**), which is commonly included in cuprates whose T_cs are above 100 K; the crystal structure shown in Fig. 1(b) is called an infinite-layer structure. That is why we have been focusing our research efforts on infinite-layer cuprates. Because the synthesis of bulk specimens of $CaCuO_2$ requires high pressure levels (3–5 GPa), single-crystalline $CaCuO_2$ specimens can be prepared exclusively by using thin-film growth methods, in our case, molecular beam epitaxy (MBE). Unlike the above-mentioned hydrides, the infinite-layer structure is stable at ambient pressure once it is formed.

2. Fabrication of ultrahigh-quality infinite-layer cuprate superconductors

While MBE has been widely used for the growth of semiconductors, we have extended it to the growth of complex transition metal oxides. Our customized MBE method is well equipped not only to synthesize novel complex transition metal oxides, for example, Sr_3OsO_6, a new ferromagnetic insulator with a Curie temperature > 1000 K [3], but also to push the limits of common crystal growth methods [4], and this is illustrated in **Fig. 2**. The vacuum recipient is 70 cm in diameter and 150 cm in height. A total of 10 metal sources are mounted at the bottom of the vacuum recipient where the elements can be evaporated by electron guns operated at 10 kV. The evaporant flux of each element is monitored and controlled by electron impact emission spectroscopy (EIES). The details of EIES are explained in another article in this issue [5].

Molecular oxygen (O_2) is insufficient for the growth of complex transition metal oxides, and therefore, the oxide MBE system is equipped with stronger oxidizing agents. This is distinct from conventional MBE. In this work, radio-frequency radical oxygen (O) was used for the growth of infinite-layer cuprates. Oxidation/reduction involves the gain/loss of electrons. Radical oxygen has two unpaired electrons and therefore a strong tendency to deprive the neighboring metal atoms of electrons. The absence of kinetic barriers in atomic oxygen is what drives the growth of complex transition metal oxides in an ultrahigh vacuum (~10^{-9} atm). In addition, the growth orientation is defined by the substrate; this phenomenon

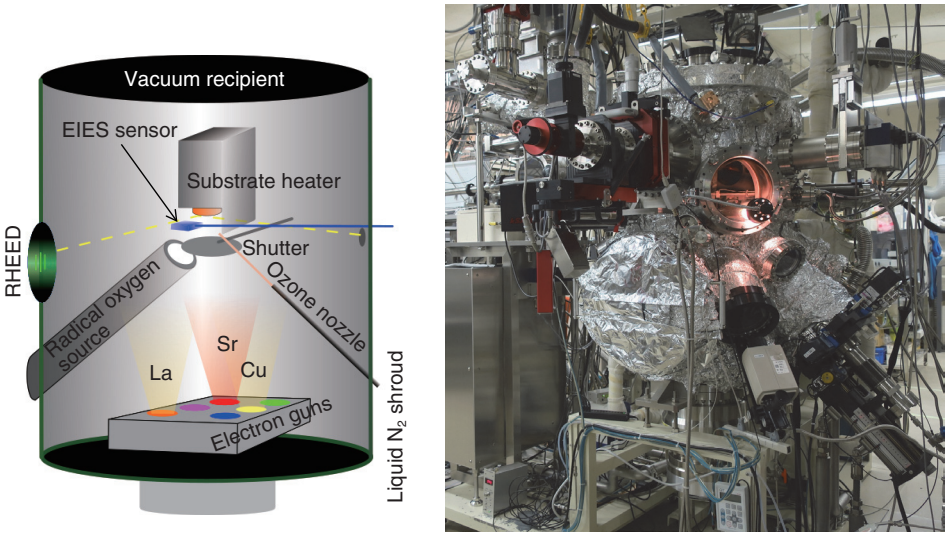

EIES: electron impact emission spectroscopy
La: lanthanum
N_2: nitrogen
RHEED: reflection high-energy electron diffraction

Fig. 2. Oxide MBE setup.

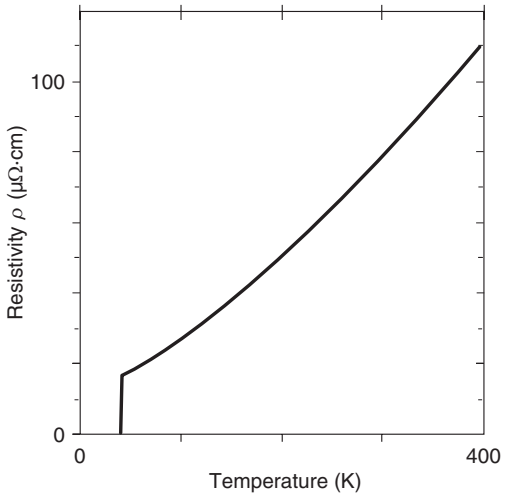

Fig. 3. Temperature dependence of resistivity for $Sr_{0.9}La_{0.1}CuO_2$ thin film.

is called *epitaxy* (in Greek, order on top). We used a single-crystal substrate with a lattice constant closer to one for infinite-layer cuprates. This mechanism enables the formation of single-crystalline infinite-layer cuprates.

We used the oxide MBE system to synthesize superconducting infinite-layer $Sr_{0.9}La_{0.1}CuO_2$ thin films [6–9]. In $Sr_{0.9}La_{0.1}CuO_2$, strontium ions (Sr^{2+} ions) are partially substituted with La^{3+} ions (lanthanum ions) to induce superconductivity. The dependence of resistivity on temperature for the $Sr_{0.9}La_{0.1}CuO_2$ thin film is plotted in **Fig. 3**. Resistivity decreases as the temperature decreases and abruptly goes to zero at 41 K. The films presented here are superior to those in other reports on superconducting infinite-layer thin films [10], as evidenced

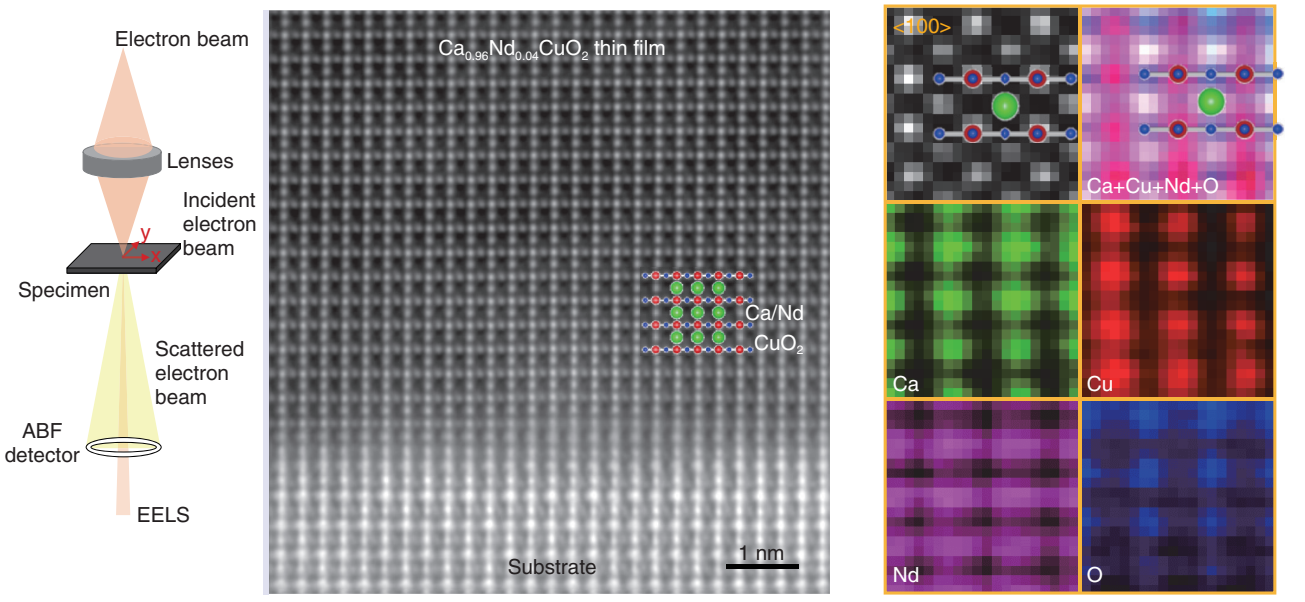

(a) STEM apparatus

(b) Atomic position of $Ca_{0.96}Nd_{0.04}CuO_2$ thin film by STEM

(c) Atomic column elemental mapping by EELS

ABF: annular bright field
Nd: neodymium

Fig. 4. Identification of superconducting state of infinite-layer $CaCuO_2$.

by the following characteristics:

- sharp superconducting transition (transition width $\Delta T_c < 1$ K)
- metal-like electronic response between 400 K and 42 K
- low resistivity value in normal state (corresponds to the intrinsic value for defect-free CuO_2 plane).

It is therefore shown that samples grown with our method are most suitable to reveal the inherent physical properties leading to understanding the mechanism of high-T_c superconductivity.

3. Infinite-layer $CaCuO_2$—elemental-resolved and atomic-resolution characterization

As already mentioned, $CaCuO_2$ is an essential structural part of high-T_c cuprates. In contrast to strontium copper oxide ($SrCuO_2$), however, little is known about the physical properties of infinite-layer $CaCuO_2$ due to the difficulty of synthesis. We synthesized infinite-layer $Ca_{1-x}Nd_xCuO_2$ thin films using MBE. In $Ca_{1-x}Nd_xCuO_2$, calcium ions (Ca^{2+} ions) are partially substituted with Nd^{3+} ions (neodymium ions) by mimicking $Sr_{0.9}La_{0.1}CuO_2$. For a composition of $x = 0.06$, we found traces of superconductivity around 10 K [11]. It is important to note that a truly superconducting state has not been established. Therefore, it is of significant importance to determine the differences between superconducting $Sr_{1-x}La_xCuO_2$ and non-superconducting $Ca_{1-x}Nd_xCuO_2$ by using scanning transmission electron microscopy (STEM) combined with electron energy loss spectroscopy (EELS).

STEM is used to visualize atomic positions in matter. The configuration of our STEM apparatus is shown in **Fig. 4(a)** [12]. Accelerated electrons at 200 kV are focused on a sample. The scattered electron beam contains information on the atomic position. This is shown in **Fig. 4(b)** for $Ca_{0.96}Nd_{0.04}CuO_2$. Because the contrast of the original bright-field image is inverted, the atomic positions appear bright in Fig. 4(b). The observed atomic column arrangements correspond to the infinite-layer structure with two-dimensional CuO_2 planes. It is evident that $Ca_{0.96}Nd_{0.04}CuO_2$ thin films are single crystalline. We used EELS to identify the constituent atomic species. This is shown in **Fig. 4(c)**. The atomic selectivity of EELS enables an atomic column identification that exactly matches the infinite-layer phase.

By measuring the distance between Cu and O

($d_{Cu\text{-}O}$) from Fig. 4(c), we determined the in-plane lattice constant of $Ca_{0.96}Nd_{0.04}CuO_2$ to be 0.386 nm. This is 0.001 nm longer than for $CaCuO_2$ [13]. Similar expansion is found for the $Sr_{0.9}La_{0.1}CuO_2$ system, where a substitution of 10% of La results in an expansion of 0.002 nm of the in-plane lattice constant [14]. It is intuitively suggested that a critical in-plane lattice constant ($d_{Cu\text{-}O}$ x 2) for the induction of superconductivity is to be expected. As the ionic size of Ca^{2+} ions is smaller than that of Sr^{2+} ions, $CaCuO_2$ has shorter $d_{Cu\text{-}O}$ than for $SrCuO_2$. During the course of our study, we found that a higher concentration of Nd causes instability of the infinite-layer phase. Consequently, it is not possible to prepare the infinite-layer phase of $Ca_{1\text{-}x}Nd_xCuO_2$ with a sufficient amount of Nd to induce a superconducting transition. This result suggests that lattice constant (the Cu-O bond length in the CuO_2 plane) engineering is important for the induction of superconductivity in cuprates.

4. Future outlook

Infinite-layer cuprates are very important to understand the physics of high-T_c superconductivity. We plan to apply our thin film growth method to further understand the mechanism of high-T_c superconductivity commonly emerging in materials containing $CaCuO_2$. This method is currently being extended to the synthesis of superlattices containing $CaCuO_2$ [15].

References

[1] A. P. Drozdov, M. I. Eremets, I. A. Troyan, V. Ksenofontov, and S. I. Shylin, "Conventional Superconductivity at 203 Kelvin at High Pressures in the Sulfur Hydride System," Nature, Vol. 525, No. 7567, pp. 73–76, 2015.

[2] M. Somayazulu, M. Ahart, A. K. Mishra, Z. M. Geballe, M. Baldini, Y. Meng, V. V. Struzhkin, and R. J. Hemley, "Evidence for Superconductivity above 260 K in Lanthanum Superhydride at Megabar Pressures," Phys. Rev. Lett., Vol. 122, No. 2, 027001, 2019.

[3] Y. K. Wakabayashi, Y. Krockenberger, N. Tsujimoto, T. Boykin, S. Tsuneyuki, Y. Taniyasu, and H. Yamamoto, "Ferromagnetism above 1000 K in a Highly Cation-ordered Double-perovskite Insulator Sr_3OsO_6," Nat. Commun., Vol. 10, No. 1, 535, 2019.

[4] H. Yamamoto, Y. Krockenberger, and M. Naito, "Multi-source MBE with High-precision Rate Control System as a Synthesis Method *sui generis* for Multi-cation Metal Oxides," Journal of Crystal Growth, Vol. 378, pp. 184–188, 2013.

[5] H. Yamamoto and H. Gotoh, "Overview of Novel Materials Creation Research at NTT," NTT Technical Review, Vol. 17, No. 10, pp. 1–6, 2019.
https://www.ntt-review.jp/archive/ntttechnical.php?contents=ntr201910fa1.html

[6] Y. Krockenberger, K. Sakuma, and H. Yamamoto, "Molecular Beam Epitaxy and Transport Properties of Infinite-layer $Sr_{0.90}La_{0.10}CuO_2$ Thin Films," Appl. Phys. Express, Vol. 5, No. 4, 043101, 2012.

[7] S. Karimoto and M. Naito, "Electron-doped Infinite-layer Thin Films with T_c over 40 K Grown on $DyScO_3$ Substrates," Appl. Phys. Lett., Vol. 84, No. 12, pp. 2136–2138, 2004.

[8] S. Karimoto, K. Ueda, M. Naito, and T. Imai, "Superconducting Thin Films of Electron-doped Infinite-layer $Sr_{1-x}La_xCuO_2$ Grown by Molecular Beam Epitaxy," Physica C Supercond., Vol. 378–381, Part 1, pp. 127–130, 2002.

[9] M. Naito, S. Karimoto, and A. Tsukada, "Epitaxy-stabilized *n*-type Superconducting Cuprates," Supercond. Sci. Technol., Vol. 15, No. 12, 1663, 2002.

[10] L. Maritato, A. Galdi, P. Orgiani, J. W. Harter, J. Schubert, K. M. Shen, and D. G. Schlom, "Layer-by-layer Shuttered Molecular-beam Epitaxial Growth of Superconducting $Sr_{1-x}La_xCuO_2$ Thin Films," J. Appl. Phys., Vol. 113, No. 5, 053911, 2013.

[11] A. Ikeda, Y. Krockenberger, and H. Yamamoto, "Molecular Beam Epitaxy of Electron-doped Infinite-layer $Ca_{1-x}R_xCuO_2$ Thin Films," Phys. Rev. Materials, Vol. 3, No. 6, 064803, 2019.

[12] S. J. Pennycook, C. Li, M. Li, C. Tang, E. Okunishi, M. Varela, Y.-M. Kim, and J. H. Jang, "Material Structure, Properties, and Dynamics through Scanning Transmission Electron Microscopy," J. Anal. Sci. Technol., Vol. 9, 11, 2018.

[13] Y. Krockenberger, A. Ikeda, K. Kumakura, and H. Yamamoto, "Infinite-layer Phase Formation in the $Ca_{1-x}Sr_xCuO_2$ System by Reactive Molecular Beam Epitaxy," J. Appl. Phys., Vol. 124, No. 7, 073905, 2018.

[14] N. Ikeda, Z. Hiroi, M. Azuma, M. Takano, Y. Bando, and Y. Takeda, "Synthesis and Superconducting Properties of the Infinite-layer Compounds $Sr_{1-x}Ln_xCuO_2$ (Ln = La, Nd, Sm, Gd)," Physica C Supercond., Vol. 210, No. 3–4, pp. 367–372, 1993.

[15] D. Di Castro, M. Salvato, A. Tebano, D. Innocenti, C. Aruta, W. Prellier, O. I. Lebedev, I. Ottaviani, N. B. Brookes, M. Minola, M. Moretti Sala, C. Mazzoli, P. G. Medaglia, G. Ghiringhelli, L. Braicovich, M. Cirillo, and G. Balestrino, "Occurrence of a High-temperature Superconducting Phase in $(CaCuO_2)_n/(SrTiO_3)_m$ Superlattices," Phys. Rev. B, Vol. 86, No. 13, 134524, 2012.

Ai Ikeda
Research Scientist, Low-Dimensional Nanomaterials Research Group, NTT Basic Research Laboratories.

She received a B.E., M.E., and Ph. D in applied physics from Tokyo University of Agriculture and Technology in 2010, 2012, and 2015. She joined NTT Basic Research Laboratories in 2015. She has been researching superconducting materials in order to push the limits of the variety of superconducting oxide materials available.

Yoshiharu Krockenberger
Senior Researcher, Low-Dimensional Nanomaterials Research Group, NTT Basic Research Laboratories.

He received a diploma in physics from the Technical University of Munich in 2002 and a Ph.D. in physics from Darmstadt University of Technology, Germany, in 2006. His principal research areas are superconductivity, strongly correlated electron systems, and thin film growth. He has been working at NTT since 2010. He also worked as a research scientist at RIKEN, Advanced Science Institute, in the cross-correlated materials research group of Prof. Y. Tokura (2006–2010).

Yoshitaka Taniyasu
Senior Researcher, Group Leader of Low-Dimensional Nanomaterials Research Group, NTT Basic Research Laboratories.

He received a B.E., M.S., and Dr. Eng. in electrical engineering from Chiba University in 1996, 1998, and 2001. He joined NTT Basic Research Laboratories in 2001. He has been engaged in wide-bandgap semiconductor research. He received the Young Scientist Award at the 2007 Semiconducting and Insulating Materials Conference, the Young Scientist Award of the International Symposium on Compound Semiconductors 2011, the Commendation for Science and Technology by the Minister of Education, Culture, Sports, Science and Technology of Japan (the Young Scientists' Prize) in 2011, and the Japan Society for the Promotion of Science Prize in 2019.

Hideki Yamamoto
Senior Research Scientist, Supervisor, Executive Manager of Materials Science Laboratory, NTT Basic Research Laboratories.

He received a B.S., M.S., and Ph.D. in chemistry from the University of Tokyo in 1990, 1992, and 1995. He joined NTT in 1995. His principal research fields are thin film growth, surface science, and superconductivity. He was a visiting scholar at the Geballe Laboratory for Advanced Materials, Stanford University, USA (2004–2005). He received the 2nd Young Scientist Presentation Award (1997) from the Japan Society of Applied Physics (JSAP) and the 20th Superconductivity Science and Technology Award (2017) from the Forum of Superconductivity Science and Technology, the Society of Non-traditional Technology. He is a member of JSAP, the Physical Society of Japan, the Japan Society of Vacuum and Surface Science, the American Physical Society, and the Materials Research Society.

High-quality Atomic-layer Materials Fabricated by Chemical Vapor Deposition

Shengnan Wang and Yoshitaka Taniyasu

Abstract

Atomic-layer materials such as graphene and hexagonal boron nitride (h-BN) are promising for their use in next-generation optoelectronic devices due to the novel and unique physical phenomena as well as superior material properties being demonstrated in such materials. Scalable fabrication methods for high-quality atomic-layer materials are essential for their industrial applications. We introduce here chemical vapor deposition growth for high-quality graphene and h-BN.

Keywords: atomic-layer materials, chemical vapor deposition, crystal orientation control

1. Atomic-layer materials

Atomic-layer materials have layered structures with a thickness of only one or a few atoms (**Fig. 1**). Graphene, a representative atomic-layer material, consists of a single layer of carbon (C) atoms arranged in a two-dimensional hexagonal lattice structure like a honeycomb, and is therefore an extremely thin material with a thickness of only one atom [1]. Graphene shows a semimetallic (or zero-gap semiconductor) character with a linearly dispersed energy band, which results in high carrier mobility (electrical conductivity) and large wavelength-independent light absorption in a wide range from infrared to visible light. Furthermore, graphene has the highest thermal conductivity and mechanical strength of any kind of material.

In addition to graphene, there are many kinds of atomic-layer materials including transition metal dichalcogenides (TMDs), MX_2 (where M is a transition metal atom such as Mo (molybdenum) or W (tungsten), and X is a chalcogen atom such as S (sulfur), Se (selenium), or Te (tellurium). Hexagonal boron nitride (h-BN) is another type of atomic-layer material. Monolayer TMDs consist of a single layer of transition metal atoms (M) sandwiched between two layers of chalcogen atoms (X); thus, the total thickness is three atoms. Some TMDs are semiconductors with bandgaps in the near-infrared to visible spectral region, and the bandgap energy varies with the number of stacked layers. TMDs have also unique properties such as spin- and valley-dependent electrical and optical properties.

The material h-BN is composed of boron (B) and nitrogen (N) and has a layered hexagonal lattice structure similar to graphene. h-BN is an insulator with a large band gap of about 6 eV and is therefore used as an insulating layer and a tunnel barrier in various types of devices made from atomic-layer materials.

There are numerous atomic-layer materials ranging from metallic, superconducting, magnetic, semiconducting, to dielectric or insulating depending on their chemical composition and crystal structure, which means they are promising for next-generation devices such as ultra-thin flexible, low-power-consumption, high-speed nanoelectronic, high-efficiency photonic, and high-sensitivity devices. Thus, the application of atomic-layer materials will lead to innovative information technology.

2. Fabrication of atomic-layer materials

Various fabrication methods for atomic-layer

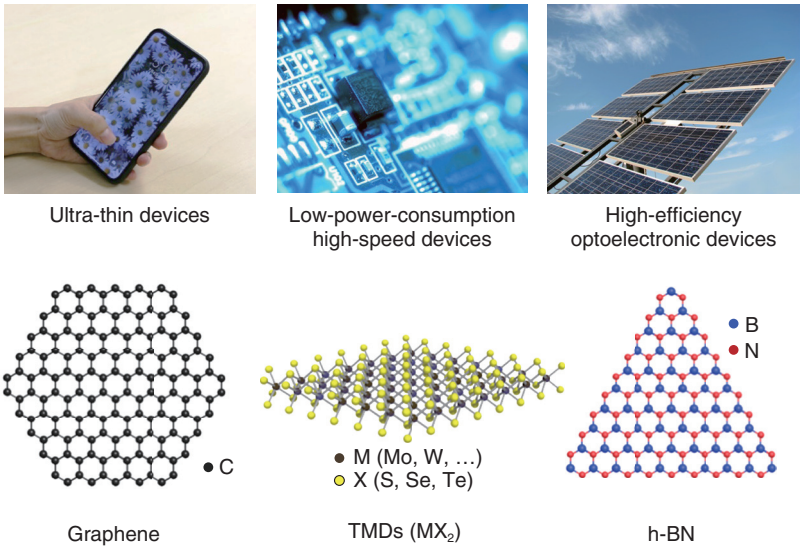

B: boron, C: carbon, N: nitrogen, Mo: molybdenum, W: tungsten, S: sulfur, Se: selenium, Te: tellurium
h-BN: hexagonal boron nitride
TMD: transition metal dichalcogenide

Fig. 1. Atomic-layer materials and their applications.

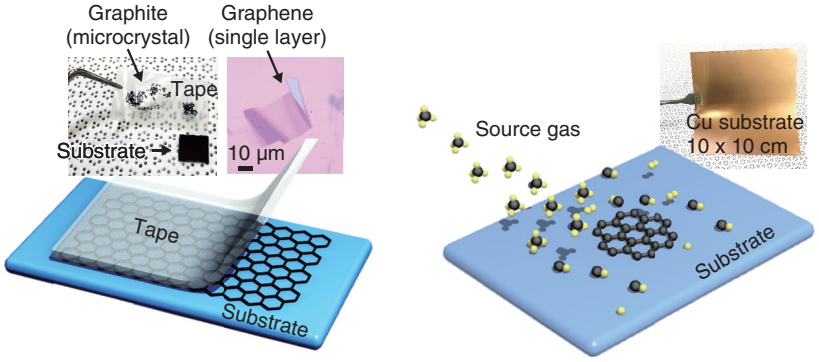

(a) Mechanical exfoliation and transfer

(b) CVD growth

Cu: copper

Fig. 2. Methods of fabricating atomic-layer materials.

materials including mechanical exfoliation and thin-film growth are proposed. In mechanical exfoliation, a monolayer flake is cleaved from a microcrystal by using adhesive tape and is transferred onto a substrate, as shown in **Fig. 2**. K. S. Novoselov and A. K. Geim, Nobel laureates in Physics in 2010, demonstrated mechanical exfoliation for graphene and showed new phenomena in quantum physics. Mechanical exfoliation has been used in fabricating atomic-layer materials in order to investigate their physical properties and to demonstrate new functional device applications. However, the size of the atomic-layer material obtained with this method is limited to the size of the microcrystals, typically about tens of micrometers (μm). This small size is not suitable for industrial applications.

Chemical vapor deposition (CVD) is a growth method for thin films on large-area wafers

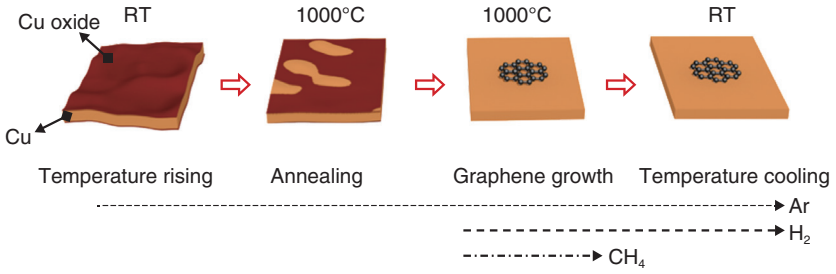

(a) CVD growth process

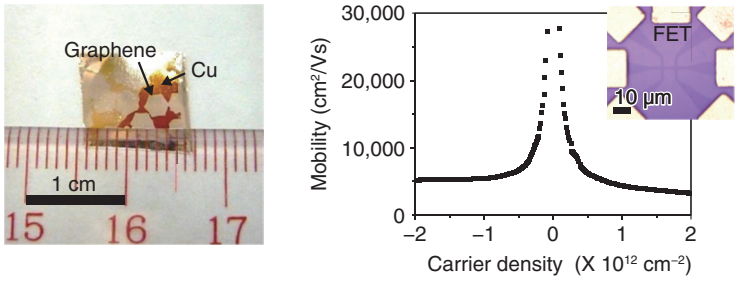

(b) Millimeter-size large graphene and its electrical property

Ar: argon, CH_4: methane, H_2: hydrogen
FET: field-effect transistor
RT: room temperature

Fig. 3. Large-size single-crystal graphene growth.

(substrates) via chemical reaction of gas sources. It is widely used in the semiconductor industry for mass production of thin films. CVD growth technology is currently under development all over the world for atomic-layer materials. Although CVD growth of atomic-layer materials on large-area substrates has been demonstrated, the crystal quality is low, mainly due to defects originating at the boundaries of randomly orientated domains. The domain size is as small as tens of micrometers, similar to that of mechanically exfoliated flakes. In this article, we introduce our CVD technology for large-area single-domain graphene and for crystal orientation control of h-BN.

3. Large-size single-crystal graphene growth

A schematic diagram of CVD growth of graphene on a copper (Cu) substrate is shown in **Fig. 3(a)**. The surface of as-received Cu is naturally oxidized. In a CVD reactor, the Cu substrate is heated to the growth temperature at ~1000°C and thermally annealed under argon (Ar) and/or hydrogen (H_2) flow to remove the natural oxide layer on the Cu surface. Then methane (CH_4) is introduced for graphene growth. When the growth starts, graphene domains (nuclei) form on the Cu surface. The domain size increases with growth time. Once the domains coalesce with nearby domains, the graphene covers the entire Cu surface. Note that the lower nucleation density results in a larger domain size. After the growth, CH_4 is shut off and the sample is cooled to room temperature.

The domain size can be controlled by the nucleation density, which depends on CVD growth conditions, the substrate material, and its surface condition. Regarding the surface conditions, the Cu oxide prevents the nucleation of graphene while graphene preferentially nucleates on the clean Cu surface without the oxide. In the thermal annealing of the substrate, the etching rate of the oxide layer depends on the ambient gas. For example, the etching rate of the Cu oxide under H_2 gas is higher than under Ar gas. To vary the coverage of the oxide layer for nucleation density control, we carried out thermal annealing of the Cu substrate under Ar gas alone and precisely

adjusted the annealing time as shown in Fig. 3(a). Consequently, we succeeded in fabricating a millimeter-size graphene single crystal that is about 100 times larger than conventional ones with domain sizes of approximately tens of micrometers [2] (**Fig. 3(b)**).

Next, we fabricated field-effect transistors in order to characterize the electrical properties of the graphene. The millimeter-size graphene showed nearly 10 times higher charge mobility than conventional CVD-grown ones. These results show that nucleation control by selective growth is a promising way to achieve large-area growth of high-quality graphene single crystals.

4. Crystal orientation control of h-BN

Similar to graphene, h-BN can be grown on Cu substrates by CVD. For h-BN growth, ammonia borane (H_6BN) was used as a BN source. The crystal orientation of thin-film materials generally depends on the surface structure and symmetry of the substrate. Cu has a face-centered cubic lattice structure. For example, on Cu (001), (101), and (111) planes, h-BN shows multiple orientations, that is, two or four orientations due to the crystal rotational symmetry mismatching between h-BN and Cu. The multiple orientations cause crystal defects formed at the boundaries of domains with different orientations (rotation angles).

The commercial Cu substrate is polycrystalline. During the thermal annealing process, the Cu substrate is recrystallized by heating. In recrystallization, polycrystalline grains coalesce and become large, and specific crystal planes of the grains appear on the substrate surface. We systematically investigated the crystal orientation of h-BN domains grown on more than 100 different Cu crystal planes. For h-BN grown on crystal planes inclined from a Cu (101) plane, as shown in the microscopic image (**Fig. 4(a)**), we found that all of the triangular h-BN domains are oriented to the same direction, indicating the formation of single-orientation h-BN [3].

We clarified the mechanisms of the single-orientation h-BN formation using theoretical calculations. In the case of a (101) plane, there are two energetically stable orientations for h-BN because the (101) plane has two-fold rotational symmetry. In contrast, for the inclined (101) plane, because the symmetry is broken, there is only one energetically stable orientation for h-BN, resulting in single-orientation h-BN formation. This mechanism is applicable to other atomic-layer materials.

To investigate the effect of the crystal orientation on the electrical properties, we measured the electrical resistance images of the multi- and single-orientation h-BN as shown in **Fig. 4(b)**. The single-orientation h-BN showed higher electrical resistance (darker contrast) than multi-orientation h-BN. This is because the single-orientation h-BN has lower defect density than multi-orientation h-BN.

Finally, we grew h-BN layers that fully covered the Cu substrate as shown in **Fig. 4(c)**. For the multi-orientation h-BN, multi-layer h-BN domains were partly formed on single-layer h-BN. In the case of the single-orientation h-BN on the other hand, no multi-layer h-BN domains were formed, and single-layer h-BN was uniformly formed on the entire Cu surface. Thus, the single-orientation control is essential to achieve high-quality atomic-layer materials.

5. Future prospects

CVD growth of heterostructures for a variety of atomic-layer materials is a challenging process to realize novel functional devices. Vertical heterostructures, in which atomic-layer materials are stacked, have demonstrated recently that material properties change greatly depending on the crystal orientation (rotation angle) of each layer. Furthermore, lateral heterostructures, in which different atomic-layer materials are atomically bonded in-plane, can lead to new physical phenomena originating from one-dimensional heterointerfaces and in-plane superlattice structures. We will continue to develop CVD growth technologies for high-quality heterostructures on large-area substrates for integrated functional devices.

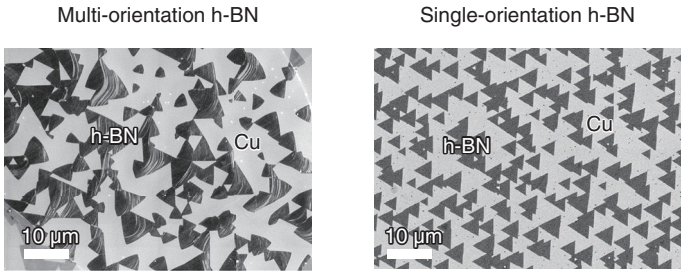

(a) Microscopic image of h-BN domains (partial coverage)

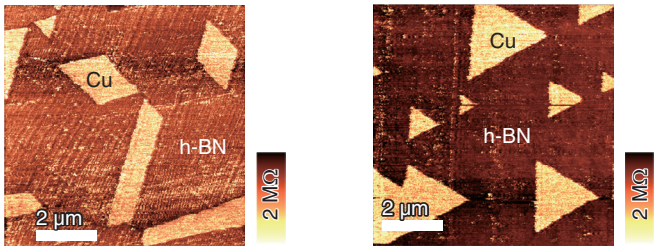

(b) Electrical resistance images

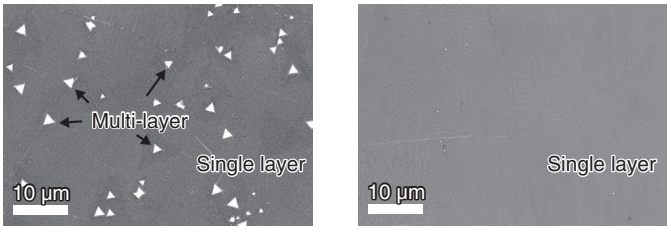

(c) Microscopic image of h-BN layers (full coverage)

Fig. 4. Crystal orientation control of h-BN.

References

[1] H. Hibino, "Graphene Research at NTT," NTT Technical Review, Vol. 11, No. 8, 2013. https://www.ntt-review.jp/archive/ntttechnical.php?contents=ntr201308fa1.html

[2] S. Wang, H. Hibino, S. Suzuki, and H. Yamamoto, "Atmospheric Pressure Chemical Vapor Deposition Growth of Millimeter-scale Single-crystalline Graphene on the Copper Surface with a Native Oxide Layer," Chem. Mat., Vol. 28, No. 14, pp. 4893–4900, 2016.

[3] S. Wang, A. E. Dearle, M. Maruyama, Y. Ogawa, S. Okada, H. Hibino, and Y. Taniyasu, "Catalyst-selective Growth of Single-orientation Hexagonal Boron Nitride toward High-performance Atomically Thin Electric Barriers," Adv. Mater., Vol. 31, 1900880, 2019.

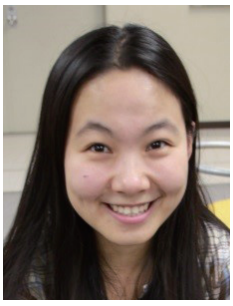

Shengnan Wang
Research Scientist, NTT Basic Research Laboratories.

She received a B.S. in light chemical engineering from East China University of Science and Technology, People's Republic of China, in 2007 and a Ph.D. in condensed matter physics from the National Center for Nanoscience and Technology, People's Republic of China, in 2012. She joined NTT Basic Research Laboratories in 2012 and has been conducting research on atomic-layer materials including graphene and h-BN. She received the Japan Society of Applied Physics (JSAP) Presentation Award at the 43rd Spring Meeting of JSAP in 2019.

Yoshitaka Taniyasu
Senior Researcher, Group Leader of Low-Dimensional Nanomaterials Research Group, NTT Basic Research Laboratories.

He received a B.E., M.S., and Dr. Eng. in electrical engineering from Chiba University in 1996, 1998, and 2001. He joined NTT Basic Research Laboratories in 2001. He has been engaged in wide-bandgap semiconductor research. He received the Young Scientist Award at the 2007 Semiconducting and Insulating Materials Conference, the Young Scientist Award of the International Symposium on Compound Semiconductors 2011, the Commendation for Science and Technology by the Minister of Education, Culture, Sports, Science and Technology of Japan (Young Scientists' Prize) in 2011, and the Japan Society for the Promotion of Science Prize in 2019.

Development of Next-generation Wide-bandgap Semiconductors

Kazuyuki Hirama, Yoshitaka Taniyasu, Hideki Yamamoto, and Kazuhide Kumakura

Abstract

Cubic boron nitride (c-BN) is a wide-bandgap semiconductor with the highest breakdown field among semiconductors. It has the potential to dramatically improve efficiency in power devices. Although c-BN is a metastable material, we have heteroepitaxially grown high-quality c-BN thin films by developing a unique growth technique. We have also used doping to control the electrical conductivity of the c-BN films. These accomplishments are major steps toward the fabrication of c-BN-based power devices.

Keywords: cubic boron nitride (c-BN), diamond, next-generation wide-bandgap semiconductors

1. Power device applications of wide-bandgap semiconductors

Wide-bandgap semiconductors are expected to serve as components of high-efficiency power devices, in which electrical power loss is significantly lower than in conventional semiconductor-based power devices. Here, silicon (Si) and gallium arsenide (GaAs) are typical conventional semiconductors. The main functions of power devices include regulation of direct current (DC) voltage, frequency conversion of alternating current (AC) voltage, and conversion between AC and DC. For example, in AC adapters used in personal computers and mobile phones, power devices convert the voltage from AC 100–200 V to DC ~20 V.

The relationship between power loss and operation voltage of power devices consisting of various semiconducting materials is shown in **Fig. 1**. Power loss is determined by the on-resistance of power devices; it becomes smaller with lower on-resistance. Increasing the carrier concentration and reducing the current-path length are both effective in reducing the on-resistance, and consequently the power loss.

Such conditions are more readily fulfilled when the breakdown field[*1] of the constituent semiconductor is higher. The high breakdown fields of wide-bandgap semiconductors, at least one order of magnitude

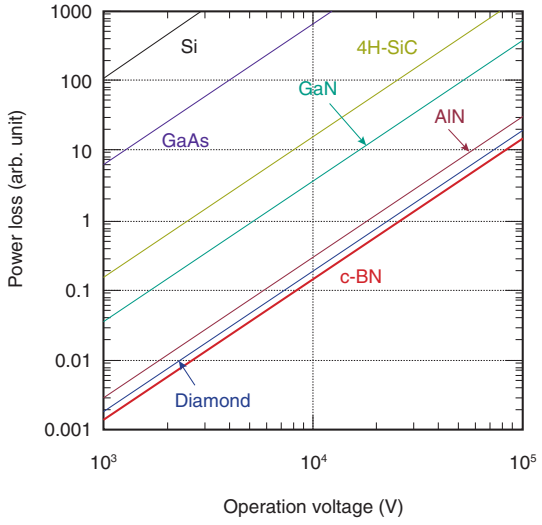

AlN: aluminum nitride, c-BN: cubic boron nitride, SiC: silicon carbide, GaN: gallium nitride

Fig. 1. Relationship between power loss and operation voltage.

*1 Breakdown field: When the electrical field is applied to an insulator or a semiconductor, the current drastically increases above a threshold value of the electrical field (i.e., the breakdown occurs). The threshold electrical field is defined as the breakdown field. Values of the inherent breakdown field vary by material.

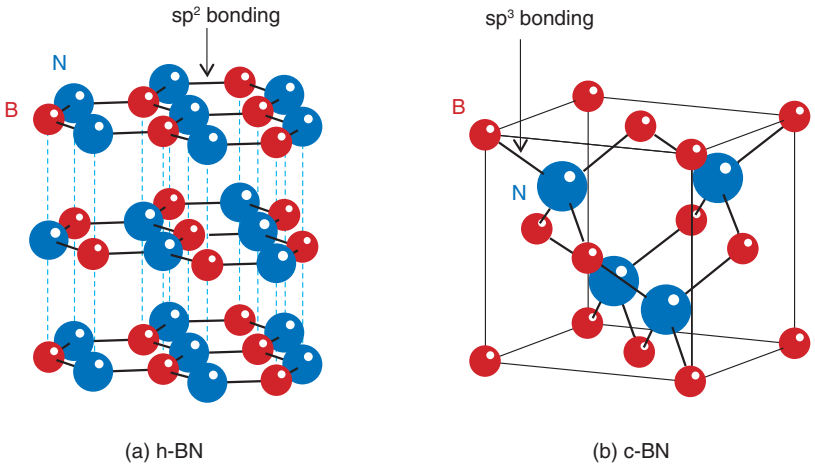

Fig. 2. Crystal structures of (a) hexagonal BN (h-BN) and (b) c-BN.

higher than those in Si or GaAs, means that the on-resistance of the power devices can be reduced by three orders of magnitude. As a result, wide-bandgap semiconductor-based power devices can operate more efficiently with lower power losses. Some wide-bandgap semiconductor-based power devices are already in practical use, as exemplified by silicon carbide (SiC)- or gallium nitride (GaN)-based ones, including high-efficiency inverters for trains.

At NTT Basic Research Laboratories, we have been studying next-generation wide-bandgap semiconductors such as cubic boron nitride (c-BN), aluminum nitride (AlN), and diamond. In the following sections, we describe the growth of c-BN thin films with the highest breakdown field among semiconductors and describe how we control their electrical conductivity. The power loss in c-BN-based power devices is expected to be four orders of magnitude lower than those in Si- or GaAs-based ones and at least one order of magnitude lower than those in SiC- or GaN-based ones (Fig. 1).

If such high-efficiency c-BN-based power devices become available, power loss can be significantly reduced in electrical vehicles, railways, and solar-power and wind-power generation systems. Accordingly, research aimed at developing c-BN-based power devices is underway, as this approach uses fewer natural resources and will contribute to constructing a sustainable society on a global scale.

2. Growth of c-BN epitaxial films using unique growth technique

Boron nitride (BN) is a compound semiconductor composed of boron and nitrogen. BN can have several crystal structures depending on the bonding character and stacking sequence. Representative crystal structures of BN are shown in **Fig. 2**. The thermodynamically stable phase under standard temperature and pressure is sp^2-bonded hexagonal BN (h-BN). In contrast, sp^3-bonded c-BN is a high-pressure and high-temperature stable phase, that is, a metastable phase under standard temperature and pressure.

To utilize c-BN with a high breakdown field for power devices, first of all, the growth of phase-pure (i.e., composed of only the sp^3-bonded phase) c-BN films is necessary. Ion irradiation to the growth surface is known to be effective for forming the metastable sp^3-bonded c-BN phase. Nevertheless, growth of a phase-pure c-BN thin film has been hampered by partial formation of the thermodynamically stable sp^2-bonded BN phase. The sp^2-bonded BN phase has a disordered h-BN structure and is called turbostratic BN (t-BN). The inclusion of the t-BN phase prevents epitaxial growth and renders the resultant BN films polycrystalline ones.

Despite the above-mentioned difficulties, we have grown phase-pure c-BN films by developing a unique growth technique, that is, ion-beam-assisted molecular beam epitaxy (MBE) (**Fig. 3**). Boron (B) atoms are supplied from an electron beam evaporator, while nitrogen radicals (N^*) are supplied from an RF (radio

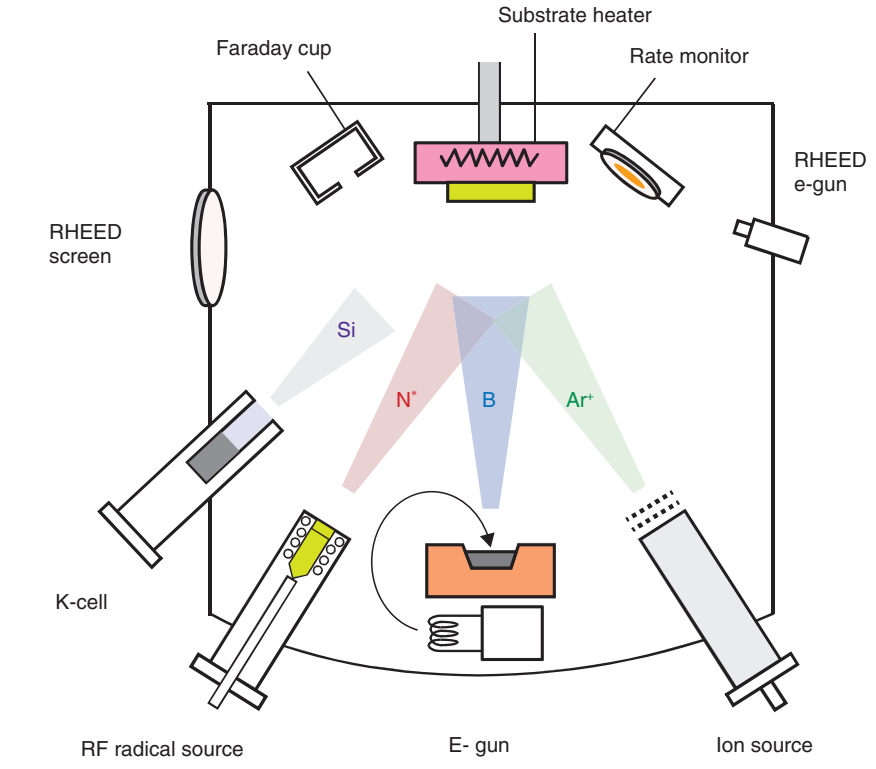

Fig. 3. Schematic of ion-beam-assisted MBE.

frequency) radical generator. At the same time, the growth surface is irradiated with argon ions (Ar^+). The Ar^+/B ratio was found to play a crucial role in forming the sp^3-bonded BN [1, 2]. The substrate is diamond with a small lattice mismatch with c-BN.

To investigate the effect of the Ar^+ irradiation during the BN growth on the bonding characteristics and crystal structures of the resultant BN films, we first grew BN films without and with Ar^+ irradiation. The Fourier transform infrared spectroscopy (FT-IR) absorption measurement*2 of the samples prepared without and with Ar^+ irradiation is shown in **Fig. 4**. In the absence of Ar^+ irradiation, two absorption peaks were observed at around 800 cm^{-1} and 1380 cm^{-1}, which are attributed to sp^2-bonded BN. No absorption peak related to sp^3-bonded BN was observed.

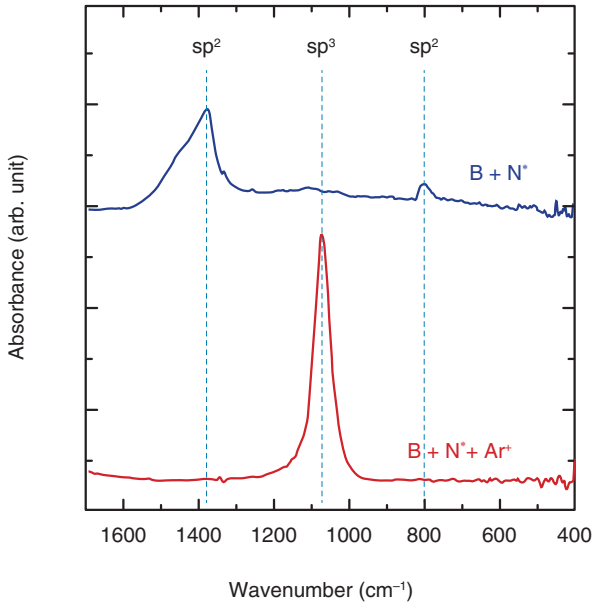

Fig. 4. FT-IR absorption spectra of BN films.

*2 FT-IR absorption measurement: An optical measurement method to characterize specific infrared (IR) absorbance in a material from the difference in intensities of transmitted and incident light. The detected signal is converted to the spectrum by Fourier transformation (FT).

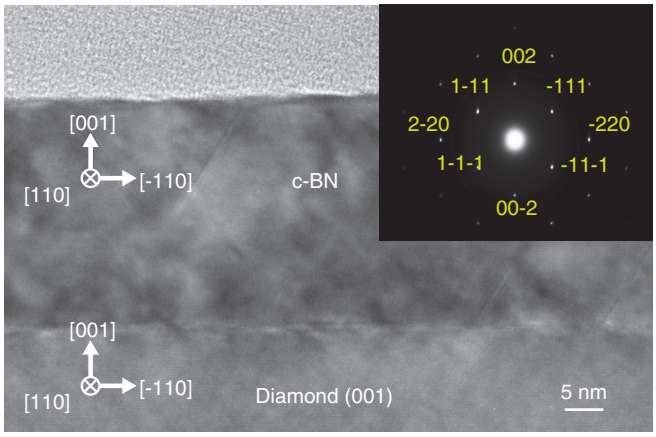

Fig. 5. Cross-sectional TEM image of c-BN film and selective-area electron diffraction pattern of c-BN region.

This means that the sp^2-bonded BN film was grown.

In contrast, in the presence of Ar^+ irradiation, only an absorption peak was observed at around 1070 cm^{-1}, which is attributed to the sp^3-bonded BN. No other peaks originating from sp^2-bonded BN were observed. Therefore, the grown film is phase-pure sp^3-bonded BN. Accordingly, the ion irradiation allows for a selective formation of the sp^3-bonded BN. We surmise that the kinetic energy and/or momentum transferred from the Ar^+ ions to the growth surface may contribute to the preferential formation of the sp^3-bonds in BN.

To identify the crystal structure, we performed cross-sectional TEM (transmission electron microscopy) measurement for the BN film prepared with the Ar^+ irradiation, which was phase-pure (sp^3-bonded BN) judging from the FT-IR measurement (**Fig. 5**). The BN film is grown uniformly from the heterointerface (interface between the diamond substrate and the BN film) to the surface. The inset in Fig. 5 shows a selective-area electron diffraction pattern of the BN film. All the diffraction spots are assigned to those for single-crystal c-BN (001) taken along the [110] zone axis. No other spots or ring patterns attributed to sp^2-bonded BN are observed. Therefore, we can conclude that the single-crystal c-BN (001) film is heteroepitaxially grown on the diamond (001) substrate [3].

3. Electrical conductivity control in c-BN films

To fabricate power devices, it is necessary to grow n-type and p-type c-BN films and control their electrical conductivity. For c-BN, Si and S (sulfur) serve as donors, while Be (beryllium) serves as an acceptor. We carried out the n-type doping first; Si was supplied as a dopant during the epitaxial growth of the c-BN (001) films by using a K-cell (Knudsen cell).*3

The dependence of carrier concentration on temperature for a Si-doped c-BN film with a Si concentration ([Si]) of 1.2×10^{18} cm^{-3} is shown in **Fig. 6**. The carrier concentration monotonically increases with the measurement temperature. The carrier concentrations at room temperature (RT) and 500°C are respectively 2.1×10^{15} cm^{-3} and 6.0×10^{17} cm^{-3}. From the fitting with the equation for the charge neutrality condition (Fig. 6, inset), the donor ionization energy (E_D), donor concentration (N_D), and acceptor concentration (N_A) are respectively estimated to be 0.20 eV, 1.1×10^{18} cm^{-3}, and 4.6×10^{17} cm^{-3}. Because N_D is almost the same as [Si], most of the doped Si atoms are considered to be substitutionally incorporated into boron sites, where they then serve as donors. Remarkably, E_D of 0.20 eV is lower than those for other next-generation wide-bandgap semiconductors such as AlN and diamond. The low E_D in c-BN is promising for higher carrier concentration and lower resistivity, suggesting the potential of c-BN to exceed AlN or diamond, once a c-BN-based power device is achieved.

The dependence of the resistivity on [Si] at RT for the Si-doped c-BN films is shown in **Fig. 7**. For comparison, the resistivity of the non-doped c-BN film is also plotted in Fig. 7. The resistivity of the non-doped c-BN film is as high as ~10^8 Ω·cm, while the Si-doped

*3 Knudsen cell: An evaporation cell, which can supply a molecular beam of a material at a precisely controlled evaporation rate by tuning the cell temperature.

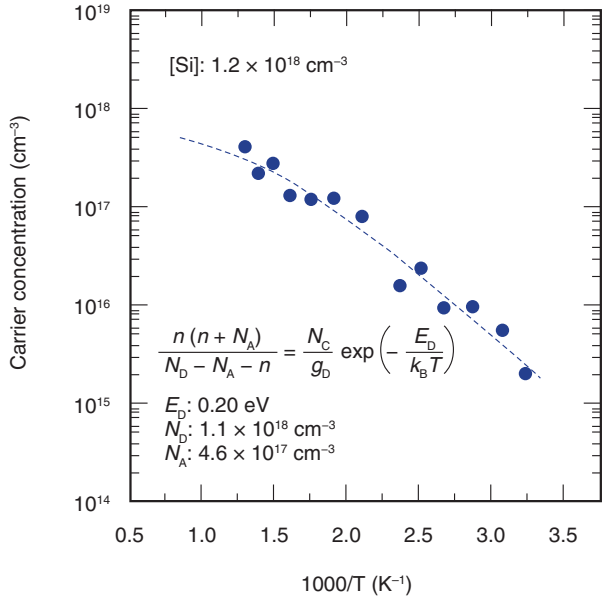

E_D: donor ionization energy
N_D: donor concentration
N_A: acceptor concentration

Fig. 6. Temperature dependence of carrier concentration in Si-doped c-BN film.

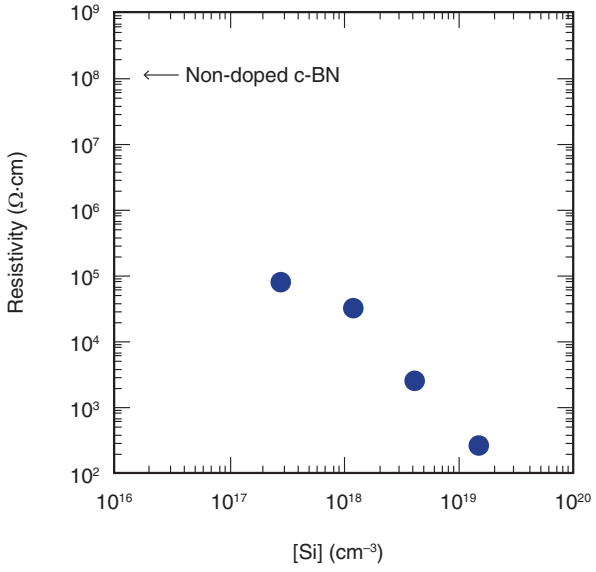

Fig. 7. Dependence of resistivity on Si concentration for Si-doped and non-doped c-BN films.

c-BN film with a [Si] of 1.5×10^{19} cm^{-3} shows low resistivity of ~260 Ω·cm. The resistivity decreases as [Si] increases, demonstrating the successful control of electrical conductivity by varying the dopant concentration, in this case, [Si].

4. Summary

We described the recent progress in research on c-BN at NTT Basic Research Laboratories. We have achieved the epitaxial growth of single-crystal c-BN thin films and control of electrical conductivity in n-type Si-doped c-BN films. These accomplishments are important steps toward the fabrication of electron devices. Further improving crystalline quality and p-type doping will pave the way to achieving high-performance c-BN-based power devices.

References

[1] K. Hirama, Y. Taniyasu, H. Yamamoto, and K. Kumakura, "Heteroepitaxial Growth of Cubic Boron Nitride (c-BN) Thin Films by Ion-beam-assisted MBE," OYO BUTURI, Vol. 85, No. 4, pp. 306–310, 2016 (in Japanese).
[2] K. Hirama, Y. Taniyasu, S. Karimoto, H. Yamamoto, and K. Kumakura, "Heteroepitaxial Growth of Single-domain Cubic Boron Nitride Films by Ion-beam-assisted MBE," Appl. Phys. Exp., Vol. 10, No. 3, 035501, 2017.
[3] K. Hirama, Y. Taniyasu, S. Karimoto, Y. Krockenberger, and H. Yamamoto, "Single-crystal Cubic Boron Nitride Thin Films Grown by Ion-beam-assisted Molecular Beam Epitaxy," Appl. Phys. Lett., Vol. 104, No. 9, 092113, 2014.

Kazuyuki Hirama
Senior Research Scientist, Thin-Film Materials Research Group, NTT Basic Research Laboratories.

He received a B.S., M.S., and Ph.D. in electrical engineering from Waseda University, Tokyo, in 2004, 2006, and 2008. He joined NTT Basic Research Laboratories in 2009. His current research interests are the growth of wide-bandgap semiconductors (c-BN, AlN, and diamond) and their device applications. He received the award for encouragement of research at IUMRS-ICA (International Union of Materials Research Societies International Conference in Asia) 2014, outstanding presentation and best poster awards at Diamond Symposium 2010 and 2012, and the young scientist presentation award at the 2008 Japan Society of Applied Physics (JSAP) meeting. Dr. Hirama is a member of JSAP.

Yoshitaka Taniyasu
Senior Researcher, Group Leader of Low-Dimensional Nanomaterials Research Group, NTT Basic Research Laboratories.

He received a B.E., M.S., and Dr. Eng. in electrical engineering from Chiba University in 1996, 1998, and 2001. He joined NTT Basic Research Laboratories in 2001. He has been engaged in wide-bandgap semiconductor research. He received the Young Scientist Award at the 2007 Semiconducting and Insulating Materials Conference, the Young Scientist Award of the International Symposium on Compound Semiconductors 2011, the Commendation for Science and Technology by the Minister of Education, Culture, Sports, Science and Technology of Japan (the Young Scientists' Prize) in 2011, and the Japan Society for the Promotion of Science Prize in 2019.

Hideki Yamamoto
Senior Research Scientist, Supervisor, Executive Manager of Materials Science Laboratory, NTT Basic Research Laboratories.

He received a B.S., M.S., and Ph.D. in chemistry from the University of Tokyo in 1990, 1992, and 1995. He joined NTT in 1995. His principal research fields are thin film growth, surface science, and superconductivity. He was a visiting scholar at the Geballe Laboratory for Advanced Materials, Stanford University, USA (2004–2005). He received the 2nd Young Scientist Presentation Award (1997) by JSAP and the 20th Superconductivity Science and Technology Award (2017) from the Forum of Superconductivity Science and Technology, the Society of Non-traditional Technology. He is a member of JSAP, the Physical Society of Japan, the Japan Society of Vacuum and Surface Science, the American Physical Society, and the Materials Research Society.

Kazuhide Kumakura
Group Leader of Thin-Film Materials Research Group, Materials Science Laboratory, NTT Basic Research Laboratories.

He received a B.E., M.E., and Ph.D. in electrical engineering from Hokkaido University in 1993, 1995, and 1998. He joined NTT Basic Research Laboratories in 1998. His current research interests include crystal growth of nitride-based semiconductors and their optoelectronic and magnetic device applications. He is a member of JSAP.

Crystal Growth of Wurtzite GaP Nanowires for Solar-water-splitting Devices

Kouta Tateno and Kazuhide Kumakura

Abstract

Gallium phosphide (GaP) is an environmentally friendly III-V semiconductor, and it has an indirect bandgap as a stable zincblende structure. However, if controlled nanowire growth is carried out, a wurtzite structure with a direct bandgap can be achieved. We successfully grew wurtzite GaP nanowires without stacking faults by using our original method using chlorine etching and repeated gallium supply. We present here our results of solar-water splitting using a p-type nanowire photoelectrode, and we explain the fabrication and properties of a pin-type nanowire solar cell.

Keywords: nanowire, gallium phosphide, solar-water splitting

1. Nanowire solar-water-splitting device

Research and development to harvest solar energy that is inexhaustible and clean has been progressing as part of efforts to achieve a sustainable society. In 1972, Fujishima et al. reported on water and carbon dioxide reduction using a semiconductor photoelectrochemical method for the first time [1]. Their method is promising for producing fuel and organic substances that can be stored and is still being researched actively.

The redox (reduction oxidation reaction) process of water using sunlight (solar-water splitting) is the simplest process because the products are hydrogen and oxygen. For this reaction, the potential difference between cathodes and anodes in an electrochemical system must be larger than 1.23 V (thermodynamically required). In addition, the materials used for solar-water splitting should be selected in consideration of low toxicity, abundance on earth, and long stability without corrosion during the reaction. Photocatalysts composed of fine powders have also been studied for solar-water splitting, but their solar-to-hydrogen conversion efficiency is low at present (about 1–2%). In practical use, an ideal device is to produce hydrogen and oxygen separately.

Our target device considering the above points is shown in **Fig. 1** [2]. The transparent tube-like structure contains dense nanowire diodes with both ends exposed to water. When the nanowire diodes absorb sunlight, the generated electrons react with hydrogen ions at the cathode side of the nanowires (outside the tube) to form hydrogen, and the holes react with water at the anode side of the nanowires (inside the tube) to form oxygen. Keeping the hydrogen and oxygen separate makes their collection easier.

Here, individual nanowire diodes independently contribute to light absorption and water splitting. Even if some nanowires fail, the device performance of others should not be affected. Since nanowires are small in diameter, we can grow good heterostructures using various materials with a relatively large difference in the lattice constant. Therefore, some semiconductors with different bandgaps can be connected axially and absorb a wide wavelength range of sunlight. In principle, such a tube-like structure can be fabricated by embedding a myriad of nanowire diodes on the substrate surface with a transparent resin, exposing the nanowire tips, peeling the resin film off the substrate, and rounding it.

There are many challenges to achieve this target device. The growth of nanowires requires a good

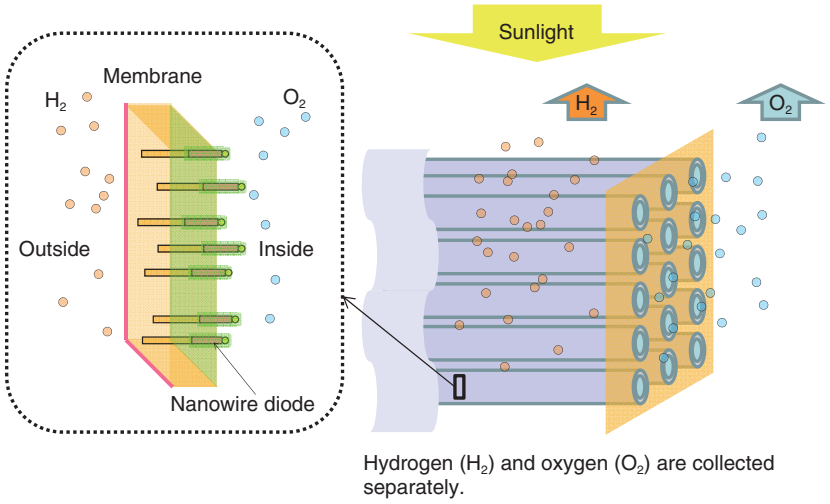

Fig. 1. Schematic illustration of our target solar-water-splitting device.

structure with uniform length and thickness and high density. In addition, techniques to grow different materials in the axial direction and to control the concentration of dopants are also required. For photoelectrochemical devices, it is necessary to develop a proper coating film with optical transparency and corrosion protection as well as cocatalysts to promote chemical reactions at the nanowire ends. The road to achieving the target device is long, but we have made progress by growing wurtzite gallium phosphide (GaP) nanowires. We have also performed p- and n-type doping in nanowires and solar-water splitting using nanowire electrodes, and we have fabricated nanowire solar cells [3, 4]. These achievements are explained in this article.

2. Wurtzite GaP nanowires

Typical GaP materials are III-V semiconductors with an indirect bandgap and are not used for high-performance devices because of their poor electronic conduction and optical absorption characteristics. However, because GaP is composed of elements abundantly present on the earth, it is suitable as a material for solar cells and photoelectrodes, which must be inexpensive and have large areas. Since the bandgap is 2.1 eV, it is possible to perform solar-water splitting without bias if the voltage loss at the electrode is small. Band structure calculations predicted that wurtzite GaP has a direct bandgap, although stable GaP normally has a zincblende structure.

A research group in Europe successfully carried out crystal growth of wurtzite GaP nanowires for the first time recently, and those nanowires showed a large increase in photoluminescence compared with zincblende GaP [5].

We also succeeded in carrying out crystal growth of wurtzite GaP nanowires [4]. The growth was carried out with the vapor-liquid-solid (VLS) method*1 using gold nanoparticles as catalysts. First, gold particles were dispersed on the substrate, and then the source gases were supplied at 400–500°C in the crystal growth apparatus. As shown in **Fig. 2(a)**, TBCl (tertiarybutylchloride) was used as a chlorine etching material, and TEGa (triethylgallium) as a group III source and TBP (tertiarybutylphosphine) as a group V source were supplied alternately. This technique enabled us to successfully grow wurtzite GaP nanowires without stacking faults.

A transmission electron microscope (TEM) image and an electron diffraction pattern of one wurtzite GaP nanowire are shown in **Fig. 2(b)**. The nanowires were about 500 nm in length, and the diameter of the gold particles was about 40 nm. The TEM image shows the gold part as hemispherical black material at the nanowire tip. The electron diffraction pattern

*1 VLS method: Vapor-liquid-solid method. A method used for growing nanowires. It is a crystal growth method in a vapor phase atmosphere using metal fine particles as a catalyst. For gold (Au) catalyzed GaP nanowires, gallium (Ga) and phosphide (P) from the gas (vapor) phase are dissolved in Au particles and become liquid. Solid crystalline GaP grows from the liquid Au-Ga-P particle.

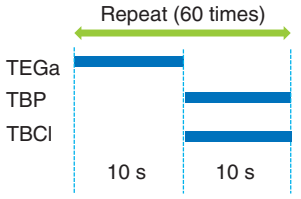

(a) Growth sequence

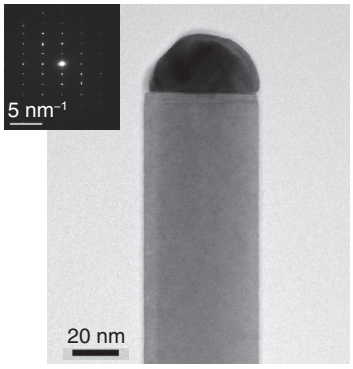

(b) TEM image & electron diffraction image

TBCl: tertiarybutylchloride
TBP: tertiarybutylphosphine
TEGa: triethylgallium

Fig. 2. Wurtzite GaP nanowire.

indicates a typical wurtzite structure. The TEM image also shows that the nanowires have smooth sidewalls without stacking faults.

3. Impurity doping in nanowires

In growing the GaP nanowires, we tried to incorporate zinc (Zn), a p-type dopant, and sulfur (S), an n-type dopant, into the nanowires. The p-type dopant source was diethylzinc (DEZn), and the n-type dopant source was DTBS (ditertiarybutylsulfide). Graphs of nanowire lengths versus flow rates are shown in **Fig. 3(a, b)**, and scanning electron microscope (SEM) and TEM images of the nanowires are shown in **Fig. 3(c)**. The lengths of the nanowires changed with the Zn and S doping. In particular, the length of the p-type ones obviously increased as the flow rate of DEZn increased, and they became wider at the bottom. These results show that the variation of the growth rate should be taken into account when fabricating devices by performing impurity doping. The TEM images show that both types of nanowires had some stacking faults due to doping, but they still had wurtzite structures.

Impurity and carrier concentrations were evaluated by secondary ion mass spectrometry (SIMS)[*2] measurements and Mott-Schottky plots[*3] from electrochemical experiments. The nanowire-grown samples were embedded in a resin or SiO_2 (silicon dioxide) film by sputter deposition and measured as average concentrations. It was confirmed that the concentration of impurities and carriers in the nanowires increased as the flow rates of the dopant sources increased. A concentration of about 10^{18} cm^{-3} was obtained for both types of doped samples for both carrier and impurity. Since the measurement methods used here provide average information on a large number of dispersed nanowires, we will continue to consider a method for measuring individual nanowires for more accurate measurements.

4. Solar-water splitting using nanowire electrodes

We grew p- and n-type wurtzite GaP nanowires and conducted photoelectrochemical experiments in order to achieve solar-water-splitting devices. The results obtained using a p-type sample as a photocathode electrode are shown in **Fig. 4**. In Fig. 4(a), we compare a p-type GaP substrate and p-type GaP nanowire samples.

We also compared nanowires with and without platinum (Pt) nanoparticles (as cocatalyst) / titanium

*2 SIMS: Secondary ion mass spectrometry is an analytical method. One spot on a sample is irradiated with an ion beam and then sputtered. The released ionized atoms and molecules are measured by mass spectrometry. The elemental concentration in the depth direction can be analyzed.

*3 Mott-Schottky plot: In an electrochemical measurement of semiconductor electrodes, carrier concentration can be determined from the slope by plotting the reciprocal of the differential capacitance against the potential. The differential capacitance is determined by impedance measurement.

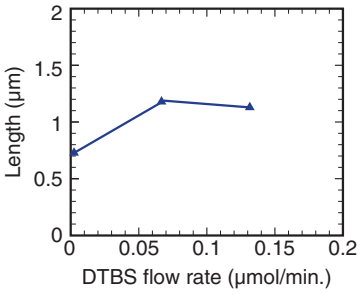

(a) S doping (n type)

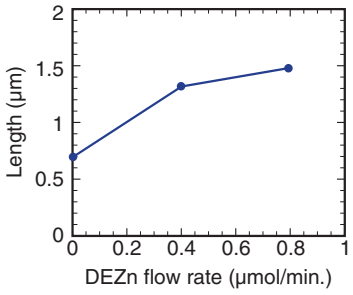

(b) Zn doping (p type)

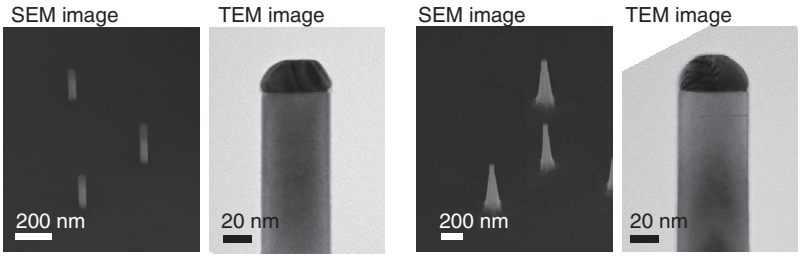

(c) SEM and TEM images of nanowires

Fig. 3. Impurity doped GaP nanowires.

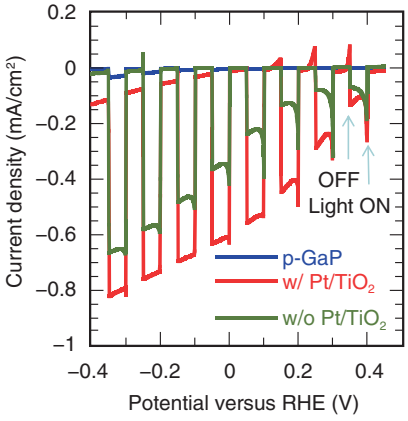

(a) Linear sweep voltammograms for p-type GaP substrate, GaP nanowires with and without Pt/TiO_2, performed under chopped illumination. The scan rate was 1 mV/s. Each ON/OFF time was 50 s.

Pt: platinum
RHE: reversible hydrogen electrode
TiO_2: titanium dioxide

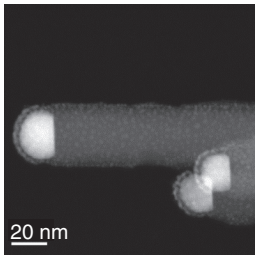

(b) Scanning TEM image of GaP nanowires with Pt/TiO_2

Fig. 4. GaP nanowire photoelectrode.

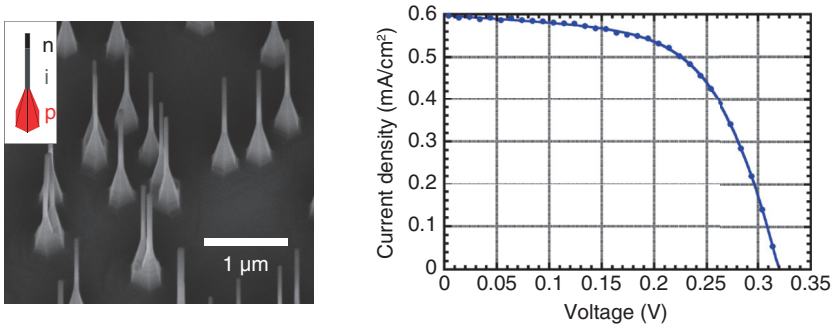

(a) SEM image of pin-type GaP nanowires

(b) Measured J-V curve of GaP nanowire solar cell under AM 1.5G one sun illumination

Fig. 5. GaP nanowire solar cell.

dioxide (TiO_2) protective thin film. The TEM image of GaP nanowires with Pt/TiO_2 is shown in Fig. 4(b), where the TiO_2 thin film covers the nanowire uniformly and Pt fine nanoparticles are dispersed. In the photoelectrochemical experiments, photocurrent was measured by repeating ON/OFF of the light while scanning the voltage using simulated sunlight (Solar simulator, AM 1.5G). The electrolyte was a 0.5-M H_2SO_4 (sulfuric acid) aqueous solution, and the counter electrode was a Pt plate. Compared with the GaP substrate, the photocurrent output of the nanowire samples was found to be large.

We also confirmed that the nanowire sample with TiO_2 dispersed with Pt fine nanoparticles showed no degradation of nanowires. The density was evaluated to be 70–110 μm^{-2}, which was relatively high, but the photocurrent itself was lower than expected due to the fact that the nanowires could not be made longer than 1 μm and the length of nanowires varied. Similar measurements were carried out on n-type nanowires. However, degradation due to corrosion was severe, even for samples with the TiO_2 protective film. We therefore need to investigate the optimum protective film for n-type photoanode electrodes.

5. Nanowire solar cell

Since the final target of the solar-water-splitting device includes pin-type nanowire photodiodes, we grew pin-type nanowires and examined the solar cell characteristics. An SEM image of the grown pin-type nanowires is shown in **Fig. 5(a)**, and the photocurrent voltage plot measured using simulated sunlight after device fabrication is shown in **Fig. 5(b)**. The device was fabricated by depositing 5 nm of alumina on the sample surface using atomic layer deposition, embedding the nanowires in resin for planarization, exposing the nanowire tips, and then forming electrodes on the back of the substrate and the sample surface. ITO (tin doped indium oxide) was used for the transparent electrode on the sample surface. The lengths of the p-, i-, and n-segments were designed to be 330, 1300, and 330 nm, respectively. The p-type segments were tapered by doping as described above, resulting in a structure with a large bottom diameter as shown in the schematic illustration. The measured result was fitted with a diode model of the following equation.

$$J = J_{sc} - (V - R_s J) / R_p - J_0 \exp(q (V - R_s J) / (n k T) - 1),$$

where q is the electron charge, k is the Boltzmann constant, T is the absolute temperature, J_{sc} is the short-circuit current density, R_s is the series resistance, R_p is the parallel resistance, J_0 is the saturation current density, and n is the ideal factor. The voltage at J = 0 is the open-circuit voltage V_{oc}.

The result was J_{sc} = 0.6 mA/cm^2, V_{oc} = 0.32 V, J_0 = 4.63×10^{-8} A/cm^2, n = 1.33, R_p = 6.5 kΩ·cm, and R_s = 40 Ω·cm, and the conversion efficiency of this sample was 0.11%. This low efficiency is due to the low nanowire density (9.8×10^7 cm^{-2}). On a single nanowire basis, J_{sc} = 160 mA/cm^2. This large photocurrent is due to the effect of the nanowires collecting the ambient light. Therefore, by optimally designing nanowire solar cells, we can expect to achieve highly efficient solar cells.

6. Future development

Through our experience in fabricating nanowire photoelectrodes and nanowire solar cells, we were able to get closer to our target solar-water-splitting devices using wurtzite GaP nanowires. The nanowires absorb light efficiently, and a large photocurrent can be expected, but a large open-circuit voltage of about 2 V, which is sufficient for water splitting, is considered to be difficult when using a single pin-type nanowire diode.

Therefore, we are planning to form a tandem type nanowire consisting of grown pin-type nanowires in series. It is also necessary to examine the material of the protective film applied to prevent corrosion. For the anode side in particular, we may have to change the electrolyte to a weak alkaline solution. It is also necessary to examine the cocatalyst. At present, precious metals such as Pt are widely used as cocatalysts due to high efficiency. Pt is a rare element and needs to be replaced with another material in the future. Corrosion prevention and cocatalysts are challenging issues, but we will continue to investigate them.

References

[1] A. Fujishima and K. Honda, "Electrochemical Photolysis of Water at a Semiconductor Electrode," Nature, Vol. 238, pp. 37–38, 1972.

[2] K. Tateno, Y. Ono, and K. Kumakura, "Photoreactor," Japanese patent application No. 2017-024024.

[3] K. Tateno, Y. Ono, and K. Kumakura, "Photoelectrochemical Properties of Wurtzite Gallium Phosphide Nanowires Grown on GaP(111)B Substrates," 2016 International Conference on Solid State Devices and Materials (SSDM 2016), PS-13-12, Tsukuba, Japan, Sept. 2016.

[4] K. Tateno, G. Zhang, S. Sasaki, M. Takiguchi, and K. Kumakura, "Wurtzite GaP Nanowire Grown by Using Tertiarybutylchloride and Used to Fabricate Solar Cells," Jpn. J. Appl. Phys., Vol. 58, No. 1, 015004, 2019.

[5] S. Assali, I. Zardo, S. Plissard, D. Kriegner, M. A. Verheijen, G. Bauer, A. Meijerink, A. Belabbes, F. Bechstedt, J. E. M. Haverkort, and E. P. A. M. Bakkers, "Direct Band Gap Wurtzite Gallium Phosphide Nanowires," Nano Lett., Vol. 13, pp. 1559–1563, 2013.

Kouta Tateno

Senior Research Scientist, NTT Basic Research Laboratories.

He received a B.S., M.S., and Ph.D. in chemistry from the University of Tokyo in 1991, 1993, and 2001. He joined NTT Opto-electronics Laboratories in 1993. His current research interests include the fabrication and physics of nanostructures using semiconductor nanowires. He is a member of the Japan Society of Applied Physics (JSAP), the Electrochemical Society of Japan, and the Materials Research Society.

Kazuhide Kumakura

Group Leader of Thin-Film Materials Research Group, Materials Science Laboratory, NTT Basic Research Laboratories.

He received a B.E., M.E., and Ph.D. in electrical engineering from Hokkaido University in 1993, 1995, and 1998. He joined NTT Basic Research Laboratories in 1998. His current research interests include crystal growth of nitride-based semiconductors and their optoelectronic and magnetic device applications. He is a member of JSAP.

High Power and High Efficiency Operation of Semiconductor Optical Amplifier Assisted Extended Reach Electroabsorption Modulated DFB Laser (AXEL) for Extension of Transmission Distance

Takahiko Shindo, Shigeru Kanazawa, Mingchen Chen, Toshihide Yoshimatsu, Yoshitaka Ohiso, Kimikazu Sano, and Hideaki Matsuzaki

Abstract

We have designed a semiconductor optical amplifier integrated with an electroabsorption modulator integrated distributed feedback laser (EML). We call this device AXEL; it is designed to enhance the power conversion efficiency and modulated light output power of EMLs. In this study, we investigated AXELs for both the L-band and O-band wavelength ranges. The results of experiments indicated that dramatically increased power conversion efficiency and modulated light output power were obtained with the fabricated AXELs. For the L-band wavelength range AXEL, a high modulated light output power of 9 dBm and an extension of 10-Gbit/s transmission distance to 80 km due to low chirp characteristics of the AXEL were simultaneously demonstrated. In addition, the 25-Gbit/s 80-km transmission achieved using the O-band wavelength range AXEL along with an avalanche photodiode was demonstrated for the first time thanks to the significantly increased modulated light output power of the AXEL.

Keywords: electroabsorption modulator, distributed feedback laser, semiconductor optical amplifier

1. Introduction

Electroabsorption modulator integrated distributed feedback (DFB) lasers (EMLs) are employed in many applications that use intensity-modulation direct-detection (IM-DD) schemes because of their high extinction ratio and low chirp characteristics compared with directly modulated lasers (DMLs) [1–3]. To meet the demand for huge data capacity, which is increasing exponentially due to the growing use of various services and devices, future optical communication systems will require a light source that can operate at high speed with high output power, and they will need to transmit over long distances. Therefore, it is very important to enhance the power conversion efficiency of the EML without degrading the transmission characteristics.

However, there is a limitation on how much the modulated light output of the EML can be enhanced without significantly increasing the power consumption.

This is because the electroabsorption modulator (EAM) has a large modulation loss, generally around 5 dB. The optical power loss in the EAM becomes large as the input power of the DFB laser diode (LD) becomes large in efforts to enhance the modulated light output. Therefore, it is intrinsically difficult to enhance the modulated light output of an EML without significantly increasing the power consumption. In other words, the intrinsic power conversion efficiency of the EML is very small compared with that of DMLs.

To overcome this limitation and efficiently enhance the modulated light output power, we have proposed a monolithically integrated semiconductor optical amplifier (SOA) with an EML [4, 5]. The device is called an SOA assisted extended reach EML, or AXEL for short. The SOA and LD in the AXEL have the same multiple quantum well (MQW) structure so as to avoid complicating the fabrication process. For the AXEL, the active region is separated into the LD and SOA components, and the input power is allocated to each component. Therefore, the SOA can independently amplify the optical output from the EAM without being affected by the large modulation loss in the EAM. As a result, the AXEL can significantly enhance the power conversion efficiency and modulated light output power.

Previously, these excellent results of the AXEL were mainly investigated in the C-band (1530–1565 nm) wavelength range. The advantages of the AXEL such as its high efficiency operation and high modulated light output, however, can be applied to all wavelength ranges. In this study, we fabricated both L-band (1565–1625 nm) and O-band (1260–1360 nm) wavelength range AXELs to extend the transmission distance. We first investigated an AXEL in the 1.57-μm wavelength range to meet the demand for a light source in 10-Gbit/s based next-generation access networks (i.e., with an extended transmission distance and increased modulated light output power). As a result, we simultaneously extended the 10-Gbit/s transmission distance to 80 km and achieved an enhanced modulated light output power of 9 dBm without significantly increasing power consumption, thanks to the high power conversion efficiency of the AXEL [6, 7].

Next, we demonstrated an AXEL in the 1.3-μm wavelength range and proposed the concept of the optical link by using the AXEL and an avalanche photodiode (APD) receiver. As a result, we successfully demonstrated a 28-Gbit/s 80-km optical link without any in-line amplifier or device for chromatic dispersion compensation [7, 8].

2. Transmission at 10 Gbit/s with L-band AXEL

To take advantage of the high efficiency characteristics of the AXEL, we first investigated the L-band wavelength range AXEL, which is intended for next-generation access networks. The main targets for future access networks are to achieve an extended transmission distance and increased power splitting ratio. In general, a high modulated light output power of over 9 dBm and a long distance transmission over 40 km are simultaneously required for the light source for 10-Gbit/s based access networks. For the L-band wavelength range in particular, low chirp characteristics are very important for the light source because large chromatic dispersion of the optical fiber severely limits the transmission distance. One advantage of the AXEL is that the SOA can act not only as an optical booster but also as a chirp compensator [9–12]. Therefore, the low chirp characteristics of the AXEL enable us to extend the transmission distance for the L-band wavelength range.

In this work, an EML having the same LD and EAM sections as those of the AXEL was fabricated on the same wafer to evaluate the superior chirp characteristics and high efficiency operation of the AXEL. Schematic views of (a) a conventional EML and (b) an AXEL are shown in **Fig. 1**. The respective lengths of the LD (DFB laser) and EAM sections were 300 and 150 μm. As explained above, the SOA section of the AXEL has the same MQW structure as that of the LD section to avoid complicating the fabrication process [4, 5]. Therefore, the AXEL can be fabricated using the same fabrication process as that of the conventional EML.

In addition, AXELs with SOA lengths of 50, 100, and 150 μm were fabricated in order to assess the lasing characteristics. In **Fig. 2(a)**, we show the injection current-light output (*I-L*) characteristics of the fabricated EML and the AXELs with various SOA lengths. In the measurement, a bias voltage V_{dc} of –2 V was applied assuming actual driving conditions. In addition, to simplify the driving method, the LD and SOA of the AXEL were electrically connected and commonly driven by the same power supply [13, 14].

For all SOA lengths, the light output power of the AXEL increased greatly compared with that of the EML. In addition, the light output power of the AXEL became higher as the length of the SOA became longer. The dependence of the power conversion efficiency on the injection current of the EML

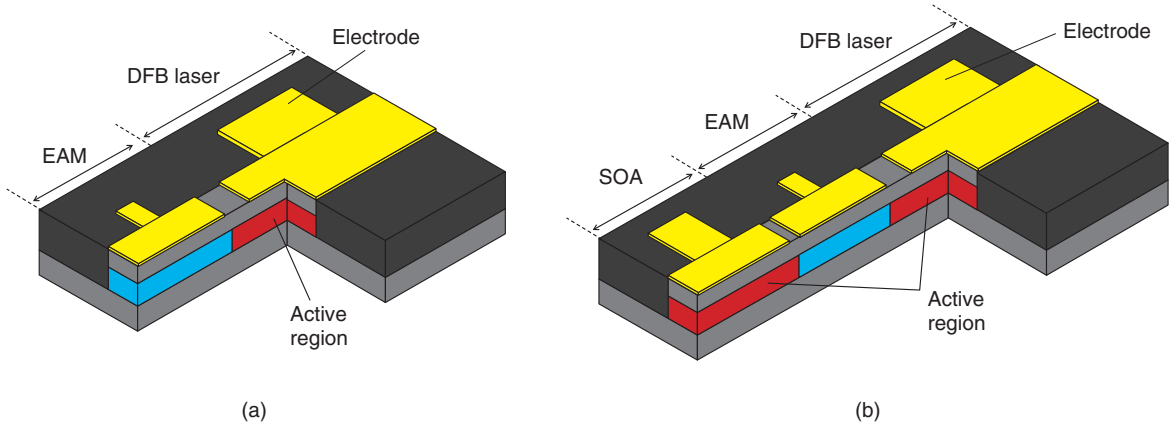

Fig. 1. Schematic device structure of fabricated (a) conventional EML and (b) AXEL for L-band wavelength range.

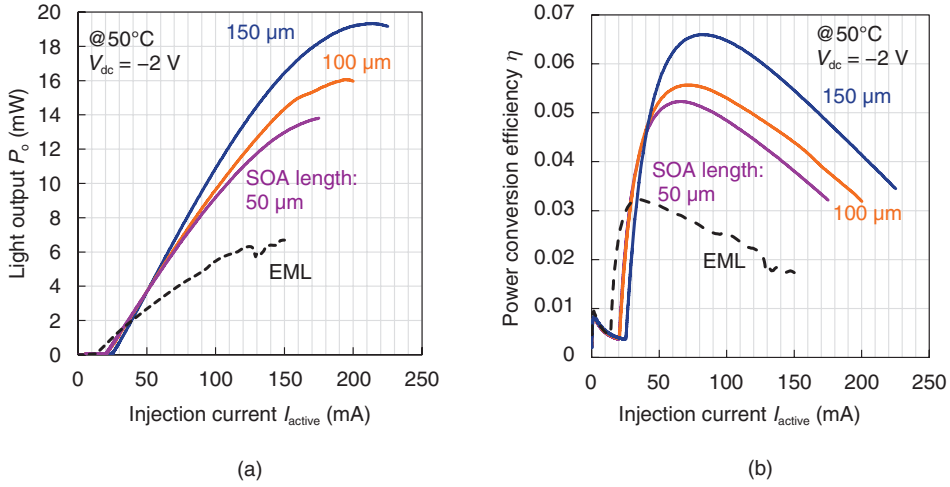

Fig. 2. (a) *I-L* characteristics and (b) dependence of power conversion efficiency on injection current of EML and AXEL with SOA lengths of 50, 100, and 150 µm.

and AXELs with various SOA lengths is plotted in **Fig. 2(b)**. It is clearly seen that the power conversion efficiency also becomes large as the SOA length becomes longer. The SOA length of 150 µm is preferred for high efficiency operation and high output power. Therefore, we used the 150-µm-long SOA for the L-band wavelength range AXEL in this investigation.

As previously described, an additional advantage of the AXEL for the L-band wavelength range is the chirp compensation effect of the SOA. To confirm this advantage, we experimentally compared the chirp characteristics of the AXEL and the conventional EML. The measured dependence of the chirp parameter on EAM bias voltage is shown in **Fig. 3**. The SOA length of the AXEL was 150 µm in this measurement. The fiber peak method was used to evaluate the chirp characteristics [15]. The driving currents I_{LD} of the EML and AXEL were set to 80 mA and 120 mA, respectively. The SOA and LD of the AXEL were electrically connected and commonly driven. As can be seen, the chirp parameter of the AXEL was relatively small compared with that of the EML, especially in the low bias voltage range. In other words, the chirp parameter of the AXEL decreased, particularly in the high optical power range. This indicates that the AXEL can extend the transmission distance because of its low chirp

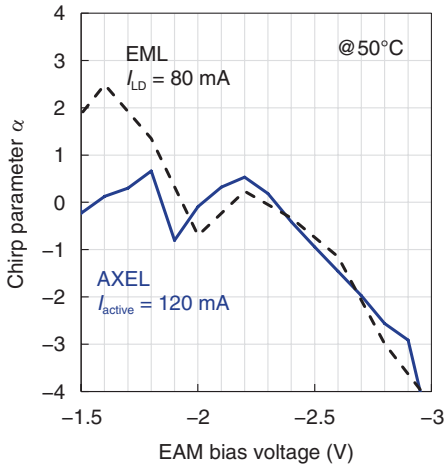

Fig. 3. Dependence of chirp parameter on EAM bias voltage of EML and AXEL.

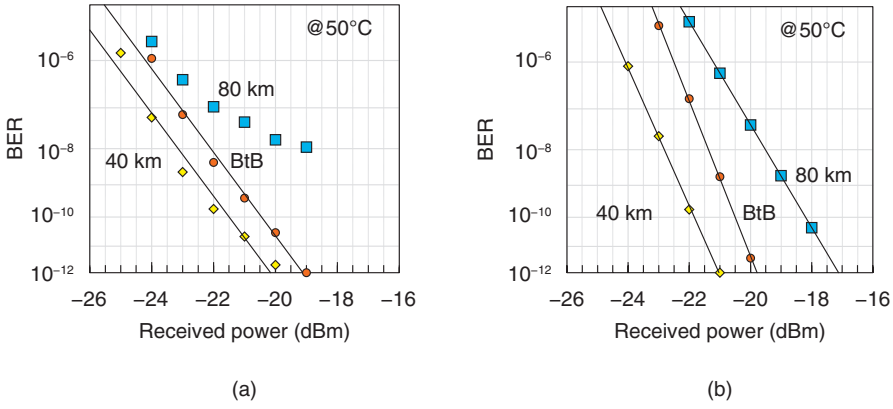

Fig. 4. Measured 10-Gbit/s BER characteristics for (a) EML and (b) AXEL.

characteristics [16].

Then we compared the 10-Gbit/s transmission characteristics of the AXEL with those of the conventional EML. The measured 10-Gbit/s bit error rate (BER) performance is shown in **Fig. 4** for back-to-back (BtB), 40-, and 80-km transmissions. In these measurements, the V_{dc} and voltage swing V_{pp} for the EAM were respectively set to –1.92 and 2.0 V. These modulation conditions were optimized to minimize the BER for 40-km transmission for the EML. The same modulation conditions were used for the AXEL. The electrical signal input was a 9.953-Gbit/s non-return-to-zero (NRZ) pseudorandom binary sequence (PRBS) of 2^{31}–1. The I_{LD} of the EML was set to 80 mA.

In contrast, the LD and SOA of the AXEL were commonly driven, and the total current of the active region was set to 126 mA. As can be seen in Fig. 4(a), error-free operation was achieved for 40-km transmission with the EML. However, the 80-km transmission with the EML could not be achieved due to large chromatic dispersion in the optical fiber. The estimated total amount of chromatic dispersion of the 80-km single-mode fiber (SMF) for 1570 nm was 1440 ps/nm. In contrast, the transmission distance was successfully extended to 80 km by using the AXEL, as shown in Fig. 4(b). This extension of the transmission distance is attributed to the AXEL's low chirp characteristics.

The measured eye diagrams for BtB and 40-km transmission are shown in **Fig. 5**. As can be seen, clear eye openings of the AXEL and EML were

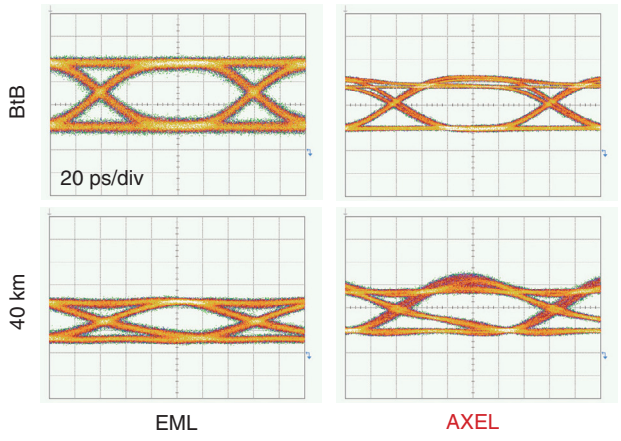

Fig. 5. Measured eye diagrams for EML and AXEL.

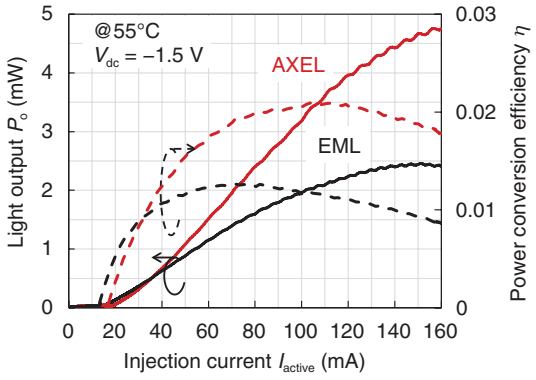

Fig. 6. Measured *I-L* characteristics and dependence of power conversion efficiency on injection current of O-band EML and AXEL.

achieved even after 40-km transmission. For the AXEL, we confirmed that there is no significant distortion of the quality of the eye diagram due to the integration of the SOA.

The modulated light output power of the EML and AXEL were also measured. The modulated light output power for the EML was as low as 6.8 dBm when the injection current I_{active} for the LD was set to 80 mA. Even when the I_{active} for the LD was 150 mA, the modulated light output power reached only 8.0 dBm. This result indicates that it is very difficult to achieve sufficient light output by using a conventional EML.

In contrast, the modulated light output power of the AXEL was 9.0 dBm with an I_{active} of 126 mA. The modulated light output power was greatly increased without an excessive increase in the injection current, thanks to the high efficiency characteristics of the AXEL. These results indicate that the AXEL is an attractive light source even for the L-band wavelength range due to its significantly increased power conversion efficiency and low chirp characteristics.

3. Transmission at 28 Gbit/s with O-band AXEL

In contrast to the L-band wavelength range, the large optical loss in the SMF limits the transmission distance for the O-band wavelength range because chromatic dispersion in the SMF is very small compared with that for the L-band. Therefore, an enhancement of the modulated light output by using the SOA is a breakthrough to overcome the limitation of large optical loss in the SMF for the O-band.

Next, we conducted experiments to demonstrate the 1.3-μm wavelength range AXEL with high-power conversion efficiency and to extend the transmission distance of a 28-Gbit/s optical link by using the AXEL. Again, we also fabricated a conventional EML that had the same LD and EAM sections as those of the AXEL by using the same fabrication process. The length of the LD and EAM were set to 300 and 150 μm, respectively. In addition, the SOA length of the AXEL was set to 100 μm.

The *I-L* characteristics of the EML and AXEL at 55°C (solid lines) are shown in **Fig. 6**. As previously described, the LD and SOA of the AXEL were electrically connected and commonly driven. In this measurement, V_{dc} of –1.5 V was applied to the EAM. The dependence of the power conversion efficiency on the injection current for the EML and AXEL are also shown in Fig. 6 (dashed lines). As can be seen, the light output power of the AXEL was significantly enhanced compared with that of the EML even for the O-band wavelength range. The light output power of the AXEL is almost two times larger than that of the EML with an I_{active} of 160 mA. In addition, the power conversion efficiency of the AXEL with I_{active} of 160 mA is also two times larger than that of the EML.

To take advantage of the high output power operation of the O-band AXEL, we focused on extending the 28-Gbit/s optical link to 80 km by using the AXEL and APD. The experimental setup used for the transmission is shown in **Fig. 7**. A standard SMF with a chromatic dispersion of –1.8 ps/nm/km and transmission loss of 0.375 dB/km for the 1.3-μm wavelength range was used for this measurement. We used an APD receiver optical subassembly (APD-ROSA), which can detect an NRZ signal of over 25 Gbit/s with a sensitivity of –21.5 dBm [17]. The estimated

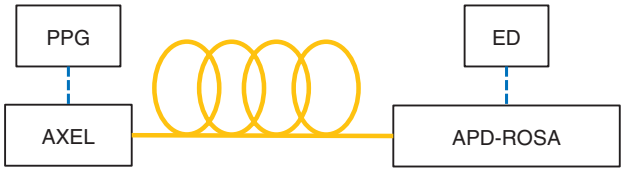

Optical fiber: 20 km x 4 = 80 km
Total chromatic dispersion: –144 ps/nm
Total optical power loss: 30 dB

APD-ROSA: APD receiver optical subassembly
PPG: pulse pattern generator
ED: error detector

Fig. 7. Experimental setup for 28-Gbit/s, 80-km transmission.

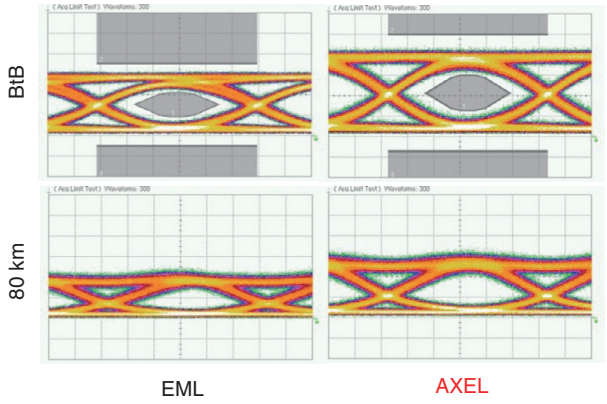

Fig. 8. Measured eye diagrams of EML and AXEL.

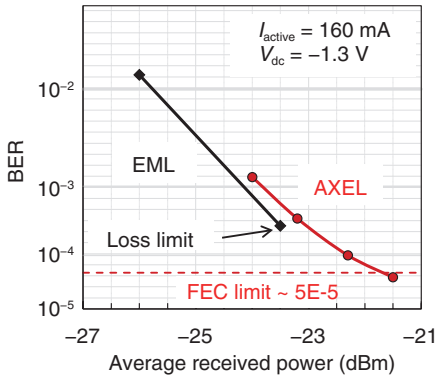

FEC: forward error correction

Fig. 9. Measured BER characteristics of the 28-Gbit/s 80-km transmission.

total optical fiber loss and dispersion were 30 dB and –144 ps/nm for 80 km with a wavelength of 1.3 μm. Therefore, the modulated light output of the AXEL should be more than 8.5 dBm in order for it to transmit sufficient light intensity to the APD-ROSA, which is 80 km ahead.

Next, we compared the 28-Gbit/s transmission characteristics of the 1.3-μm AXEL with those of the conventional EML. Measured eye diagrams for BtB and after 80-km transmission with the AXEL and EML are shown in **Fig. 8**. For both the AXEL and EML, an I_{active} of 160 mA was applied, and the modulation V_{pp} and the V_{dc} were 2.0 and –1.3 V, respectively. The electrical signal we used for the measurement was a 28-Gbit/s NRZ PRBS of 2^{31}–1. As a result, the dynamic extinction ratio (ER) and mask margin (MM) determined from the measured eye diagrams were 8.7 dB and 8% for the EML.

Almost the same quality of the eye diagram for the AXEL with an ER of 8.9 dB and MM of 9% was confirmed. Furthermore, the modulated light output power of the AXEL and EML was 5.7 and 8.5 dBm, respectively. We therefore confirmed that the AXEL successfully enhanced the modulated light output by about 2.8 dB.

The measured BER characteristics of the AXEL and EML after 80-km transmission are shown in **Fig. 9**. In this measurement, we assumed the RS (Reed Solomon; 528,514) forward error correction (FEC; KR4-FEC) and set a target BER of 5.0E-5. As can be seen in the figure, we could not achieve the target BER of 5.0E-5 by using the EML due to the limitation of the modulated light output power. In contrast, the AXEL successfully extended the transmission distance to 80 km with sufficient receiver sensitivity. Therefore, we can conclude that the significantly improved power conversion efficiency and

modulated light output power of the AXEL enabled us to extend the 28-Gbit/s NRZ transmission distance.

4. Conclusion

An SOA integrated EML, called an AXEL, was experimentally investigated for both the O-band and L-band wavelength ranges in order to extend the transmission distance. We first investigated a 1.57-μm wavelength range AXEL with various SOA lengths. Both the power conversion efficiency and modulated light output power of the AXEL with an SOA length of 150 μm were significantly enhanced compared with those of the conventional EML that was fabricated using the same process.

The low chirp characteristics of the AXEL were also confirmed compared with those of the conventional EML, which enabled us to extend the transmission distance. The measured BER characteristics of the AXEL and EML showed that the 10-Gbit/s transmission distance was successfully extended to 80 km with sufficient light output power of 9 dBm.

Next, the 1.3-μm wavelength AXEL with an SOA length of 100 μm was also investigated to see whether it was possible to overcome the limitation of transmission distance due to large optical fiber loss for the 1.3-μm wavelength range. We confirmed that the modulated light output power was increased to almost twice that of the conventional EML. Furthermore, we experimentally demonstrated a 28-Gbit/s optical link by using the AXEL and APD-ROSA and achieved 80-km transmission with a BER of less than 5.0E-5. These results indicate that the AXEL has significantly enhanced power conversion efficiency, and it can be applied for various optical networks using the IM-DD scheme with any wavelength range.

References

[1] T. Fujisawa, K. Takahata, W. Kobayashi, T. Tadokoro, N. Fujiwara, S. Kanazawa, and F. Kano, "1.3 μm, 50 Gbit/s Electroabsorption Modulators Integrated with DFB Laser for Beyond 100G Parallel LAN Applications," Electron. Lett., Vol. 47, No. 12, pp. 708–710, 2011.

[2] K. Naoe, N. Sasada, Y. Sakuma, K. Motoda, T. Kato, M. Akashi, J. Shimizu, T. Kitatani, M. Aoki, M. Okayasu, and K. Uomi, "43-Gbit/s Operation of 1.55-μm Electro-absorption Modulator Integrated DFB Laser Modules for 2-km Transmission," Proc. of the 31st European Conference on Optical Communication (ECOC 2005), Glasgow, Scotland, UK, Th2.6.4, Sept. 2005.

[3] W. Kobayashi, M. Arai, T, Yamanaka, N. Fujiwara, T. Fujisawa, T. Tadokoro, K. Tsuzuki, Y. Kondo, and F. Kano, "Design and Fabrication of 10-/40-Gb/s, Uncooled Electroabsorption Modulator Integrated DFB Laser with Butt-joint Structure," J. Lightw. Technol., Vol. 28, No. 1, pp. 164–171, 2010.

[4] W. Kobayashi, M. Arai, T. Fujisawa, Y. Shibata, T. Sato, T. Ito, K. Hasebe, T. Yamanaka, and H. Sanjoh, "40-Gbit/s EADFB Laser Integrated with Short Cavity SOA Improving Chirp Characteristics with Low Power Consumption," Proc. of the 40th European Conference on Optical Communication (ECOC 2014), Cannes, France, Mo4.4.5, Sept. 2014.

[5] W. Kobayashi, M. Arai, T. Fujisawa, T. Sato, T. Ito, K. Hasebe, S. Kanazawa, Y. Ueda, T. Yamanaka, and H. Sanjoh, "Novel Approach for Chirp and Output Power Compensation Applied to a 40-Gbit/s EADFB Laser Integrated with a Short SOA," Opt. Exp., Vol. 23, No. 7, pp. 9533–9542, 2015.

[6] T. Shindo, W. Kobayashi, N. Fujiwara, Y. Ohiso, K. Hasebe, H. Ishii, and M. Ito, "High Modulated Output Power over 9.0 dBm with 1570-nm Wavelength SOA Assisted Extended Reach EADFB Laser (AXEL)," J. Sel. Top. Quant., Vol. 23, No. 6, 2017.

[7] T. Shindo, W. Kobayashi, N. Fujiwara, Y. Ohiso, T. Yoshimatsu, H. Ishii, K. Sano, and H. Matsuzaki, "An SOA-integrated EADFB Laser for Enhancement of Modulated Light Output Power and Extension of Transmission Distances," Proc. of SPIE Photonics West 2018, San Francisco, CA, USA, Vol. 10560, 1056008, Jan. 2018.

[8] W. Kobayashi, N. Fujiwara, T. Shindo, Y. Ohiso, T. Yoshimatsu, S. Kanazawa, T. Ohno, K. Hasebe, H. Ishii, and H. Matsuzaki, "Low-power Consumption 28-Gb/s 80-km Transmission with 1.3-μm SOA-assisted Extended-reach EADFB Laser," J. Lightw. Technol., Vol. 35, No. 19, pp. 4297–4303, 2017.

[9] P. A. Yazaki, K. Komori, S. Arai, A. Endo, and Y. Suematsu, "Chirping Compensation Using a Two-section Semiconductor Laser Amplifier," J. Lightw. Technol., Vol. 10, No. 9, pp. 1247–1255, 1992.

[10] T. Watanabe, N. Sakaida, H. Yasaka, F. Kano, and M. Koga, "Transmission Performance of Chirp-controlled Signal by Using Semiconductor Optical Amplifier," J. Lightw. Technol., Vol. 18, No. 8, pp. 1069–1077, 2000.

[11] M. N. Ngo, H. T. Nguyen, C. Gosset, D. Erasme, Q. Deniel, N. Genay, R. Guillamet, N. Lagay, J. Decobert, F. Poingt, and R. Brenot, "Electroabsorption Modulated Laser Integrated with a Semiconductor Optical Amplifier for 100-km 10.3 Gb/s Dispersion-penalty-free Transmission," J. Lightw. Technol., Vol. 31, No. 2, pp. 232–238, 2013.

[12] K.-C. Chang, S.-W. Shen, M.-C. Hsu, Y.-J. Chiu, C.-C. Wei, and C.-K. Lee, "Negative-chirped EAM-SOA for Distance-insensitive Optical OFDM Transmission in Long-reach OFDMA PONs," Proc. of 37th Optical Fiber Communication Conference (OFC 2014), San Francisco, CA, USA, Tu3H.4, Mar. 2014.

[13] W. Kobayashi, Japan patent JP5823920B (October 16, 2015).

[14] W. Kobayashi, N. Fujiwara, T. Shindo, S. Kanazawa, K. Hasebe, H. Ishii, and M. Itoh, "Ultra Low Power Consumption Operation of SOA Assisted Extended Reach EADFB Laser (AXEL)," 21st Optoelectronics and Communication Conference, (OECC 2016) WD3-2, Niigata, Japan, July 2016.

[15] F. Devaux, Y. Sorel, and J. F. Kerdiles, "Simple Measurement of Fiber Dispersion and of Chirp Parameter of Intensity Modulated Light Emitter," J. Lightw. Technol., Vol. 11, No. 12, pp. 1937–1940, 1993.

[16] K. Yamada, K. Nakamura, Y. Matsui, T. Kunii, and Y. Ogawa, "Negative-chirp Electroabsorption Modulator Using Low-wavelength Detuning," IEEE Photon. Technol. Lett., Vol. 7, No. 10, pp. 1157–1158, 1995.

[17] T. Yoshimatsu, M. Nada, M. Oguma, H. Yokoyama, T. Ohno, Y. Doi, I. Ogawa, H. Takahashi, and E. Yoshida, "Compact and High-sensitivity 100-Gb/s (4 x 25 Gb/s) APD-ROSA with a LAN-WDM PLC Demultiplexer," Opt. Exp., Vol. 20, No. 26, pp. B393–B398, 2012.

Takahiko Shindo
Research Engineer, NTT Device Innovation Center.

He received a B.E., M.E., and Ph.D. in electrical and electronic engineering from Tokyo Institute of Technology in 2008, 2010, and 2012. He received a research fellowship for young scientists from the Japan Society for the Promotion of Science for the years 2010 to 2012. In April 2013, he joined NTT Photonics Laboratories (now NTT Device Innovation Center), where he is researching optical semiconductor devices. Dr. Shindo is a member of the Institute of Electrical and Electronics Engineers (IEEE) Photonics Society, the Japan Society of Applied Physics (JSAP), and the Institute of Electronics, Information and Communication Engineers (IEICE).

Shigeru Kanazawa
Senior Research Engineer, NTT Device Innovation Center.

He received a B.E., M.E., and Ph.D. in electronic engineering from Tokyo Institute of Technology in 2005, 2007, and 2016. In April 2007, he joined NTT Photonics Laboratories (now NTT Device Innovation Center). He is engaged in the research and development (R&D) of optical semiconductor devices and integrated devices for optical communications systems. Dr. Kanazawa is a senior member of IEEE/Photonics Society and a member of JSAP and IEICE.

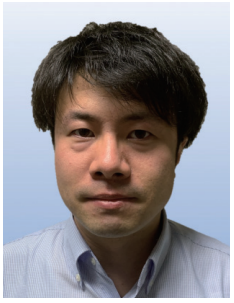

Mingchen Chen
Researcher, NTT Device Innovation Center.

He received a B.E. and M.E. in electronic engineering from the University of Electro-Communications, Tokyo, in 2010 and 2012 and a Ph.D. in engineering from the University of Electro-Communications in 2015. He joined NTT Device Technology Laboratories in 2015. He is engaged in R&D of tunable laser sources.

Toshihide Yoshimatsu
Senior Research Engineer, NTT Device Innovation Center.

He received a B.E. and M.E. in applied physics from Tohoku University, Miyagi, in 1998 and 2000. He joined NTT Photonics Laboratories (now NTT Device Innovation Center) in 2000. He is involved in researching and developing ultrafast optoelectronic devices. He received the International Conference on Solid State Devices and Materials (SSDM) Paper Award in 2004. He is a member of IEICE and JSAP.

Yoshitaka Ohiso
Senior Research Engineer, NTT Device Technology Laboratories.

He received a B.S., M.S., and Ph.D. in electrical engineering from Keio University, Kanagawa, in 1989, 1991, and 2003. Since joining NTT in 1991, he has been researching and developing optical semiconductor devices such as vertical cavity surface emitting lasers, optical filters and optical modulators of electroabsorption and Mach-Zehnder modulators. He also has been involved in the epitaxial growth of III-V compound semiconductors using metal organic chemical vapor deposition. Dr. Ohiso is a member of JSAP and IEICE.

Kimikazu Sano
Project Manager, NTT Device Innovation Center.

He received a B.S., M.S., and Ph.D. in electrical engineering from Waseda University, Tokyo, in 1994, 1996, and 2004. He joined NTT in 1996. Since then, he has been engaged in the design and evaluation of high-speed integrated circuits (ICs) and optoelectronic ICs for large-capacity optical networks. From 2005 to 2006, he was a visiting researcher at the University of California, Los Angeles (UCLA), where he researched a microwave/millimeter-wave sensing system. From 2012 to 2014, he was with NTT Electronics, where he developed high-speed analog ICs and packaged modules for coherent optical systems. He is currently with NTT Device Innovation Center, where he manages the development of lasers, photodiodes, analog/digital circuits for optical metro-access networks. He served as a member of the Technical Program Committee for IEEE Compound Semiconductor IC Symposium (CSICS) from 2008 to 2010.

Hideaki Matsuzaki
Senior Research Engineer, Supervisor, NTT Device Technology Laboratories.

He received a B.S. and M.S. in physics from Kyoto University in 1993 and 1995. He joined NTT's Atsugi Electrical Communications Laboratories in 1995. He is currently involved in R&D of compound semiconductor devices, photodiodes, and laser diodes. He is a member of IEICE.

Surviving in the Digital Transformation Era; Technical Trends and Issues from the Perspective of The Telecommunication Technology Committee

Mai Kaneko

Abstract

As a standards development organization certified by the Ministry of Internal Affairs and Communications of Japan, The Telecommunication Technology Committee (TTC) has been contributing to standardization activities in the field of information and communication technology by developing and disseminating standards for information and communications networks for more than 30 years. The role of TTC is changing as the environment surrounding information and communications undergoes dramatic changes such as the development of digital transformation. This article describes the current status and challenges of Japanese companies in the global market and explains the latest technological trends and TTC's initiatives to serve as a reference for future business strategies.

Keywords: digital transformation, SDGs, innovation

1. Introduction

An overview of The Telecommunication Technology Committee (TTC) and some examples of the areas of standardization the TTC handles are explained in this section.

1.1 TTC overview

The TTC is certified by the Ministry of Internal Affairs and Communications of Japan to standardize information and communication technology (ICT). The purpose of this organization is to contribute to standardization in the information and telecommunications field and to promote the spread of standardization by creating standards related to information and telecommunications networks.

TTC is a members-only organization in which 95 companies, including the NTT Group, information and telecommunications companies, and information technology (IT)-related companies, participate. Members can participate in standardization activities by participating in working groups (WGs) and can also participate in seminars and events for free or for a fee. Members actively interact with each other through activities of the WGs and other events.

1.2 TTC standardization activities through WGs

The TTC has 18 WGs that are organized in 5 technical fields. This organization is based on the layered structure of a telecommunications network. The WGs gather information on related technologies and hold discussions related to standardization. In addition to the WGs, there are sub-WGs, ad hoc groups, and liaison committees (**Fig. 1**).

The Telecommunications System Committee of the Ministry of Internal Affairs and Communications has decided to refer upstream activities concerning all study groups (SGs)[*1] (excluding SG3 and SG9) and

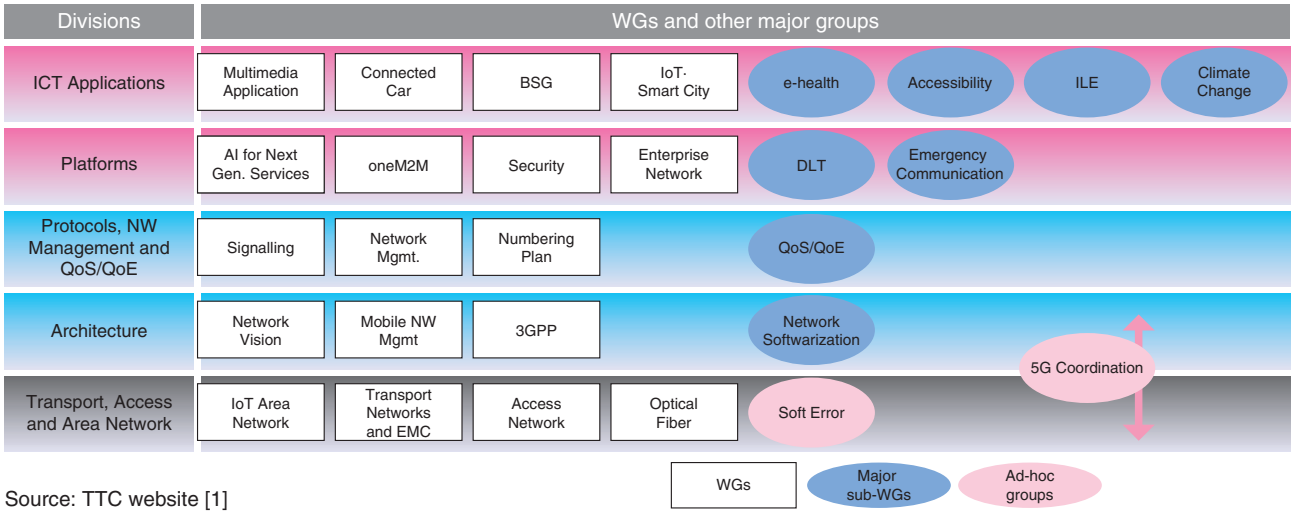

Source: TTC website [1]

AI: artificial intelligence
BSG: Bridging the Standardization Gap
DLT: distributed ledger technology
EMC: electromagnetic compatibility
5G: fifth-generation mobile communications
ILE: immersive live experience
IoT: Internet of Things
M2M: machine to machine
NW: network
QoE: quality of experience
QoS: quality of service
3GPP: 3rd Generation Partnership Project

Fig. 1. Organization of WGs in TTC (as of June 2019).

the Telecommunication Standardization Advisory Group (TSAG)*2 of the International Telecommunication Union - Telecommunication Standardization Sector (ITU-T)*3 to TTC. These activities include deliberating in advance on Japanese contribution letters (proposal documents), drawing up a Japanese response policy, and, if necessary, submitting proposals to the Telecommunications System Committee. In addition, the TTC is recognized as a qualified standardization organization that ITU-T can exchange information with; ITU-T can also use TTC documents as a reference in ITU-T standardization documents, according to ITU-T Recommendations A.5*4 and A.6*5. WGs within the TTC conduct these activities.

1.3 TTC standardization examples

Here, two examples of standardization addressed by TTC in 2018 are introduced. The first example concerns immersive live experience (ILE), which is represented by NTT's Kirari! technology. ILE enables real-time transmission of sports events and entertainment performances to remote locations and provides an ultra-realistic live experience. Service scenarios and frameworks of ILE were standardized based on a proposal from Japan.

The second example is an international standard that defines design, test, and evaluation methods and quality standards for countermeasures against soft errors, which are malfunctions of terrestrial communications equipment caused mainly by cosmic rays. A soft error is not an error that permanently causes the device to fail, but a temporary failure that can be recovered by, for example, restarting the device. It has recently become possible to measure the effects of soft errors on telecommunications equipment by using a compact accelerator-driven neutron source. Consequently, design and evaluation indices of soft errors were required. This is an example of Japan's proactive proposal that embodies the strategy of *the standard is not to follow; it is to make*.

*1 SG: A group of researchers working on a particular topic.
*2 TSAG: A group providing advice on the management and operation of standardization activities in parallel with SGs.
*3 ITU-T: The ITU is a specialized agency of the United Nations that is responsible for establishing international standards and regulations. ITU-T is the division responsible for the development of standards in the telecommunications field.
*4 Recommendation A.5: Generic procedures for including references to documents of other organizations in ITU-T Recommendations.
*5 Recommendation A.6: Cooperation and exchange of information between the ITU Telecommunication Standardization Sector and national and regional standards development organizations.

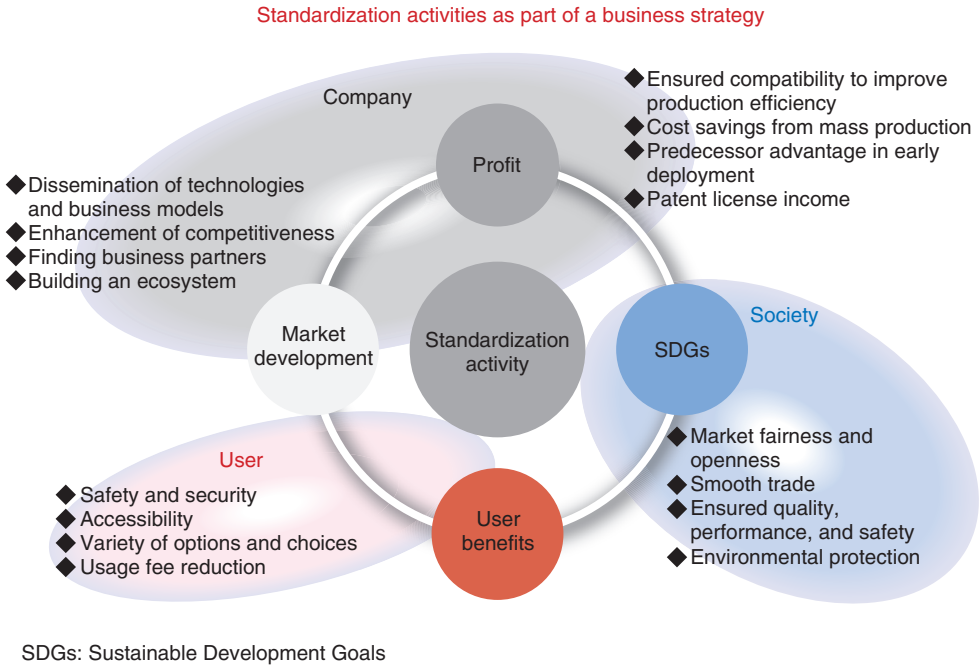

Fig. 2. Benefits of standardization from a business perspective.

2. Significance of standardization

Here, the benefits and strategic use of standardization in business are explained.

2.1 Benefits of standardization from a business perspective

Standardization provides many benefits as part of a business strategy. By ensuring compatibility and consistency through standardization, companies can improve production efficiency. Standardization also leads to cost reductions through mass production and simplification. Furthermore, the early adoption of standardization technology will lead to first-mover profits and license income. Finally, it is possible to create an ecosystem in which technologies and business models become more prevalent, competitiveness increases, and ultimately all stakeholders benefit.

In this way, the opening of the market promotes social trade, and the establishment of rules to meet the environment and standards leads to improvements in safety and security.

Not only is safety guaranteed for users, but a variety of companies participate in standardized specifications, and a variety of products are available on the market, which broadens the range of choices. Standardization is therefore a strategy that benefits all stakeholders (**Fig. 2**).

2.2 Strategic use of standards

Standards are classified into three categories: de jure, forum, and de facto, and they need to be strategically used for different purposes.

(1) De jure standards

De jure standards are established by formal standards organizations, for example, the ITU. The TTC is also classified as an organization that develops de jure standards. De jure standards have great impact on global markets and developing countries, but because of the involvement of national administrations, deliberation and coordination may take time.

(2) Forum standards

Forum standards can be formed through the efforts of multiple companies or organizations to speed up the development of standards. Representative examples of such organizations are the Internet Engineering Task Force (IETF)[*6], the Institute of Electrical and Electronics Engineers (IEEE)[*7], and the World Wide Web Consortium (W3C)[*8]. Forum standards

*6 IETF: A voluntary organization promoting standardization of Internet technology.
*7 IEEE: An organization that standardizes electrical and electronic communications specifications.
*8 W3C: A nonprofit organization that standardizes web technology.

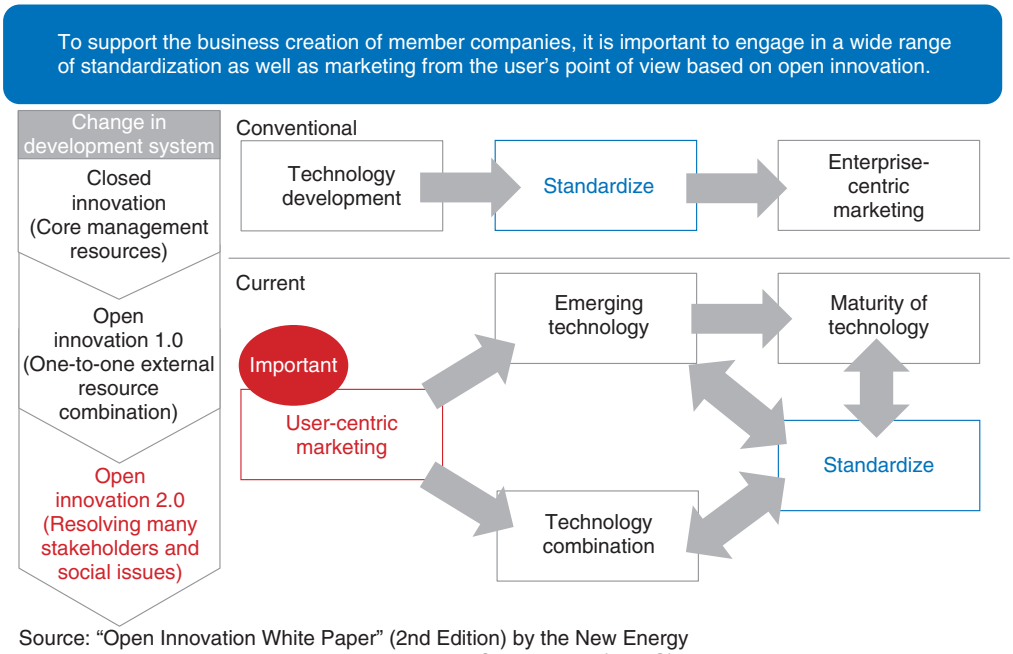

Source: "Open Innovation White Paper" (2nd Edition) by the New Energy and Industrial Technology Development Organization (NEDO) and the Japan Open Innovation Council (JOIC) [2]

Fig. 3. Expanded role of standardization.

are disadvantageous for small businesses and developing countries because standardization is influenced by power relationships centered on developed companies.

(3) De facto standards

De facto standards, also known as market-driven standards, are standards that are adopted widely by an industry and customers. One example is typified by the Windows operating system.

It is important that standardization is carried out strategically in consideration of the balance between the areas of cooperation that are open to the market through standardization and the areas of competition that are not standardized in terms of improving competitiveness.

2.3 Standardization as the role expands

In this age where the market has matured and customer needs have diversified, it is more difficult to create innovative services, and it is not easy to keep up with the changes that are accelerating with the development of ICT. Until now, the worldwide trend has been to develop technologies that make the best use of existing management resources and then to standardize and commercialize them. However, as many companies feel that creating services on their own is time consuming and costly, they have shifted to an open innovation system in which they create services beyond the confines of their company and have been moving to a user-oriented development system in which we think about services based on user issues and the way the services should be. As a result, the role of the TTC has been shifting from technology to marketing in corporate support (**Fig. 3**).

3. Environment surrounding information and communications

This section presents information on various trends and issues facing Japanese companies today.

3.1 Digital transformation and Sustainable Development Goals (SDGs) required for enterprises

The evolution of technologies such as the Internet of Things, big data, and artificial intelligence (AI), which affect the way society should be (i.e., a modern, well-functioning society), has accelerated cross-industry collaboration, and the transformation of the industrial structure has been remarkable. The digital transformation (DX) is progressing; this refers not only to the digitization of existing businesses but also

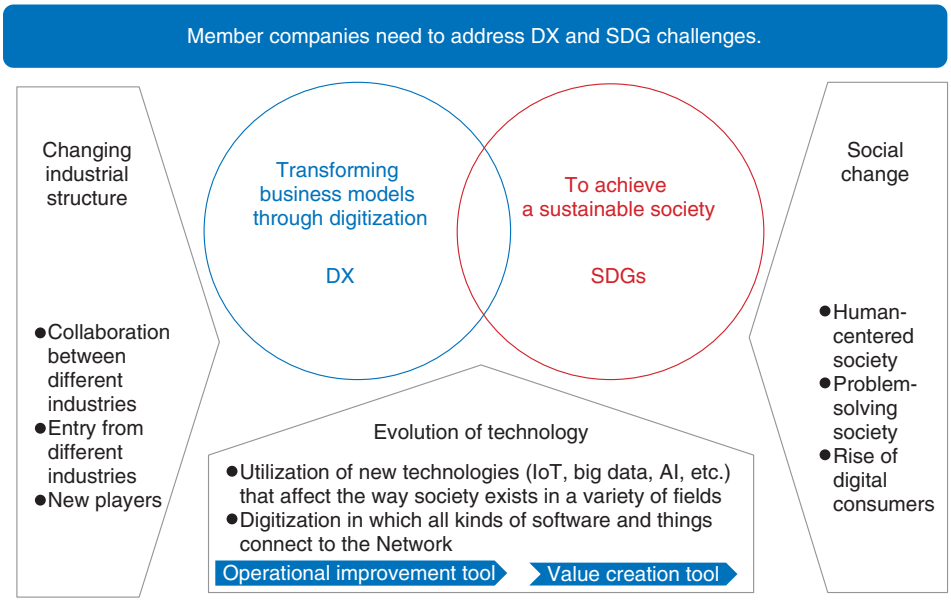

Fig. 4. DX and SDGs required for enterprises.

the transformation of business models using digital technology. Achieving the United Nations SDGs has become a common practice in global markets, and Japanese companies also face an urgent need to promote activities to achieve them (**Fig. 4**).

3.2 Reality of Japanese companies in the global market

Japanese companies face a difficult situation in the global market. About 30 years ago, there were 32 Japanese companies in the top 50 in the world market capitalization ranking, but in 2018, there was only 1, Toyota. In contrast, the United States had 32 companies in the ranking. IT companies are on top, and the rise of Chinese companies is obvious (**Table 1**).

3.3 Trends at the Consumer Electronics Show (CES) 2019

Samsung from South Korea won numerous Innovation Awards at CES 2019, topping the list of companies with the number of wins. CES is the world's largest consumer electronics trade show and is held annually in Las Vegas, US. Japan had little presence at the event, including exhibition booths. Many of the exhibits from other countries featured combinations of existing technologies such as robots and beauty appliances that were popular in Japan some years ago, but with sensors and other advances. Innovation is not only about developing cutting-edge technology but also about combining existing technologies and reworking them in innovative ways.

3.4 Trends in ITU-T participating companies

The membership of ITU-T, which is a representative de jure standardization organization, has increased significantly in recent years. More than half of the participating companies are in the traditional IT communication field, involved in areas such as quantum communication, digital currency, MVNO (mobile virtual network operator), and over-the-top (OTT). However, insurance companies and those in the automobile industry are also participating, and the range of fields represented by the participating companies is expanding. Since 2017, 4 companies in Japan (Canon, Murata Manufacturing, Softbank, and Internet Initiative Japan) have joined ITU-T, in addition to 13 companies in China and 15 in the US. China leads the number of ITU-T contributions by country, with 27%, followed by South Korea with 11%, the United States with 10%, and Japan with 4%. In China, companies as well as the government actively participate in standards activities.

3.5 Global responses to SDGs

No Japanese company has been selected as one of the 50 leading companies in the world that support SDGs. The overwhelming majority are in the United States, and half are in Europe. In Asia, companies in

Table 1. Comparison of world market capitalization rankings.

	1989	Country name	Type of industry	2018	Country name	Type of industry
1	NTT	Japan	Telecommunications	Apple	USA	IT
2	Industrial Bank of Japan	Japan	Banking	Amazon.com	USA	IT
3	Sumitomo Bank	Japan	Banking	Alphabet, Inc.	USA	IT
4	Fuji Bank	Japan	Banking	Microsoft	USA	IT
5	Dai-Ichi Kangyo Bank	Japan	Banking	Facebook	USA	IT
6	IBM	USA	Computers	Berkshire Hathaway	USA	Investing
7	Mitsubishi Bank	Japan	Banking	Alibaba Group Holdings	China	IT
8	Exxon	USA	Oil	Tencent Holding	China	IT
9	Tokyo Electric Power Company	Japan	Energy	J.P. Morgan Chase & Co.	USA	Financial
10	Royal Dutch Shell PLC	UK	Oil	Exxon Mobil	USA	Oil
11	Toyota Motor Corporation	Japan	Automotive	Johnson & Johnson	USA	Healthcare
12	GE	USA	Conglomerate	Visa	USA	Financial

Source: Diamond Weekly, August 25 issue, 2018 [3], prepared by the author

Hong Kong and Singapore are most prominent. By industry, there are many medical, infrastructure, and chemical manufacturers. As Japan is lagging behind other countries in SDG efforts, it can be expected that the formulation of SDG rules will proceed mainly through the efforts of Europe and the United States.

4. Key technology and TTC initiatives in 2019

The TTC is constantly monitoring ITU-T trends. ITU-T is promoting standardization under the slogan *Smart ABC (AI, banking, cities) – Innovative use of ICT to improve quality of life, service efficiency, and competitiveness*. There are six topics for standardization: 1) new standards for optical fiber, 2) 5G (fifth-generation mobile communications), 3) framework for cooperation between OTT operators and network operators, 4) quality of service (network quality) and quality of experience (user experience quality) such as in video streaming, 5) interoperability for personal health, and 6) key performance indicators for achieving smart cities. TTC is focusing on trends that ITU-T will discuss in the future such as connected cars, quantum communications and cryptography, digital currency and blockchains, AI, and Network 2030 beyond 5G, with various activities being carried out in the TTC WGs (**Table 2**).

5. Innovation study group for service innovation

To help Japanese companies develop human resources capable of adapting to the changing times, the TTC established a practical study group to create use cases for innovative services using an open innovation approach. The five-part program consists of learning how to generate the ideas needed in the service creation process, listening to innovative examples from key players in advanced companies that develop and provide services from the user's perspective, and experiencing open innovation through collaboration with participants from different organizations. The TTC launched this initiative to address the growing role of standards in 2018.

6. Conclusion

Japanese companies are falling behind in terms of both competitiveness and SDG compatibility in the global market. It is hoped that the TTC will help to develop innovative services, expand into global markets, and promote cross-industry catch-up and open innovation. The TTC website [4] contains more information on standardization and the latest technical information not covered in this article.

Table 2. ITU-T trends and TTC activities.

Development of new business and ICT services in the DX era		
MaaS	Connected Car WG	• Specific examination of automobile communications technology, next-generation mobility services, and disaster response using cars
ILE	Multimedia Application WG (ILE-SWG)	• Advanced MMT—elemental technology of NTT's Kirari!—is ultra-realistic media synchronization technology that makes it possible to realize a variety of video services. This WG promotes international standardization of ILE.
e-health	Multimedia Application WG (e-health SWG)	• Promoting standardization of work items for remote medical care and ICT health care using the latest multimedia ICT technology • Downstreaming international standards for safe listening (volume restriction function to prevent hearing disabilities, etc.)
Response to new standardization themes such as quantum communication and AI		
Quantum communication	Security WG	• Inviting experts to study groups and holding collaborative seminars with the Information Processing Society of Japan (IPSJ)
Digital currency		• Establishing SWGs and starting reviews
AI	AI for Next Gen. Services WG	• Collecting and analyzing examples of use cases using AI
Contributing to building infrastructures in the future with the Network 2030		
Network 2030/5G	Network Vision WG	• Discussing future networks such as inter-industry linkage with OTT services and open API
Contribution to SDGs to solve social issues		
SDG	International coordination	• To achieve SDGs, we held TTC seminars for executives and the public, and organized connections between SDG efforts and TTC activities. • At the TSAG meeting, we showed the mappings between the ITU-T SG issues and the 17 SDG goals and proposed clarification of the rationale. Proposal of a mapping guideline from Japan is planned.
Smart City	IoT·Smart City WG OneM2M WG	• Analyzing and understanding IoT and smart city use cases, and implementing cases and disseminating them to domestic companies.

API: application programming interface
MaaS: mobility as a service

References

[1] Website of TTC, Organization, Working groups, https://www.ttc.or.jp/e/org/workin-groups
[2] NEDO and JOIC, "Open Innovation White Paper," 2nd Edition, June 2018 (in Japanese).
[3] Diamond Weekly, August 25 issue, 2018 (in Japanese).
[4] TTC, https://www.ttc.or.jp/e

Trademark notes

Mai Kaneko
Director, Planning and Strategy, The Telecommunication Technology Committee.

She received a B.S. in mathematics from Tokyo Woman's Christian University in 1997 and an MBA from Yokohama National University in 2014. She joined NTT in 1997 and was in charge of designing and building large-scale information systems, including one for the National Museum of Emerging Science and Innovation, as a system engineer in corporate sales. She collaborated with various companies as an alliance strategist from 2002 to 2006. Among her accomplishments, she devised a new tablet service that originated in Japan and initiated a project in the product development division in 2009. She was in charge of training planning and labor management for 100 young technical employees as a manager from 2010 to 2012. She was temporarily transferred to the Center for International Public Policy Studies (CIPPS), where she engaged in policy recommendation work. She returned to NTT EAST in 2015 and worked as a sales manager for the Kanagawa area. She took up her current position in 2018.
Books authored:
Individual Number Card, Pioneering the Future (contributed as a member of Nomura Institute of Capital Markets Research)
Medical Care and Individual Number Card (co-author)
Japan's Growth Strategy Considered in 10 Points (co-author)

Introduction to Troubleshooting Cases Related to Telephone Systems in Customer Premises

Technical Assistance and Support Center, NTT EAST

Abstract

In this article, we introduce two cases involving problems that occurred in telephone systems. In the first case, a connection could not be established even when the customer dialed the correct number. In the second case, silence suddenly occurred during the connection. We investigated and solved these problems using various measurement tools and analysis methods. This is the fifty-fourth article in a series on telecommunication technologies.

Keywords: key telephone system, IP phone, PSTN

1. Introduction

The Network Interface Engineering Group at the Technical Assistance and Support Center provides technical support and on-site troubleshooting for difficult-to-solve problems in Internet protocol (IP) services such as the FLET'S HIKARI NEXT fiber-optic broadband service and public switched telephone network (PSTN) services such as plain old telephone services (POTS).

The rapid progression of information and communication technology (ICT) has led to our support of various ICT services. Thus, when we investigate the cause of a problem, we use a variety of measurement methods and equipment. For IP services, we obtain IP packets in a network using packet capture tools, and we analyze those packets using various methods. For PSTN services, we analyze signals using waveform recorders and ISDN (integrated services digital network) protocol analyzers. To inspect key telephone systems, we collect and analyze specific signals in a cable between the master equipment and terminal telephone sets using the α line monitoring system (a tool developed by the Technical Assistance and Support Center). Two recent cases of problems that occurred in customer premises are introduced in this article.

2. Introduction to troubleshooting cases in customer premises

This section describes in detail the two problems that occurred in customer premises.

2.1 Case 1: Connection cannot be established even if customer dials correct number

2.1.1 Overview and investigation method

In this case, the customer's key telephone system (αGX-M) was connected to five POTS lines. The customer claimed that a connection could not be established even if the correct number was dialed. On site, the master equipment unit and telephone sets were replaced by service personnel, but the problem persisted.

Thus, we conducted an investigation to solve the problem. This consisted of collecting and analyzing data when the problem occurred. The configuration of the measurement setup and tools used in the

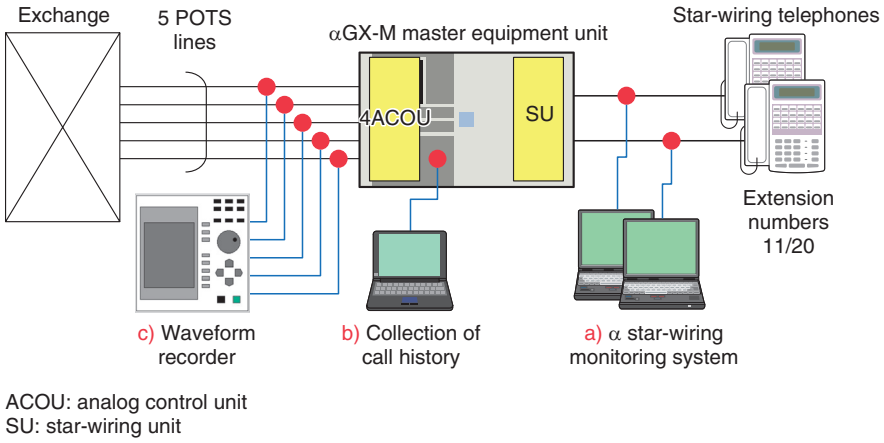

Fig. 1. Configuration of call analysis system and measurement points.

Table 1. System status at problem occurrence.

Date/time	Outside line	Extension number	Number dialed
Date/Month/2018 at 10:00	2	20	02xx-xx-xxxx
Date/Month/2018 at 10:20	3	20	02yy-yy-yyyy
Date/Month/2018 at 10:21	2	20	02zz-zz-zzzz

investigation are shown in **Fig. 1**. The red circles indicate the measurement points. We investigated the following using several measurement tools.

a) Monitoring telephone operation using the α line monitoring system
b) Collecting call history using a personal computer, that is, the maintenance console of the system, and checking the call-connection status at the time of the problem
c) Checking outgoing-call sequence/selection signals (push button (PB) signals) by monitoring the voltage between the L1-L2 lines using the waveform recorder

The customer explained that the problem occurred three times during the investigation period. After conducting the investigations above, we analyzed the collected data. The system status at the time the problem occurred is summarized in **Table 1**.

2.1.2 Results of analyzing collected data

a) α line monitoring system

When the telephone operation was checked at the time the problem occurred, it was found that the customer was operating the telephone normally by connecting to an outside line using the line key and pressing the dialing buttons corresponding to the destination telephone number.

b) Collection of call history via maintenance console

When the call history of the master equipment was checked, it was found that the number dialed by the customer on the telephone was recorded; that is, it indicated that the customer was operating the telephone correctly.

c) Voltage monitoring between L1-L2 lines by waveform recorder

The following information was obtained from the waveform recorder. The waveforms obtained when the problem occurred are shown in **Fig. 2**.

- The PB signal of the first digit dialed (‘0’) was transmitted approximately 640 to 790 ms after connecting to an outside line (loop closure).
- The dial tone (DT) was received from the exchange after the PB signal of the first digit had already been transmitted (‘0’).
- The DT stopped when the second digit was dialed (‘2’).
- It took approximately 800 to 900 ms for the DT to be received in the customer’s environment.

2.1.3 Cause of problem and countermeasure

This problem occurred because the PB signal of the

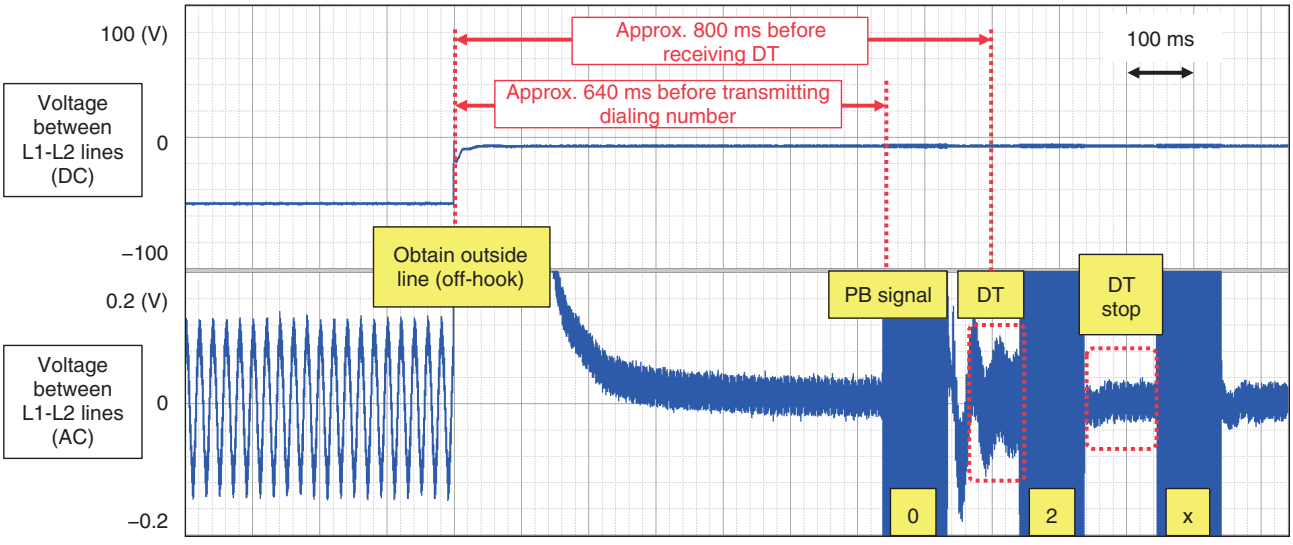

AC: alternating current
DC: direct current
DT: dial tone

Fig. 2. Waveforms at time of problem.

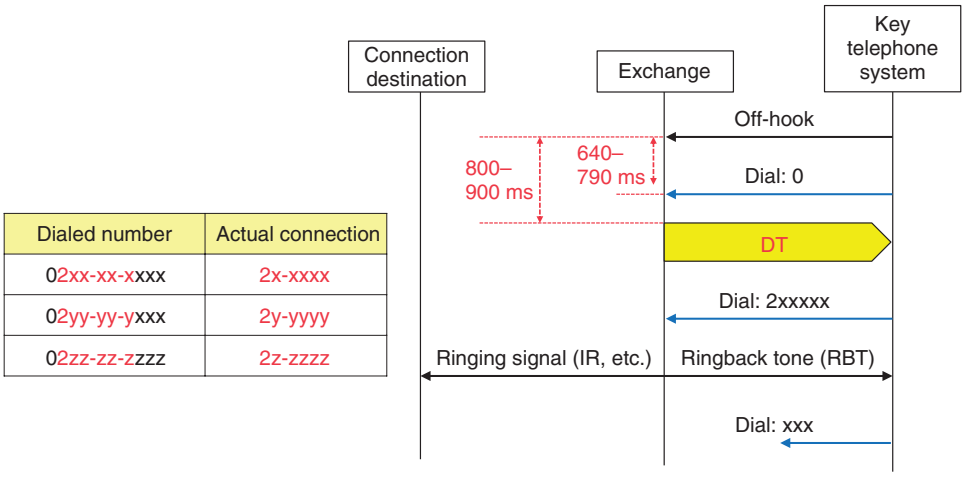

Dialed number	Actual connection
02xx-xx-xxxx	2x-xxxx
02yy-yy-yxxx	2y-yyyy
02zz-zz-zzzz	2z-zzzz

IR: inter ringing

Fig. 3. Calling sequence at time of problem.

first digit dialed (‘0’) was transmitted from the telephone before receiving the DT from the exchange, preventing that digit from being recognized by the exchange. Furthermore, since the PB signal of the second digit dialed (‘2’) (transmitted after receiving the DT) was processed by the exchange, and given that the first digit of a local office number is ‘2,’ a connection was made to an existing 6-digit local telephone number. The calling sequence is shown in **Fig. 3**. This problem was solved by changing the initial value of the guard interval before transmitting the first digit of the dialed number from 600 ms to 1000 ms. This can be easily set by using the αGX-M master equipment system data, that is, the 07–47 early dialing prevention timer for making an outside call. The waveforms when setting this value to 1200 ms

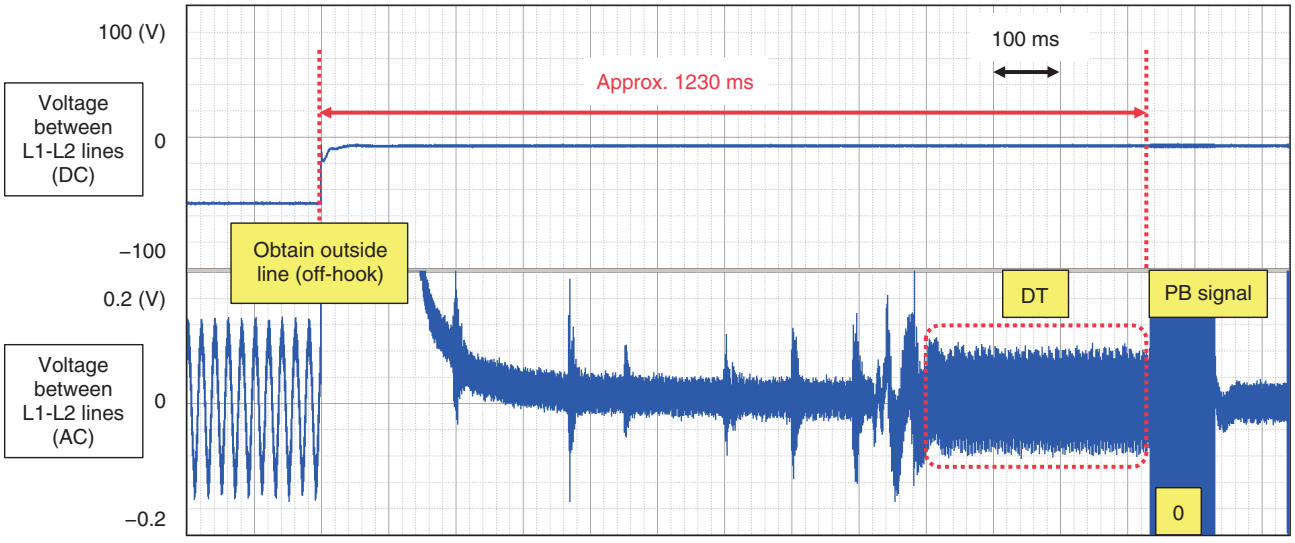

Fig. 4. Waveforms for guard interval set to 1200 ms.

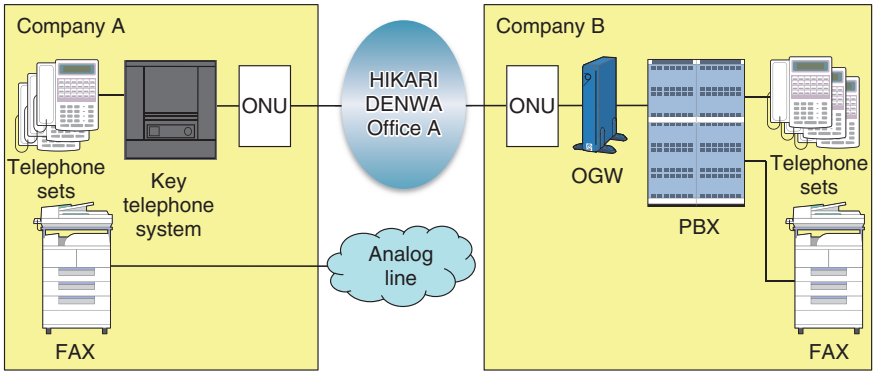

FAX: facsimile
ONU: optical network unit

Fig. 5. Equipment configuration.

are shown in **Fig. 4**.

2.2 Case 2: Voice suddenly disappears in connection with specific destination

2.2.1 Overview and investigation method

A customer (Company A) was using the NTT HIKARI DENWA IP phone service in its key telephone system. The customer claimed that a voiceless condition occurred during calls with Company B. Company B, meanwhile, was using the NTT HIKARI DENWA (via OGW (Office Gateway) with Primary Rate Interface) in its private branch exchange (PBX). The equipment configuration at both locations is shown in **Fig. 5**. We captured IP packets using packet-capturing equipment near the ONU (optical network unit) at both locations. Then the data at the time of the problem occurred were analyzed.

2.2.2 Results of analyzing collected data

Six incidents were reported by the customer during the time the packet-capturing equipment was installed. The captured data revealed the following information. These were common to the six incidents.

- At Company A, the incidents always occurred when the telephone set was used on extension number 25.
- Analysis by Wireshark (local area network

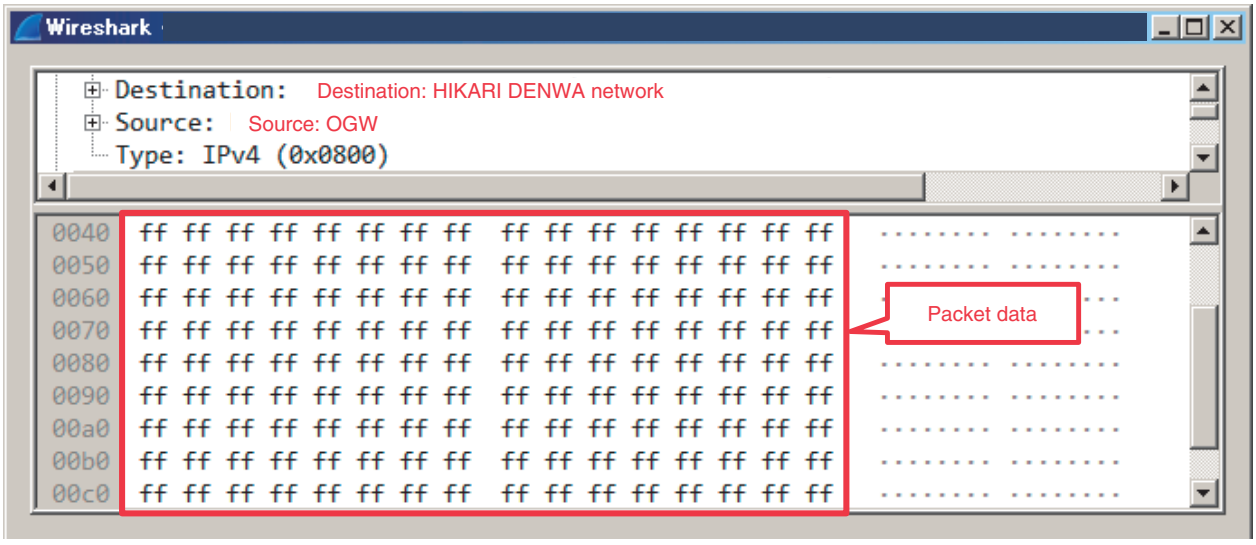

Fig. 6. Voice packet data from Company B.

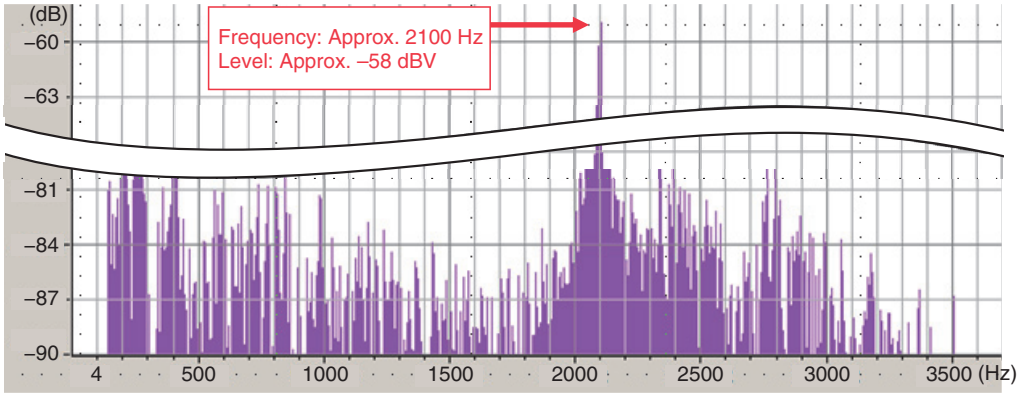

Fig. 7. Results of analyzing frequency components.

analyzer) revealed that voice packet data from Company B contained "ff," which indicates complete silence (**Fig. 6**). This state continued until the call was disconnected.

- Analysis of voice packet data indicated that the sound of facsimile (FAX) communications was mixed in with the voice call from Company A.
- This mixed-in sound is the called terminal identification (CED) tone (frequency: 2100 Hz), which is the response signal issued on receiving a FAX (**Fig. 7**).

2.2.3 Inference of cause and countermeasure

After analyzing the collected data, we inferred that one of the causes of this problem was the mixing in of the FAX CED tone from Company A during the call. Consequently, on checking the surroundings near the telephone set at Company A, we found that the telephone set having extension number 25 was installed about 1 m away from the FAX machine, and the machine was transmitting the sound of FAX communications from the speaker used for monitoring its operation. Thus, the monitor sound during FAX communications was picked up by the microphone of telephone number 25. To avoid unintended pickup of the sound, the volume of the monitor sound during FAX communications was decreased.

2.2.4 PBX operation check

In addition, we also checked the operation of the

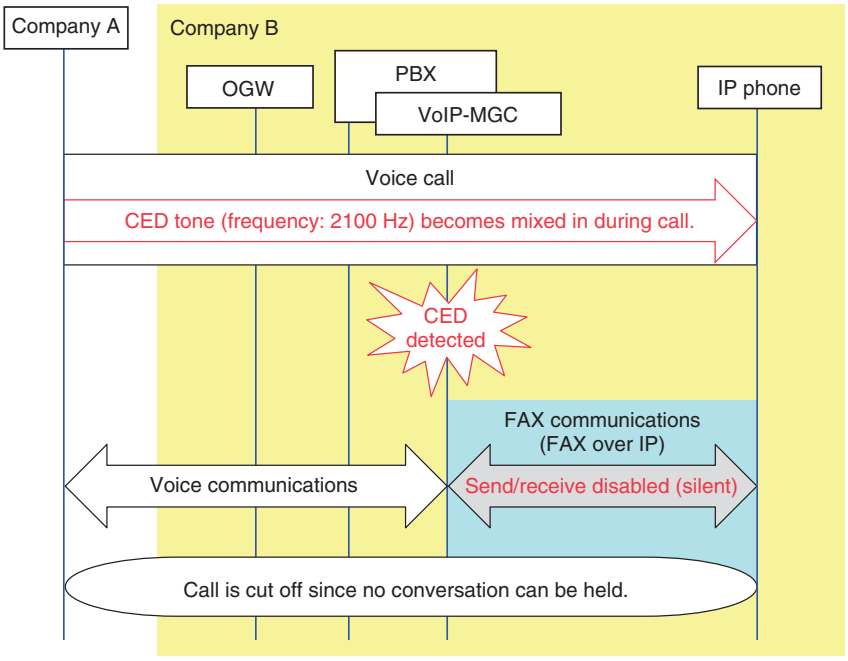

VoIP-MGC: Voice over Internet Protocol Media Gateway Card

Fig. 8. Conditions of problem occurrence.

PBX at Company B. We added a 2100-Hz signal to the voice communication between Company A and Company B. As a result, the voice communication was disabled. Furthermore, on checking the specifications of the PBX equipment, we found that this problem would occur under the following conditions, as shown in **Fig. 8**.

- The equipment configuration included IP phones (with a Voice over Internet Protocol (VoIP) Media Gateway Card installed) used as extension telephones.
- The VoIP Media Gateway Card would switch to the FAX communications mode (FAX over IP) from the voice communications mode when it detected a CED tone (2100 Hz).
- A voiceless condition would occur after the card switched to FAX communications mode because the telephone set (i.e., IP phone) was not a FAX machine.

We confirmed that the equipment configuration at Company B was the same as that at Company A. This means that there was a possibility that the same problem could occur when Company B was making a call with another destination. Therefore, we proposed that the PBX (VoIP Media Gateway Card) should be set to disable the switching to FAX communications mode during a call (set FAX over IP to *disabled*). This proposal was accepted and implemented, and then problem was solved.

3. Conclusion

This article introduced two case studies of problems occurring in telephone systems in customer premises. The first one described a problem in a key telephone system caused by the timing of transmission of a dial tone in POTS. The other involved a problem in which a PBX would have a misoperation due to picking up a sound in the surrounding area. As we explained here, we use not only modern IP technologies but also conventional PSTN technologies to solve problems in the field. The Technical Assistance and Support Center will continue to provide solutions to problems in the field by using various tools and methods in order to ensure safe and secure telecommunication services.

External Awards

Outstanding Catalyst Depicting Business Assurance Awareness

Winner: Skynet catalyst program (The member includes Kenichi Tayama, Shingo Horiuchi, and Chao Wu, NTT Access Network Service Systems Laboratories.)
Date: May 16, 2019
Organization: TM Forum

For "Skynet Catalyst proof of concept (PoC)."

The Skynet is a TM Forum catalyst project and it aims for an end-to-end service orchestration and monetization on a 5G network slice in hybrid network for large enterprises with multiple global locations. Its catalyst champions include BT, Chunghwa Telecom, Deutsche Telekom, Du, NTT Group, Orange, Verizon, Vodafone, Telenet Group, Telecom Italia, and Telus. Participants include Amartus, BearingPoint, Ericsson, EXFO, Infosys, and RIFT. At Digital Transformation World 2019, Skynet demonstrated PoC operation of remote medical services using a network resource management technology prototype.

Best Paper Award

Winner: Yousuke Takahashi, NTT Network Technology Laboratories; Keisuke Ishibashi, International Christian University; Masayuki Tsujino, NTT Network Technology Laboratories; Noriaki Kamiyama, Fukuoka University; Kohei Shiomoto, Tokyo City University; Tatsuya Otoshi, Yuichi Ohsita, and Masayuki Murata, Osaka University
Date: June 6, 2019
Organization: The Institute of Electronics, Information and Communication Engineers (IEICE)

For "Separating Predictable and Unpredictable Flows via Dynamic Flow Mining for Effective Traffic Engineering."
Published as: Y. Takahashi, K. Ishibashi, M. Tsujino, N. Kamiyama, K. Shiomoto, T. Otoshi, Y. Ohsita, and M. Murata, "Separating Predictable and Unpredictable Flows via Dynamic Flow Mining for Effective Traffic Engineering," IEICE Trans. Commun., Vol. E101-B, No. 2, pp. 538–547, 2018.

Best Paper Award

Winner: Ryo Kikuchi, NTT Secure Platform Laboratories; Nuttapong Attrapadung, National Institute of Advanced Industrial Science and Technology; Koki Hamada and Dai Ikarashi, NTT Secure Platform Laboratories; Ai Ishida, Takahiro Matsuda, Yusuke Sakai, and Jacob C. N. Schuldt, National Institute of Advanced Industrial Science and Technology
Date: July 4, 2019
Organization: The 24th Australasian Conference on Information Security and Privacy (ACISP) 2019

For "Field Extension in Secret-shared Form and Its Applications to Efficient Secure Computation."
Published as: R. Kikuchi, N. Attrapadung, K. Hamada, D. Ikarashi, A. Ishida, T. Matsuda, Y. Sakai, and J. C. N. Schuldt, "Field Extension in Secret-shared Form and Its Applications to Efficient Secure Computation," ACISP 2019, Christchurch, New Zealand, pp. 343–361, July 2019.

Best Paper Award

Winner: Yuto Sagae, Takashi Matsui, and Kazuhide Nakajima, NTT Access Network Service Systems Laboratories
Date: July 10, 2019
Organization: The 24th OptoElectronics and Communications Conference (OECC 2019)

For "Ultra-low-XT Multi-core Fiber with Standard 125-μm Cladding for Long-haul Transmission."
Published as: Y. Sagae, T. Matsui, and K. Nakajima, "Ultra-low-XT Multi-core Fiber with Standard 125-μm Cladding for Long-haul Transmission," OECC 2019, Fukuoka, Japan, July 2019.

Best Paper Award

Winner: Sayaka Yagi, Kimio Tsuchikawa, and Kohji Tsuji, NTT Access Network Service Systems Laboratories
Date: July 18, 2019
Organization: 23rd International Conference Information Visualisation

For "A Heatmap-based Visualization Technique for Finding Operational Problems."
Published as: S. Yagi, K. Tsuchikawa, and K. Tsuji, "A Heatmap-based Visualization Technique for Finding Operational Problems," 23rd International Conference Information Visualisation (IV19) - Part II, pp. 110–115, Adelaide, Australia, July 2019.

Technical Committee on Communication Quality Best Research Award

Winner: Takuto Kimura, NTT Network Technology Laboratories; Tatsuaki Kimura, Osaka University; Arifumi Matsumoto and Jun Okamoto, NTT Network Technology Laboratories
Date: July 18, 2019
Organization: IEICE Technical Committee on Communication Quality

For "Video Engagement Control with Bayesian Optimization."
Published as: T. Kimura, T. Kimura, A. Matsumoto, and J. Okamoto, "Video Engagement Control with Bayesian Optimization," IEICE Tech. Rep., Vol. 118, No. 503, CQ2018-100, pp. 43–48, 2019.

Papers Published in Technical Journals and Conference Proceedings

Women in Security: Building a Female InfoSec Community in Korea, Japan, and Taiwan

S. Kang, A. Nakajima, and H. Yen

Black Hat USA 2019, Las Vegas, NV, USA, August 2019.

The information security industry has historically been a male-dominated field, and today, unfortunately, this situation has not changed much. Indeed, the survey conducted by Frost & Sullivan in 2017 concluded that women represented only 11% of the current information security workforce. While more women are expected to join the information security industry to reach new levels of innovation, still, it is difficult to increase their number because women face many obstacles, such as stereotype bias. One way to bridge this gap is a female community, which can support and motivate women, and produce more role models. In this talk, we will introduce three representative Asian female communities, Power of XX, CTF for GIRLS, and HITCON GIRLS, which were established in Korea, Japan, and Taiwan, respectively. We will first explain how we build and maintain each female community and then go into the details of how we tackled various challenges, such as building a sustainable community and attracting and retaining new members.